# UC Santa Barbara
## UC Santa Barbara Electronic Theses and Dissertations

**Title**

Mechanisms and Characteristics of Landfalling Atmospheric Rivers Affecting Southern California

**Permalink**

https://escholarship.org/uc/item/39k557kf

**Author**

Harris, Sarah May

**Publication Date**

2017

Peer reviewed|Thesis/dissertation

# UNIVERSITY OF CALIFORNIA
## Santa Barbara

# Mechanisms and Characteristics of Landfalling Atmospheric Rivers Affecting Southern California

A dissertation submitted in partial satisfaction

of the requirements for the degree Doctor of Philosophy

in

Geography

by

Sarah M. Harris

Committee in charge:

 Professor Leila M. V. Carvalho, Chair

 Professor Bodo Bookhagen

 Professor Charles Jones

 Professor Marilyn Raphael

January 2018

The dissertation of Sarah M. Harris is approved.

_____
Bodo Bookhagen

_____
Charles Jones

_____
Marilyn Raphael

_____
Leila M. V. Carvalho, Committee Chair

November 2017

# Acknowledgments

First and foremost, I would like to express my sincere appreciation to my advisor and the chair of my committee, Professor Leila M. V. Carvalho. Without her this work would not have been possible. She has been a wonderful mentor and has provided me with academic and professional guidance as well as emotional support. I am grateful for her assistance and endless patience. I would also like to thank my committee members, Professor Bodo Bookhagen, Professor Charles Jones, and Professor Marilyn Raphael, for their input, guidance, and the encouragement to pursue my academic interests. Additional thanks to Professor Tommy Dickey for his optimism and reassurance throughout my graduate student career.

I would like to acknowledge the University of California, Santa Barbara (UCSB), Graduate Division who provided me with the financial support to finish my dissertation. Also, UCSB's Department of Geography and the Earth Research Institute for their support throughout the years.

I owe my deepest gratitude to Professor Grant. D. McKenzie who provided important insights to this project. His creative advice and constant encouragement has been invaluable and has kept me going. Also, a huge thank you to our families for their care, understanding, and support during these past years.

Finally, a special thanks to current and former members of the CLIVAC research group, the 2010 fall cohort, as well as all the friends I have made along the way. Thank you for making graduate school an unforgettable experience!

## EDUCATION

**Ph.D. Geography**                                    (estimate) December 2017
University of California, Santa Barbara, CA
Committee Chair: Leila M. V. Carvalho, Ph.D.
   Mechanisms and Characteristics of Landfalling Atmospheric Rivers Affecting Southern
   California

**M.A. Geography**                                                      June 2013
University of California, Santa Barbara, CA
Committee Co-chairs: Leila M. V. Carvalho, Ph.D. and Bodo Bookhagen, Ph.D.
   A comprehensive analysis of precipitation in Santa Barbara, California on hourly to
   interannual timescales

**B.A. Geography**                                                       May 2009
**B.S. Psychology (biobehavioral concentration)**
University of Vermont, Burlington, VT

## PUBLICATIONS

Harris, S.M. and L.M.V. Carvalho. 2017. Characteristics of southern California atmospheric rivers.
Theoretical and Applied Climatology. DOI: 10.1007/s00704-017-2138-1

Harris, S.M. and L.M.V. Carvalho, Backward trajectories analysis of southern California
atmospheric rivers. Under preparation.

Harris, S.M. and L.M.V. Carvalho, Impacts of atmospheric rivers and the Madden-Julian
Oscillation on precipitation in Santa Barbara, CA. Under preparation.

## PROFESSIONAL EXPERIENCE & DEVELOPMENT

**Graduate Student Researcher**
Earth Research Institute                                    April 2014-September 2014
University of California, Santa Barbara, CA
Supervisor: Leila M. V. Carvalho, Ph.D.
Atmospheric river occurrence, variability, and effects on southern California

Earth Research Institute                                    April 2011-June 2011
University of California, Santa Barbara, CA                 April 2012-September 2012
Supervisor: Charles Jones, Ph.D.
Extreme precipitation in Santa Barbara, CA

**Instructor of Record**
University of California, Santa Barbara, CA                 September 2016-December 2016
People, Place, and Environment (GEOG 5)
Undergraduate course covering the basic concepts of human geography, with emphasis on
people, place, and environment.

University of California, Santa Barbara, CA                    June 2013-August 2013
Oceans and Atmosphere (GEOG 3A)
Undergraduate course that introduces students to Earth's atmosphere and ocean systems and
explains their role in climate and weather patterns.

**Lead Teaching Assistant**
University of California, Santa Barbara, CA              September 2014-August 2015
Dept. of Geography

**Summer Teaching Institute for Associates Certificate**
University of California, Santa Barbara, CA                           Summer 2013
Instructional Development

**Teaching Assistant**
University of California, Santa Barbara, CA              September 2010-December 2010
People, Place, and Environment (GEOG 5)                      July 2011-August 2011
                                                       September 2013-December 2013
                                                        August 2015-September 2015
                                                           January 2017-March 2017

University of California, Santa Barbara, CA                       April 2013-June 2013
Maps and Spatial Reasoning (GEOG W12)                            March 2015-June 2015

University of California, Santa Barbara, CA                    January 2015-March 2015
Geography of Latin America (GEOG 155)

University of California, Santa Barbara, CA               October 2014-December 2014
Teaching Assistant Training (GEOG 500)

University of California, Santa Barbara, CA                    January 2011-March 2011
Introduction to Meteorology (GEOG 110)                       January 2012-March 2012
                                                             January 2013-March 2013
                                                             January 2014-March 2014

University of California, Santa Barbara, CA              September 2012-December 2012
Tropical Meteorology (GEOG 133)

University of California, Santa Barbara, CA              September 2011-December 2011
Oceans and Atmosphere (GEOG 3A)

# Abstract

# Mechanisms and Characteristics of Landfalling Atmospheric Rivers

# Affecting Southern California

By

Sarah M. Harris

Atmospheric rivers (ARs) are filamentary channels of water vapor flux that play a vital role in the meridional transport of heat and moisture to midlatitudes. These features travel horizontally through the low atmosphere and over the open oceans. When they interact with orographic barriers such as coastal mountain ranges they are often responsible for high-intensity storms. In Southern California (SCA), an area that receives most of its annual precipitation from relatively few storms per season, ARs are important components of the region's hydrological cycle. They provide significant proportions of annual precipitation totals within only a handful of storms and are responsible for many high-intensity rainfall events leading to hazards such as flooding. There is abundant AR research that analyzes the events affecting North America's west coast. Yet, few examine ARs that landfall in SCA and instead focus on latitudes farther north. This research analyzes the AR events that make landfall in SCA, about their dynamics, characteristics, and lifecycles on the day of and in the days before landfall. It is the goal of this research to increase our understanding of these events to enhance AR modeling and forecasts for SCA. This may improve general preparedness, mitigate against hazards, and aid with water resources management.

In this dissertation, we create an algorithm to identify ARs within reanalysis fields to determine the historical events affecting the west coast of North America (30°-55°N) during the last four decades. We categorize these events according to landfall areas and create composites of regional events using additional reanalysis fields to establish atmospheric characteristics on the day

of and the days before landfall. We aim to determine the defining characteristics of SCA ARs. We find that all ARs landfalling in western North America have landfall day characteristics consistent with baroclinic wave trains in the position and organization of moisture, temperature, and geopotential (500mb) heights. In the days before landfall, we determine that the position, phase, and amplitude of the wave train are important drivers behind SCA ARs which we see in the development of 500mb trough-ridge couplets in the western Pacific and subsequent changes to the 200mb jet core ($\geq 60 \text{ms}^{-1}$). We also investigate the relationship between these ARs and modes of variability, the El Niño Southern Oscillation, the Madden-Julian Oscillation and the Pacific North American Teleconnection Pattern. We find that there are no strong relationships between these modes with AR landfall locations indicating that while these modes may increase AR frequency for North America's west coast, they are not the drivers of specific AR landfall locations. We also complete a backward trajectories model of identified west coast ARs to determine the hourly movement and lifecycles of air parcels from these events at various atmospheric levels. We run the model from the hour of landfall and hourly for the 72 hours before landfall. For all ARs, we find that variables indicative of orographic uplift occur in the hours (0–15 hours) right before landfall. However, we find that SCA ARs are slower and warmer, giving them the potential to hold more moisture. Significantly higher specific humidity values confirm these observations. A case study analysis of a particularly strong SCA AR is also introduced. We find commonalities between this AR and the average AR characteristics but also differences in along-trajectory variables of temperature and specific humidity values as well as temporal characteristics that highlight why this event was so extreme.

Collectively these analyses show us fundamental differences between SCA ARs and ARs landfalling farther north along North America's west coast. These characteristics need to be accounted for to improve event modeling and/or forecasting.

# TABLE OF CONTENTS

# List of Figures

# List of Tables

# Chapter 1

# Introduction

Southern California (SCA) is loosely defined as the area north of the U.S. Mexico western border to a variable northern boundary and encompasses several large cities including Los Angeles and San Diego. Regional coastal areas have Mediterranean climates with distinct rainy seasons although SCA precipitation has large intra-seasonal and interannual variability. Annual rainfall totals occur from relatively few storms per season and provide water to millions of residents as well as its prominent industries including agriculture and tourism (Dettinger et al. 2011; Kim et al. 2013). The area is also prone to high-intensity cool-season precipitation as well as rainfall-induced hazard events that affect both humans and the natural environment. Understanding regional precipitation is imperative as any changes to storm frequency and/or intensity may have dramatic consequences for this area.

The boundaries encompassing SCA are not defined borders but are subjective transitions based upon experience and opinion. SCA's southern boundary is typically identified as the border between California and Mexico (~32.5°N) with the exclusion of Baja California as its climate is greatly affected by the North American Monsoon (Mechoso et al. 2005). SCA's northern boundary is more difficult to identify and is often based on locations of cities and/or mountain ranges. Some define the northern boundary as several mountain groups including the Santa Ynez Mountains in Santa Barbara County (~35.0°N), which are a unique landmark of SCA's landscape. The Santa Ynez Mountains comprise a portion of the Transverse Ranges, a mountain chain positioned in an east-west direction rather than the more common northwest-southeast orientation of other California mountains (e.g., the Sierra Nevada) (Schoenherr 1992). This alignment as well as the intersection with mountains of the Coastal and Peninsular Ranges affects how storms behave

within the region (Neiman et al. 2004; Schoenherr 1992). The area also has a unique coastal orientation with an east-west alignment from Point Conception to Ventura and Los Angeles Counties where the coast shifts to the more common northwest-southeast direction. Additionally, various islands are near the coastline and in some cases, shelter coastal regions from incoming storm systems (Schoenherr 1992).

Major orographic effects throughout the state result in fundamental climatic differences particularly between coastal and inland areas. SCA coastal regions experience Mediterranean climates with warm, dry summers and cool, wet winters with defined rainy seasons. Upon moving inland, desert climates dominate the landscape (Schoenherr 1992). For coastal SCA, precipitation-bearing storms are infrequent and have high rainfall intensity variability with some events reaching intensities like those of hurricanes affecting the U.S. southeast and Gulf coasts (Dettinger et al. 2011; Kim et al. 2013; Ralph and Dettinger 2012). High inter-and intra-seasonal precipitation variability poses problems for storm forecasting and water resources management.

Storm frequency and intensity resulting from orographic rainfall are important for a variety of reasons. SCA is prone to various precipitation-induced hazards including landslides and flooding (e.g., Ryan 1994). Landslides alter landscapes and can occur within seconds. The 2005 La Conchita, CA landslide seriously damaged or destroyed 36 houses, killed 10 people, and is among the most dramatic examples of the power and abrupt nature of landslides, a hazard which is intrinsically linked to rainfall (Caine 1980; Iverson 2000; Jibson 2005). Floods, such as the one that occurred during the 1997-1998 season in Santa Barbara, CA (Naftaly et al. 1998), can cause short- and long-term changes to an area through soil movement and alteration of the water cycle (Anderson and Anderson 2010). In SCA flooding is especially hazardous since the region is prone to flash floods that occur in a matter of minutes (www.fema.gov). On the other end of the spectrum, seasons with little to no precipitation may lead to drought as well as fire. The 2012-2016

2

CA drought is a stark reminder of what continual seasons of little to no rainfall will do to a landscape. During 2016 there were 11 fires in San Luis Obispo, Santa Barbara, Ventura, Los Angeles, Orange, and San Diego counties with 4 of these fires burning over 10,000 acres (www.calfire.ca.gov/). Fire can have many ramifications for a landscape including changes to soil cohesion and evapotranspiration rates due to burning of vegetation (Shakesby 2011). As most the area's population resides along coastal cities including Los Angeles, San Diego, Ventura, and Santa Barbara (www.census.gov), these regions are vulnerable to hazards and thus, are affected by changes of precipitation patterns and events. Additionally, as CA generates much of the U.S.'s agricultural produce, any changes to storm intensity and/or frequency may have dramatic effects for the entire country. Thus, it is important to understand and predict storms that may lead to these events in SCA.

The phenomena that influence precipitation vary both spatially as well as temporally and depend on systems ranging from large-to small-scales and their interactions with topography and other geographic features. In SCA multiple phenomena on varying timescales including the El Niño Southern Oscillation (ENSO) (Mo and Higgins 1998), the Madden-Julian Oscillation (MJO) (Madden and Julian 1994), and atmospheric rivers (ARs) (Zhu and Newell, 1994) influence rainfall intensity and duration through ocean-atmospheric interactions and dynamical forcings. It is well known that ENSO and the MJO influence storms that occur in SCA through processes such as modulation of the upper-level jet and low-level moisture flux (e.g., Jones 2000; Mo and Higgins 1998; Zhang 2005). Although much insight has been gained in understanding the climatology of ARs that affect North America's west coast (e.g., Dettinger et al. 2011; Neiman et al. 2008b), the spatiotemporal characteristics and atmospheric forcings driving ARs to SCA needs to be further addressed.

The following sections provide background information and known impacts of AR events. The final section presents this dissertation's objectives and organization.

**1.1 Synoptic atmospheric river characteristics**

ARs are long (>2000km), narrow (<1000km) channels of high water vapor flux that transport moisture horizontally from lower to higher latitudes through the low troposphere (Neiman et al. 2008a, 2008b; Ralph et al. 2005, 2006, 2011; Zhu and Newell 1994, 1998) (Fig. 1.1a). These synoptic features are comparable to highways of water vapor and are responsible for over 90% of Earth's meridional water vapor movement while covering a small percentage (<10%) of Earth's surface (Neiman et al. 2008a, 2008b; Newell et al. 1992; Ralph et al. 2004; Zhu and Newell 1994, 1998). ARs form and traverse over the oceans (Neiman et al. 2008b) and all continents experience these events. Newell et al. (1992) found that at any given time, there are four or five ARs present globally (Fig. 1.1b).
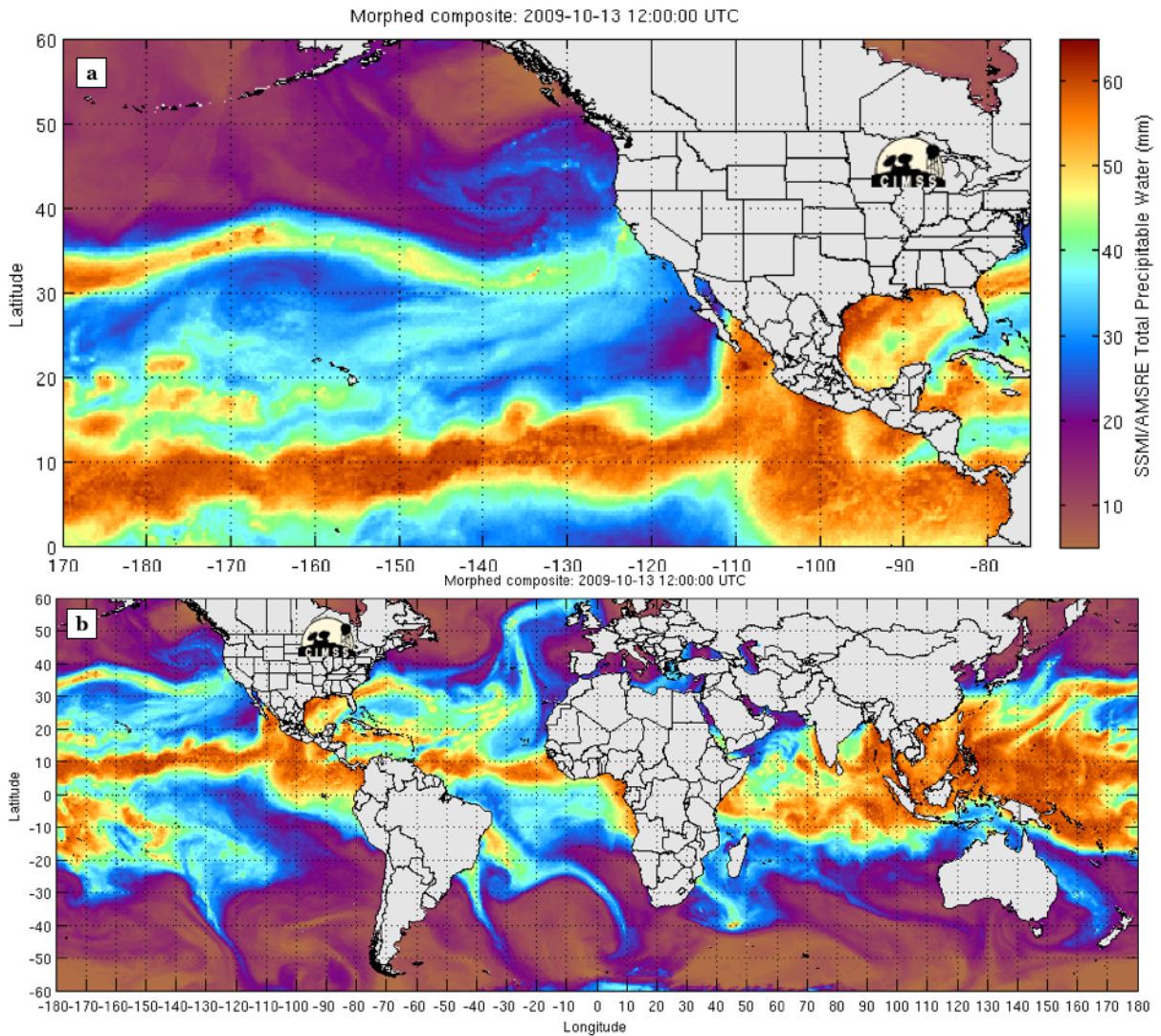
**Fig. 1.1** Morphed composites of total precipitable water illustrating AR events on 12:00 UTC 13 October 2009 for **a** SCA and **b** globally. Figures from the Cooperative Institute for Meteorological Satellite Studies (tropic.ssec.wisc.edu)

ARs have warm temperatures, high moisture contents ($\geq$20mm), and strong winds ($\geq$12.5ms$^{-1}$) resembling low-level jets. Additionally, AR cores occur within the bottom 2.5km of the atmosphere where they tend to have weak moist static stability. All this results in rapid water vapor movement (Dettinger et al. 2011; Neiman et al. 2008a; Ralph and Dettinger 2011, 2012;

5

Ralph et al. 2003, 2004, 2005, 2006; Sodemann and Stohl 2013). Once this warm, water dense, horizontally moving air moves over land (herein landfall), particularly along mountainous coastlines, orographic forcing often leads to high-intensity rainfall (Martinković et al. 2017; Neiman et al. 2002, 2008a, 2008b; Ralph and Dettinger 2011) (**Fig. 1.2**; Ralph et al. 2005).
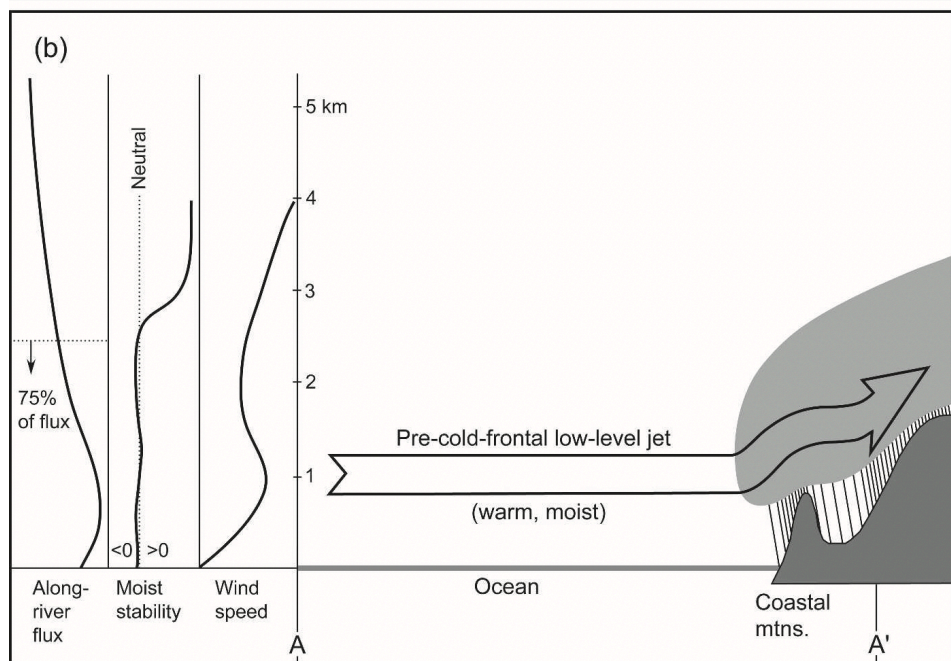


**Fig. 1.2** Cross section schematic denoting AR offshore vertical structure of along-river moisture flux, moist static stability, and wind speeds on the left. Schematic showing orographic forcing of landfalling AR conditions is on the right. Figure is from Ralph et al. (2005)

ARs are intrinsically linked to extratropical cyclone activity and are found within the pre-cold frontal warm sectors (Bao et al. 2006; Dettinger 2004; Dettinger et al. 2011; Martinković et al. 2017; Neiman et al 2008a, 2008b, 2011; Ralph et al. 2004, 2005, 2006; Zhu and Newell 1994). This provides one method of moisture acquisition through convergence of local water vapor along the extratropical cyclone's cold front. This results in continuous cycling of moisture contributing to AR maintenance and formation (Bao et al. 2006; Newman et al. 2012; Sodemann and Stohl

2013). However, other events suggest that some ARs transport water vapor directly to the midlatitudes with few losses to precipitation over the oceans (Bao et al. 2006; Stohl et al. 2008).

**1.2 Atmospheric rivers and the western coast of North America**

The western coast of North America is one region that experiences repeated AR events (e.g., Neiman et al. 2008b; Ralph and Dettinger 2012). In this area, AR storms often lead to high-intensity rainfall (Dettinger 2004; Neiman et al. 2008a, 2008b; Ralph and Dettinger 2012; Ralph et al. 2011), extreme winds (Waliser and Guan 2017), flooding and other hazards (e.g., Neiman et al. 2011). Additionally, they also present challenges for local water management agencies through methods such as changes to regional snowpack totals (e.g., Guan et al. 2013). Yet, ARs affecting North America's west coast vary in strength, source areas, as well as trajectories (Neiman et al. 2008a).

AR frequency and intensity varies according to latitude and proximity to coasts (Kim et al. 2013; Neiman et al. 2008a; Rutz et al. 2014). A study by Neiman et al. (2008a) establishes that AR storms landfalling in western North America form over the Pacific Ocean and are characterized by baroclinic midlatitudes wave trains resulting in offshore troughs and southwesterly flow. Troughs vary in depth and placement depending on AR landfall location. Upon landfall, most AR conditions dissipate leeward of mountain barriers due to orographic forcing along the various ranges of the coastal west (Dettinger et al. 2011; Neiman et al. 2008a; Rutz et al. 2014). In effect, the strongest AR conditions are along the coasts with weakening conditions upon moving inland. Nevertheless, Rutz et al. (2015) determine that ARs resulting in inland storms have the highest moisture contents and/or strongest winds of all ARs. A subset of ARs, the Pineapple Express (PE), is a predominant AR known to affect the western coast of North America (Ralph et al. 2004; Zhu and Newell 1998). PEs have a specific orientation and are associated with direct transport of

7

tropical water vapor from Hawaii to North America (Bao et al. 2006; Dettinger 2011; Dettinger et al. 2011; Neiman et al. 2008ab; Ralph et al. 2011).

ARs landfall throughout the entire western coast of North America although less so in SCA than latitudes farther north (Kim et al. 2013; Neiman et al. 2008a). Some areas of SCA experience only several ARs per season; despite this, ARs are still significant contributors to SCA annual water budgets (Dettinger et al. 2011; Neiman et al. 2013; Rutz et al. 2014). Dettinger et al. (2011) determine that in some regions of SCA, ARs provide up to 45% of annual precipitation totals whereas a study by Rutz and Steenburgh (2012) concludes that in parts of SCA (including Baja California) ARs are responsible for up to 50% of seasonal (November-April) precipitation totals. ARs have also been responsible for some of area's highest-intensity rainfall (e.g., Dettinger et al. 2011; Kim et al. 2013; Rutz and Steenburgh, 2012) and according to Rutz et al. (2014) some of the longest-duration storms. A 2017 AR storm in SCA brought about high-intensity precipitation, measured winds of over 60 knots (with gusts >90 knots in some places), and rogue waves all concentrated over a narrow region of populated coastline (weather.com[1]). This led to mudslides, flooding of local sloughs and roads, et cetera (latimes.com[2]). Due to SCA's large population and sensitivity to meteorological events, it is imperative to investigate the role of ARs within SCA and how various phenomena may affect these features. Additionally, as infrequent AR events provide large rainfall totals to SCA and AR frequency is expected to change in a changing climate (Dettinger 2011), understanding the background dynamics behind AR development is crucial. Furthermore, although the characteristics of ARs affecting North America's west coast are generally understood and well examined (e.g., Neiman et al. 2008a), the characteristics and mechanisms of those affecting SCA have not been thoroughly investigated yet.

---

[1] Web article at weather.com/forecast/regional/news/california-record-wet-water-year-forecast-feb2017

[2] Web article at latimes.com/local/lanow/la-live-powerful-storms-moving-l-area-20170216-htmlstory.html

**1.3 Dissertation scope and objectives**

This research takes a new approach to AR analysis in the isolation and examination of ARs affecting SCA. We investigate the atmospheric characteristics, pre-landfall dynamics, association with various modes of variability, as well as distance and trajectory characteristics of ARs that landfall in SCA and how they differ from ARs affecting latitudes farther north. The specific objectives of this dissertation are:

1. Design an algorithm that identifies historical AR events landfalling along the western coast of North America within reanalysis fields (Chapter 2);

2. Organize and categorize said AR events according to landfall regions and determine the climatological atmospheric characteristics during SCA ARs. Differentiate SCA ARs from ARs landfalling farther north on the day of as well as the days leading to AR landfall (Chapter 2);

3. Determine the relationships of defined AR groups with modes of variability known to affect western North America (Chapter 2);

4. Investigate the movement and change of AR groups and their along trajectory characteristics in the hours before landfall using a backward trajectories model (Chapter 3).

Implications of these studies are a better understanding of the formation and dynamics of SCA ARs and their conditions in the days before and during landfall. This in turn can help to improve regional forecasting and hazard mitigation.

In Chapter 2 I introduce a method for AR detection in reanalysis fields of total precipitable water (TPW) using a fit-ellipse approach. This detection algorithm builds upon a previous approach and is used to identify AR events affecting western North America during the October-

9

March seasons of 1979-2013. Once identified, ARs are categorized according to separate landfall areas designated by latitude. Daily composites of atmospheric variables for the day of and several days prior to-landfall are created for each region to determine the climatological characteristics and dynamics of AR groups. I summarize the dominant modes affecting AR frequency for western North America and the statistical occurrences of AR events during various modes and their phases are also investigated. Work in chapter 2 is a slightly modified version of a previously published journal article available in Theoretical and Applied Climatology as:

Harris, S.M. and L.M.V. Carvalho. 2017. Characteristics of southern California atmospheric rivers. Theoretical and Applied Climatology. 1-17, DOI: 10.1007/s00704-017-2138-1.


In Chapter 3 I discuss the main approaches found in the literature for AR trajectory analysis including the Lagrangian trajectory model used. I use the model to analyze seasonal (October-March) ARs affecting the U.S. west coast between December 2004 and December 2015 in the hour of and up to 72 hours before landfall at one hour time-steps. Statistical analyses of distances and along-trajectory characteristics for regional ARs are determined. This work is being prepared for publication in the journal of Theoretical and Applied Climatology and is published here with only minor changes.

Chapter 4 summarizes the work completed and conclusions made. Additionally this chapter discusses a possible direction of future AR research.

# Chapter 2

# Characteristics of Southern California Atmospheric Rivers

As appears in:

**Abstract**

Atmospheric rivers (ARs) are channels of high water vapor flux that transport moisture from low to higher latitudes on synoptic timescales. In areas of topographical variability, ARs may lead to high intensity precipitation due to orographic forcing. ARs landfalling along North America's west coast are linked to extreme events including those leading to flooding and landslides. In Southern California (SCA), proper AR forecasting is important for regional water resources as well as hazard mitigation and as the area's annual precipitation totals occur from relatively few storms per season, any changes to storm frequency and/or intensity may have dramatic consequences. Yet, as most regional AR studies focus on the Pacific Northwest, there is little information about SCA ARs.

We develop an algorithm to identify ARs landfalling on North America's west coast between 1979-2013 within total precipitable water reanalysis fields. ARs are then categorized according to landfall region. To determine and differentiate the characteristics and spatial distributions of ARs affecting these areas, we examine lag composites of various atmospheric variables for each landfall region. SCA ARs differ from ARs landfalling farther north in the days prior to landfall with the position and amplitude of a trough offshore from the Asian continent and ridge over Alaska, as well as the displacement and eastward extension of the jet core that potentially guides AR moisture southwards. The relationships between AR landfalls and the El

Niño/Southern Oscillation (ENSO), the Madden-Julian Oscillation (MJO), and the Pacific/North American Teleconnection Pattern (PNA) are also investigated.

## 2.1 Introduction

Using a combination of satellite as well as station rainfall data, Dettinger et al. (2011) determines that during 1998 to 2008 ARs landfalling on North America's west coast between 32.5°-52.5°N latitudes contributed between 30% to 45% of rainfall in all California with SCA ranging from 20% to ~35% along the coast. In a similar analysis by Rutz and Steenburgh (2012), ARs crossing over the Baja Peninsula are also accounted for increasing the AR contributing proportion between 20 to ~40% in SCA during the cool season of November-April. With few events but high precipitation totals, ARs are often of high-intensity and/or of long duration (Rutz et al. 2014). As SCA is characterized by vast mountainous terrain, particularly along the coast, high-intensity precipitation is often associated with a landfalling AR in the area (e.g. Rutz et al. 2014).

ARs are influenced by the interactions of tropical and extratropical phenomena. It is generally understood that the Madden-Julian Oscillation (MJO), considered the most important tropical mode on intraseasonal timescales (e.g. Madden and Julian 1994), alters North Pacific atmospheric circulation, modulating regional air and moisture movement and affecting meteorological events that occur in North America including ARs (Bell and Higgins 2005). The propagation of the MJO's convection and associated pattern of atmospheric circulation over the Pacific and Indian Oceans (Bell and Higgins 2005; Guan et al. 2012; Mo and Higgins 1998; Ralph et al. 2011) is known to assist ARs, particularly a specific subset of ARs known as the Pineapple Express (Dettinger 2004; Dettinger et al. 2011). For seasons with frequent and/or exceptionally strong MJOs, numerous and/or higher-intensity ARs may occur causing an increase in the

frequency and/or intensity of extreme precipitation events in SCA (Jones 2000; Jones et al. 2011; Payne and Magnusdottir 2014).

Payne and Magnusdottir (2014) investigate the link between MJO phases with ARs and determine that ARs affecting western North America increase in frequency during MJO phases 3, 6, 7, and 8 with the highest increase during phase 6 and the smallest increase during phase 3. This is semi-consistent with Guan et al. (2012) who compares MJO phases and AR activity to snow water equivalent (SWE) values in the Sierra Nevada and determines that positive SWE anomalies are most prominent during MJO phases 3 and 6 whereas phase 8 is associated with negative SWE anomalies.

The El Niño Southern Oscillation (ENSO) is another phenomenon known to influence precipitation in SCA through processes such as the modulation of the upper level jet and low-level moisture flux (e.g., Mo and Higgins 1998). Studies regarding ARs and ENSO reveal mixed findings. Payne and Magnusdottir (2014) determine that the frequency of landfalling ARs increases during warm ENSO phases and is at a minimum during cold ENSO phases. They also find that AR landfall latitudes shift southward during warm ENSO events. Bao et al. (2006) argue that direct "river-like" transport of moisture is most likely to occur during ENSO-neutral years and least likely during warm ENSO years. Like most AR studies, investigations of the relationships between ARs and the MJO as well as ENSO is limited to ARs events affecting northern latitudes or the west coast of North America as whole, and is not specific to SCA.

This study investigates the atmospheric characteristics of ARs landfalling in SCA and the differences from ARs affecting latitudes farther north. This is accomplished first through an algorithm that detects AR activity by identifying plume-like features using reanalysis. Mechanisms associated with AR activity are examined with composites of various atmospheric variables for the identified AR events, organized by landfall region. Additionally, this study uses MJO and ENSO

13

indices to describe the statistical significance of these phenomena over SCA landfalling ARs. This paper is organized as follows. Section 2.2 describes the datasets and methodologies used. Sections 2.3, 2.4, and 2.5 present the results of the validations, composites, and statistical analyses of the MJO and ENSO, respectively. Conclusions and implications are presented in section 2.6.

## 2.2 Datasets & Methods

We develop an algorithm to identify AR activity affecting North America's west coast and particularly SCA based on an AR detection algorithm from Jiang et al. (2014). Daily total precipitable water (TPW) fields calculated from the National Oceanic and Atmospheric Administration's (NOAA) National Centers for Environmental Prediction's Climate Forecast System Reanalysis (CFSR) (Saha et al. 2010) at a $0.5°×0.5°$ spatial resolution are used to identify ARs events from 1979 to 2013. CFSR are used because of its high spatial resolution, the coupling to the ocean, and the assimilation of satellite radiances for the entire period of study (Saha et al. 2010). TPW (in kg m$^{-2}$) is an equivalent to integrated water vapor as it reflects the water total within an atmospheric column (vertically integrated, surface – 200mb) if all water vapor is condensed into liquid water with 1 kg m$^{-2}$ equal to 1 mm (Campmany et al. 2010).

A previous record of AR activity created by Neiman et al. (2008a) and later extended by Dettinger et al. (2011) uses Special Sensor Microwave Imager (SSM/I) data to identify AR activity affecting North America's west coast expanding water years 1998 to 2011. Here we use TPW from reanalysis due to SSM/I's limited temporal span. Extending the record provides additional AR cases (from 1979 to 2013) to adequately investigate the characteristics and dynamical forcings of these high-intensity episodes.

This algorithm modifies a previous AR detection procedure first introduced in Jiang and Deng (2011) and later modified in Jiang et al. (2014) that identifies AR plumes using the National

Aeronautical and Space Administration's Modern Era Retrospective-Analysis for Research and Applications (MERRA) at a 0.5°latitude × 0.667°longitude spatial resolution. A summary of the tracking algorithm is described in Steps 1-5 below. Note that steps 1-2 are based on Jiang et al. (2014) criteria while steps 3-5 describe the methodologies that were developed in the present study and differ from Jiang et al. (2014).

1) TPW grid point values ($Q_r$) north (south) of 15.0°N (15.0°S) that meet the following listed criteria are identified.

$$Q_r \geq Q_{zmean} + A(Q_{zmax} - Q_{zmean}) \qquad \text{(Eq. 2.1)}$$

$$Q_r \geq Q_{mmean} + B(Q_{mmax} - Q_{mmean}) \qquad \text{(Eq. 2.2)}$$

$$Q_r \geq q_{cut} = 20\text{mm} \qquad \text{(Eq. 2.3)}$$

Where $Q_{zmean}$, $Q_{zmax}$, $Q_{mmean}$, and $Q_{mmax}$ refer to the zonal (latitudinal, $z$) and meridional (longitudinal, $m$) mean and max values of $Q_r$ (i.e. TPW) respectively. Parameters A and B are meant to preserve the elongated shape of the AR and are identified as 0.3 and 0.1 respectively. Variable $q_{cut}$ is a threshold parameter referring to the minimum TPW value required to be considered an AR (Jiang and Deng 2011; Jiang et al. 2014).

2) Of the identified $Q_r$ points, contiguous areas meeting or exceeding an area threshold mark of $5.0 \times 10^5$ km$^2$ are determined and smaller regions are dismissed as they are considered too small to be ARs. Jiang et al. (2014) uses an area threshold of $2.5 \times 10^5$ km$^2$ which we conclude is too small as it classifies extraneous filamentary features as ARs.

3) ARs exhibit elongated geometry. To identify the elongation of the AR candidates we calculate the first two (orthogonal) eigenvectors (or Principal Components) that explain most of the spatial variance of each large contiguous region. The first two eigenvectors (PC-1 and PC-2 respectively) can be interpreted as the two axes of an ellipse that best fits to the area. From the ellipse axes we are able to calculate eccentricity, defined as the ratio between the minor

(PC-2) and major (PC-1) axes of the ellipse. This fit ellipse procedure is the most prominent difference between this algorithm and the one described in Jiang et al. (2014) that uses an aerial fraction criterion to determine AR eligibility.

4) Ellipses with eccentricities less than 0.40 as well as widths less than 1,000 km are classified as ARs. The 0.40 criterion is used to guarantee the AR's elongated structure. If the feature is greater than 1,000 km wide, then the eccentricity must be less than 0.30. Although a width of 1,000 km or less is used as a defining AR characteristic (e.g. Neiman et al. 2008ab; Ralph et al. 2005, 2006, 2011; Zhu and Newell 1994, 1998), an AR may occur within a broader region of high TPW and using the 0.30 eccentricity criterion for wider TPW areas attempts to capture these features.

5) For all identified ARs, ellipse orientation is calculated using the $1^{st}$ eigenvector (PC-1) and determining the degrees counter clockwise from the x-axis (east-west orientation). ARs affecting North America are often oriented between 0.0° - 90.0° due to the dominant wind patterns and Coriolis force. Features that meet all of the above criteria are defined as ARs landfalling along the western coast of North America.

Dates classified as ARs by the AR algorithm (steps 1-5) but not meeting a visual inspection of AR criteria are identified and removed so as not to skew composites. From the total record of 762 identified events, 43 are removed leaving 719 AR events. ARs are then categorized according to landfall region.

Even though SCA experiences high-intensity ARs responsible for significant proportions of regional annual precipitation (e.g. Dettinger et al. 2011; Kim et al. 2013; Rutz and Steenburgh 2012), fewer ARs occur in SCA compared to latitudes farther north (Neiman et al. 2008ab; Rutz et al. 2014) therefore, it is important to determine if SCA ARs have unique characteristics.

Additionally the orientation of much of SCA's coastline as well as a local mountain range, the Transverse Range, run in an east-west direction rather than the typical north-south common to the rest of western North America (Schoenherr 1992). This affects how storms make landfall and ultimately how they interact with the environment in this region. We conduct composite analyses to determine if the overall features of SCA ARs differ from other ARs. In the record from Neiman et al. (2008a) and Dettinger et al. (2011), AR activity affecting North America's west coast from 32.5° to 52.5°N is identified where the coast is divided into two domains "south-coast" (i.e. CA; 32.5°-41.0°N) and "north-coast" (i.e. Oregon, Washington, and/or British Columbia; 41.0°-52.5°N). To maintain consistency with the previous record, composites are performed over the latitudinal domain of 32.5°-52.5°N. However, as we intend to investigate the role of ARs in SCA, the subdomains are partitioned into smaller groups. For simplicity we divide the domain into four subdomains each with similar latitudinal ranges: SCA ($32.5° \leq$ latitude $\leq 37.0°$), Northern California (NCA, $37.0° <$ latitude $\leq 42.0°$), Southern Pacific Northwest (SPNW, $42.0° <$ latitude $\leq 47.0°$), and Northern Pacific Northwest (NPNW, $47.0° <$ latitude $\leq 52.5°$). These ranges additionally capture the change of coastal and mountain orientation for SCA discussed earlier.

To perform a comprehensive analysis of AR features and identify AR characteristics according to region of landfall, lag-composites of various atmospheric variables (from CFSR) are created for different landfalling regions for the dominant rainy season months of October through March (Oct-Mar). Lag-composites are created from 10 days prior to the day of the event (0 Lag days), to 3 days after the AR landfall. Atmospheric variables examined include TPW, TPW anomalies, 500mb geopotential heights (h500), h500 anomalies, as well as two-meter surface temperature (t2m) anomalies. Daily anomalies are calculated at each grid point by removing the smoothed annual cycle.

**2.3 Validation and Case Studies**

First, we assess the modified algorithm's ability to detect AR events compared to the algorithm identified in Jiang et al. (2014). We applied both algorithms using CFSR for the December, January, February (DJF) months of 1979-2005 to obtain AR climatology according to latitude (between 30.0°-55.0°N) (Fig. 2.1). Our algorithm (Fig. 2.1a) exhibits a peak of approximately 9% of all landfalling ARs affecting western North America at about 40°N whereas Jiang et al.'s (2014) algorithm (Fig. 2.1b) shows a peak of 8% around 39ºN. The latitudinal variation of AR landfall probability is comparable between both methods with AR probability decreasing farther away from 40°N. However, our algorithm indicates a greater decrease in AR probability toward latitudes equatorward of 40ºN compared to Jiang et al. (2014). For instance the AR landfall probability at 35ºN drops to about 2.5% in our algorithm compared to 4.5% for Jiang et al. (2014). The regional AR climatology obtained with MERRA and discussed in Jiang et al. (2014) suggests a maximum AR probability of approximately 10% around 40°N for DJF 1979-2005 (see Jiang et al. 2014, Fig. 2.1), whereas our algorithm run using MERRA found approximately 8% of all landfalling ARs around 40°N and a similar profile (not shown).
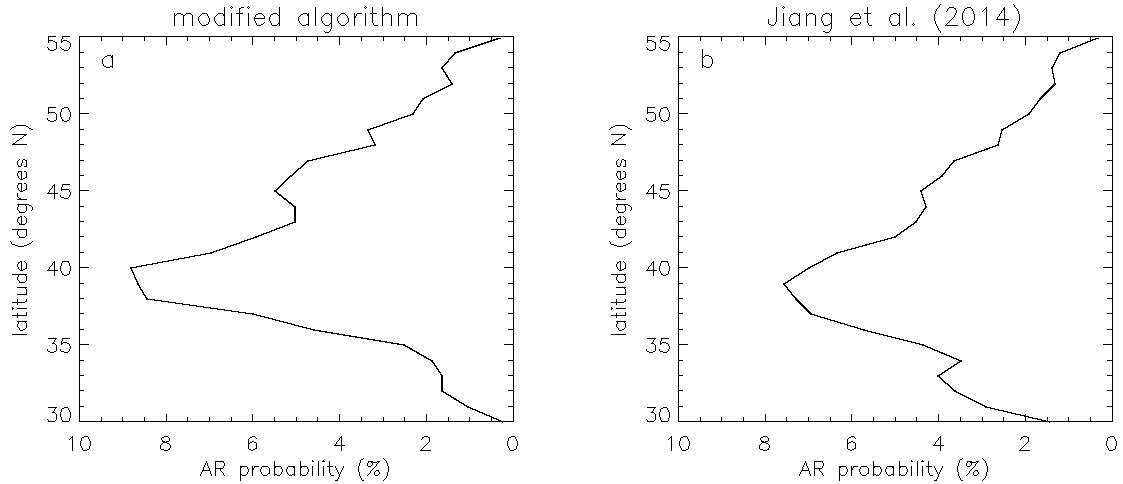
**Fig. 2.1** Landfalling AR climatology for North America's west coast (30.0°-55.0°N) outputted from **a** the modified algorithm and from **b** the criteria described in Jiang et al. (2014). AR activity is derived using CFSR and covers DJF from 1979 to 2005

Additionally, four independent AR dates affecting North America's west coast identified in previous analyses (Ralph and Dettinger 2012; Ralph et al. 2011) are examined using outputs from both algorithms with CFSR as inputs (Fig. 2.2). Case study dates include March 26, 2005, November 7, 2006, October 13, 2009, as well as December 18, 2010. Outputs of these dates are visually assessed in order to investigate how well each algorithm identifies AR features. Both identification algorithms detect all four ARs; still, differences between each set of outputs can be identified in terms of recognition of extraneous features not directly related to the investigated AR. For example, for March 26, 2005 an AR extending from the Hawaiian Islands northeastward to the Oregon coast is identified by both the modified algorithm (Fig. 2.2a) as well as the original algorithm (Fig. 2.2e). However, while the modified algorithm identifies this plume as the only feature affecting North America, the original algorithm identifies another component affecting the U.S. east coast and the Gulf of Mexico. This feature may be associated with high TPW values from an existing storm. It is important that the algorithm does not identify these features as we

want to eliminate characteristics that do not classify as ARs (such as the movement of the Monsoon, hurricanes, etc.). Overall, the modified algorithm (Fig. 2.2a-d) gives a more precise identification of AR plumes and excludes objects not directly related to the event of interest. This is most likely due to the criterion of eccentricity adopted in the modified method (step 3) as the first two eigenvectors accurately capture the elongated AR shape.

03/26/2005

11/07/2006

10/13/2009

12/18/2010
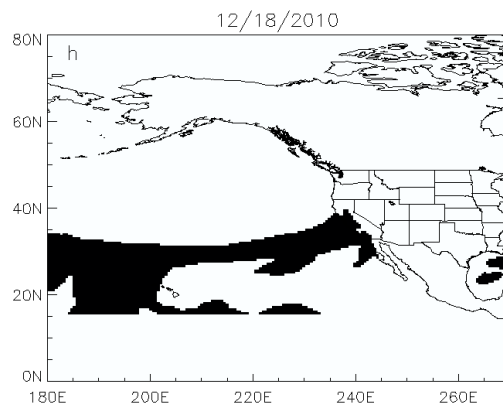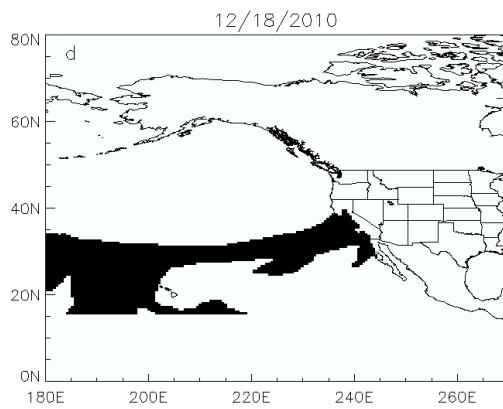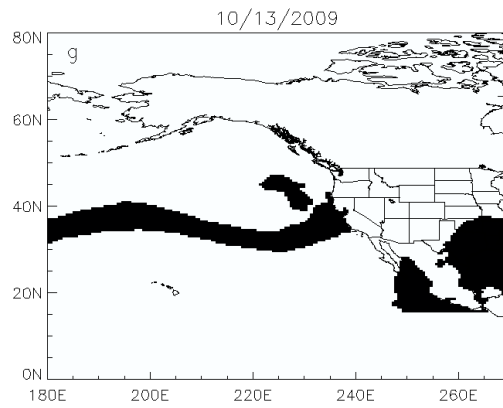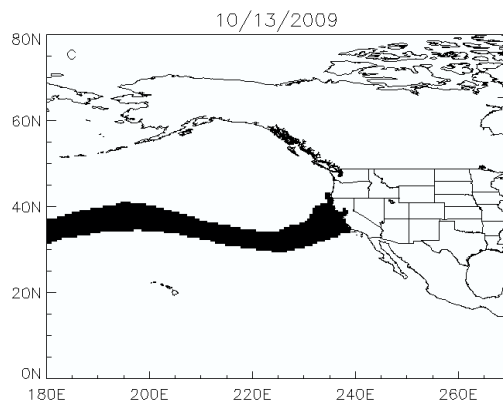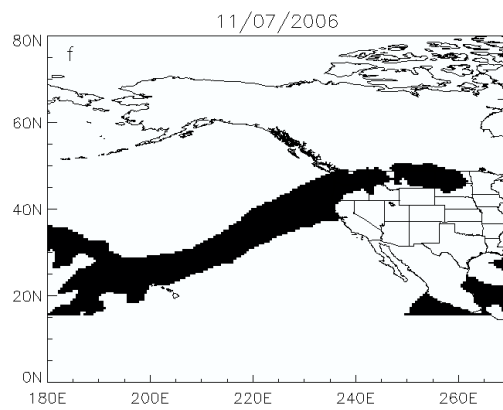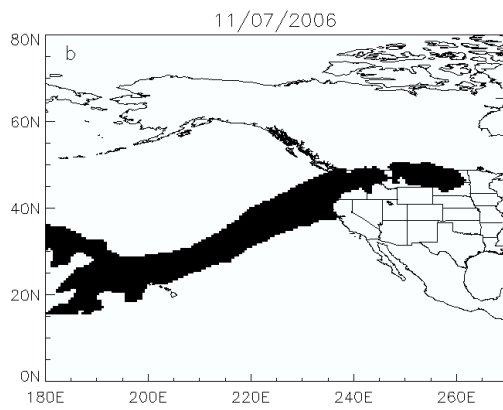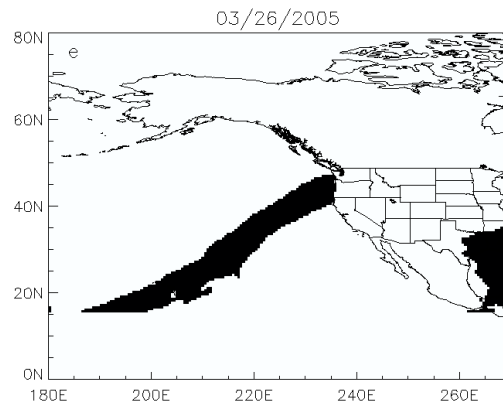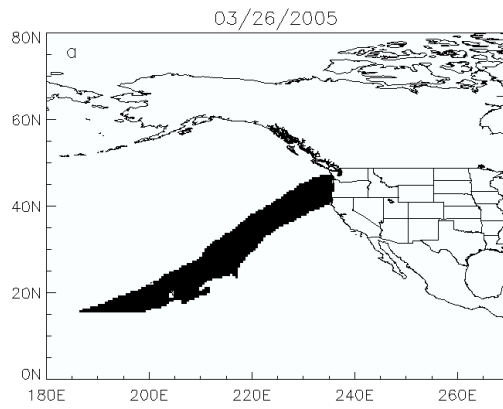
**Fig. 2.2** AR events as identified by the algorithm presented in this paper (a-d) as well as the algorithm described in Jiang et al. 2014 (e-h) using CFSR data. Case study dates include a, e March 26, 2005, b, f November 7, 2006, c, g October 13, 2009, and d, h December 18, 2010. Areas identified as an AR are indicated by black shading

## 2.4 Synoptic characteristics

The numbers of independent AR events during Oct-Mar from 1979 to 2013 separated according to landfall regions are 72 SCA, 213 NCA, 183 SPNW, and 160 NPNW (Table 2.1), in agreement with previous literature in that AR landfalls are greatest between northern California and southern Canada with decreased frequencies upon moving southward (e.g. Rutz et al. 2014). Independent events are defined as ARs with no other AR events within $\pm 3$ days of landfall. In spite of large year-to-year variability in the frequency of AR events (not shown), no significant trends in AR occurrence is observed for any of the investigated landfall regions during the examined time period (1979-2013). In SCA, there are several seasons with zero detected AR events. As AR storms bring about large proportions of SCA's annual rainfall totals (e.g. Dettinger et al. 2011; Kim et al. 2013; Rutz and Steenburgh 2012), a lack of these extreme events may lead to a severe reduction in seasonal rainfall totals.

**Table 2.1** Landfall regions and the number of identified landfalling ARs during Oct-Mar seasons from 1979 to 2013

| Name | Abbr. | Lat. Covered (°N) | Landfalling ARs |
|---|---|---|---|
| Southern California | SCA | 32.5°-37.0° | 72 |
| Northern California | NCA | 37.0°-42.0° | 213 |
| Southern Pacific Northwest | SPNW | 42.0°-47.0° | 183 |
| Northern Pacific Northwest | NPNW | 47.0°-52.5° | 160 |
| All ARs | - | 30.0°-55.0° | 719 |

The main objective of this study is to examine dynamical mechanisms associated with ARs affecting North America's west coast at different latitudes and particularly SCA. Figures 2.3-2.12 show composites of atmospheric variables for all landfall regions. ARs are characterized by baroclinic wave trains propagating through the Pacific resulting in northeastward extending moisture plumes (Neiman et al. 2008a). These plumes are flanked to the northwest and southeast by areas of dryness as indicated by anomalous TPW values that appear days prior to AR landfall with both positive and negative anomalies strengthening as an AR approaches landfall (Fig. 2.3-2.6). After landfall moisture plumes retreat from the coast and dissipate (not shown).

Composites of TPW and TPW anomalies (Fig. 2.3-2.6) on AR landfall days (0 Lag days) for all landfall regions display, as expected, positive TPW anomalies within regions of high TPW (i.e. the AR moisture plume) with neighboring negative anomalies to the northwest and southeast, consistent with a midlatitude wave-train pattern. These anomalies appear similar in terms of area covered for all regions. Additionally, all ARs display comparable maximum positive anomalies (+10 kg m$^{-2}$ SCA, Fig. 2.3; +9 kg m$^{-2}$ for all other landfall regions, Fig. 2.4-2.6) as well as negative

anomalies, including negative anomalies to the southeast of the AR plume (-6 kg m$^{-2}$ SCA, Fig. 2.3; -3 kg m$^{-2}$ NCA, Fig. 2.4; -2 kg m$^{-2}$ SPNW, Fig. 2.5; -3 kg m$^{-2}$ NPNW, Fig. 2.6). For all landfall regions the strongest positive anomalies on AR landfall days appear offshore, near the coastline and do not stretch farther inland. As these are areas of mountainous terrain it suggests that the topography impedes on AR progression possibly affecting AR persistence and intensity (Rutz et al. 2014).
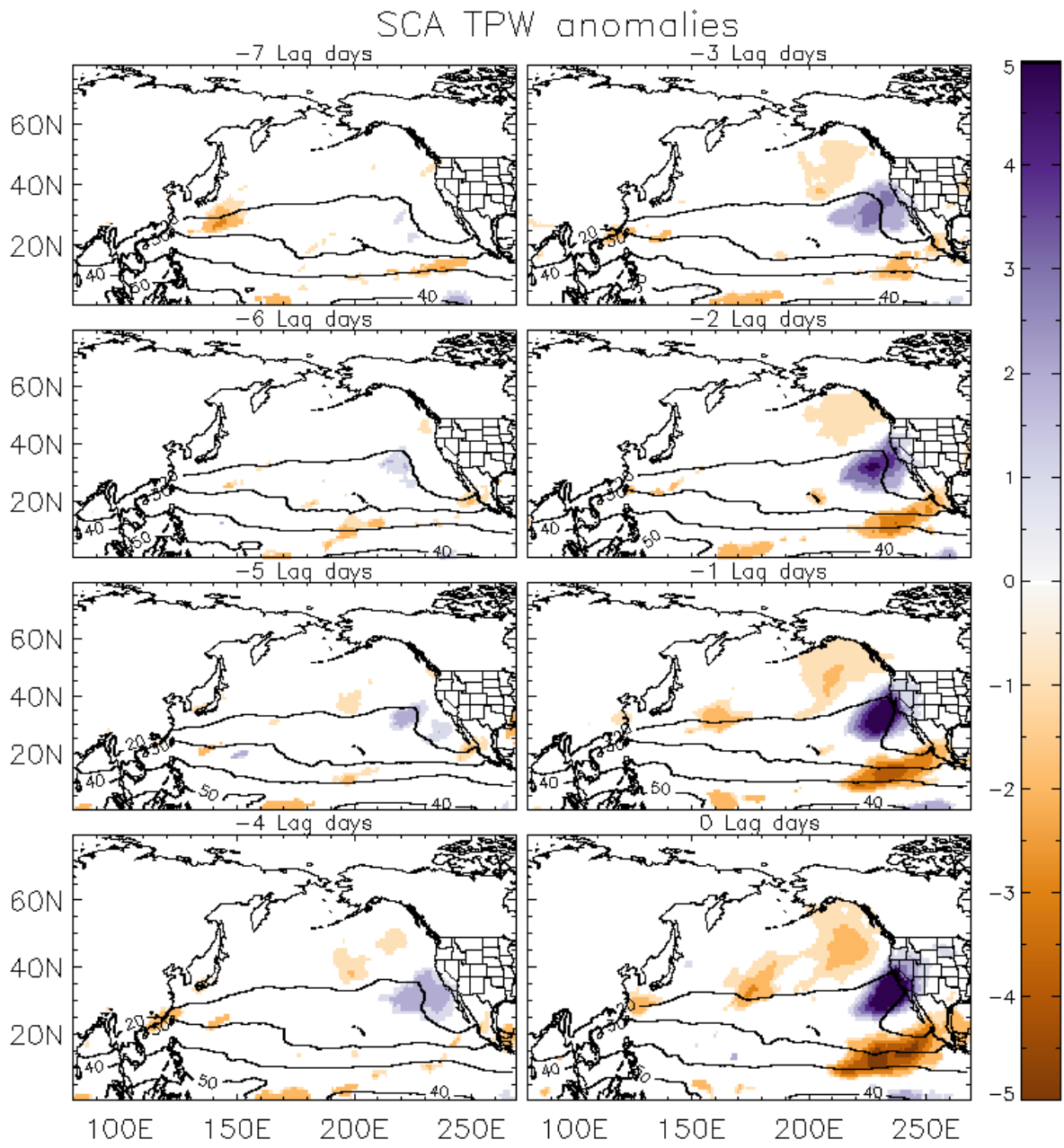
**Fig. 2.3** Composites of TPW anomalies (colored shading; kg m$^{-2}$) overlaid with TPW (contours) starting seven days prior to AR landfall (-7 Lag days) and continuing to the day of AR landfall (0 Lag days) for ARs affecting SCA. Anomalies are calculated at the 95% level using a Student's t-test. TPW contours indicate regions of high moisture and begin at 20 kg m$^{-2}$ with a contour interval of 10
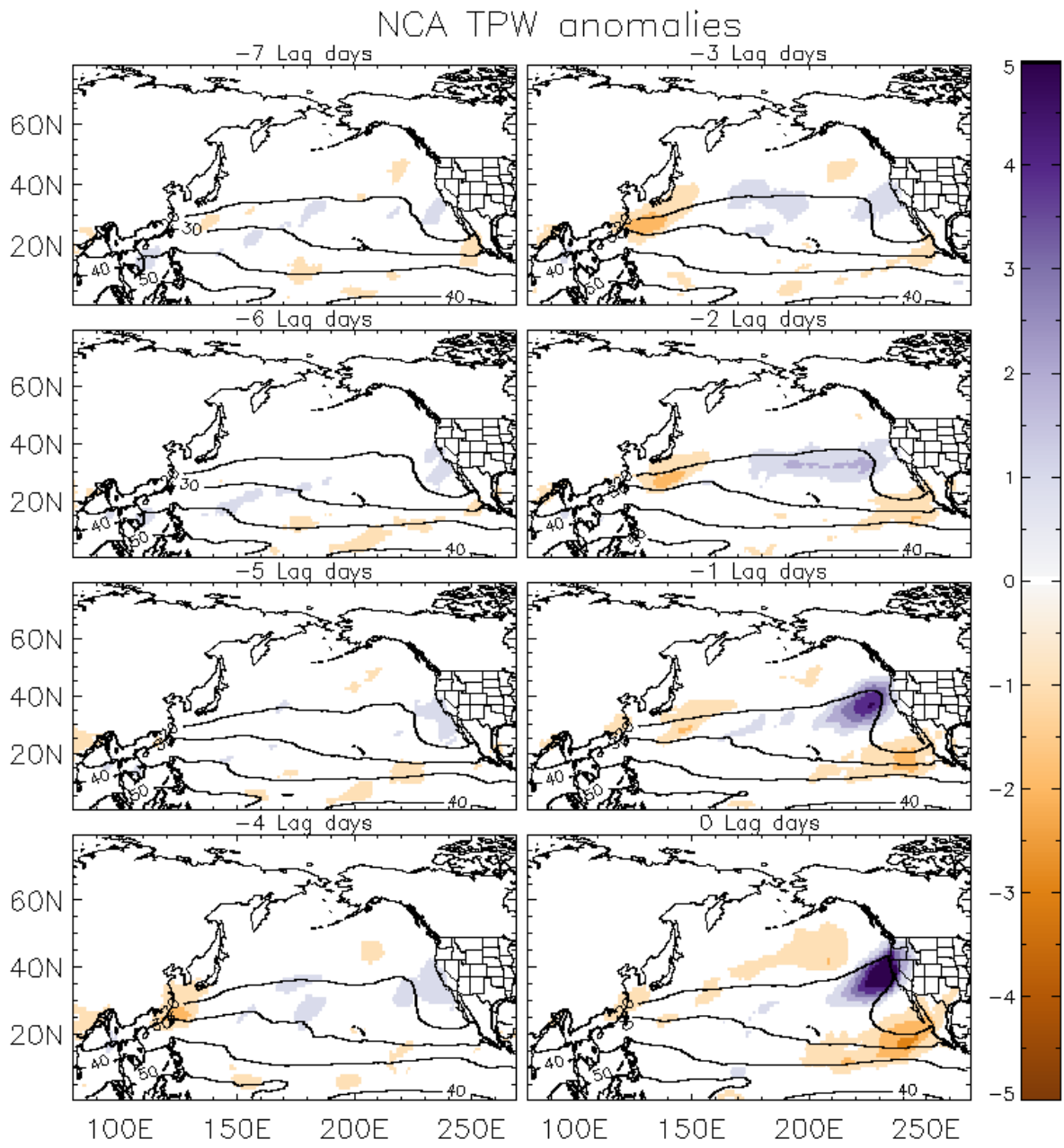
**Fig. 2.4** Same as Fig. 2.3, but for ARs affecting NCA
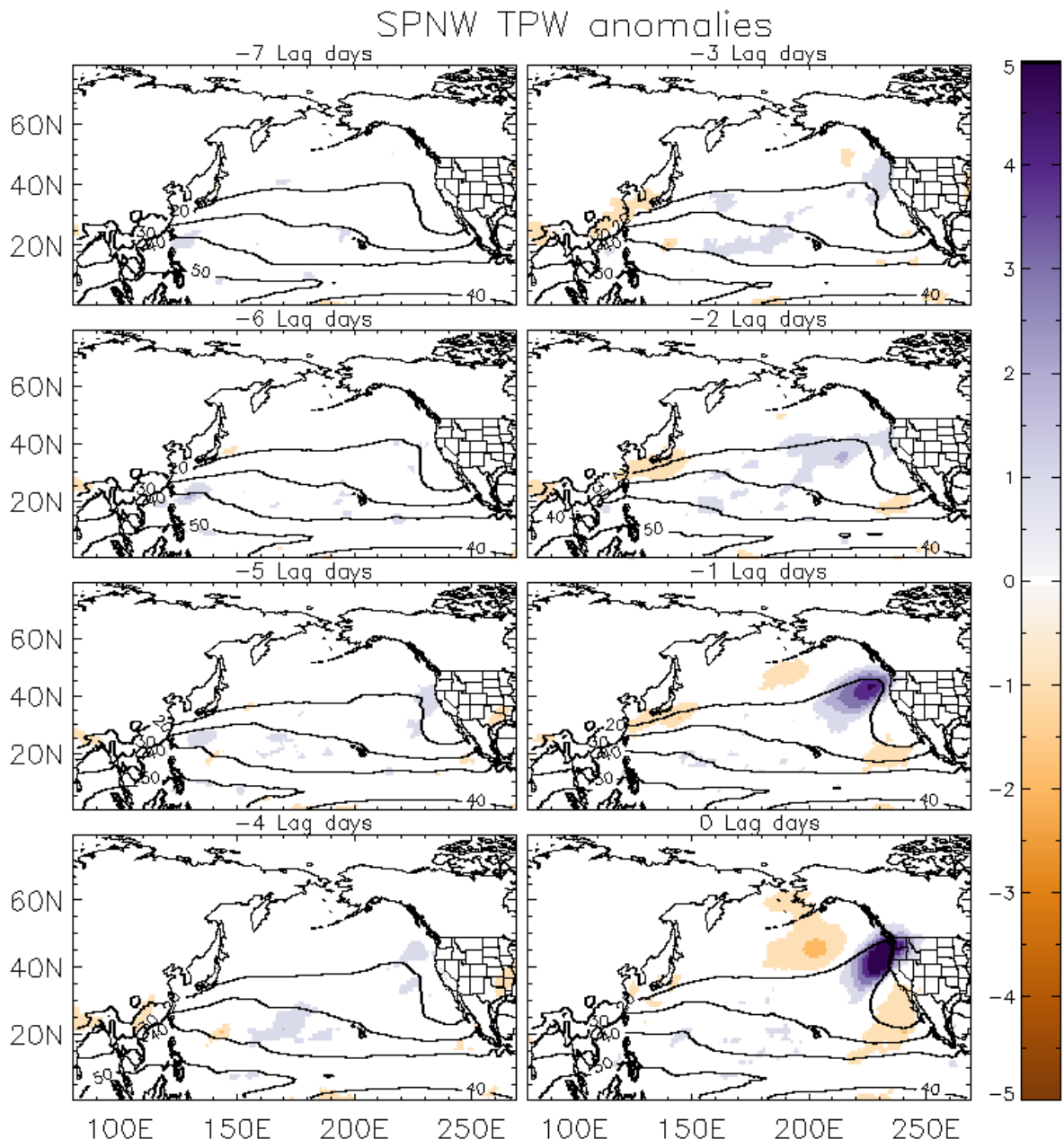
**Fig. 2.5** Same as Fig. 2.3, but for ARs affecting SPNW
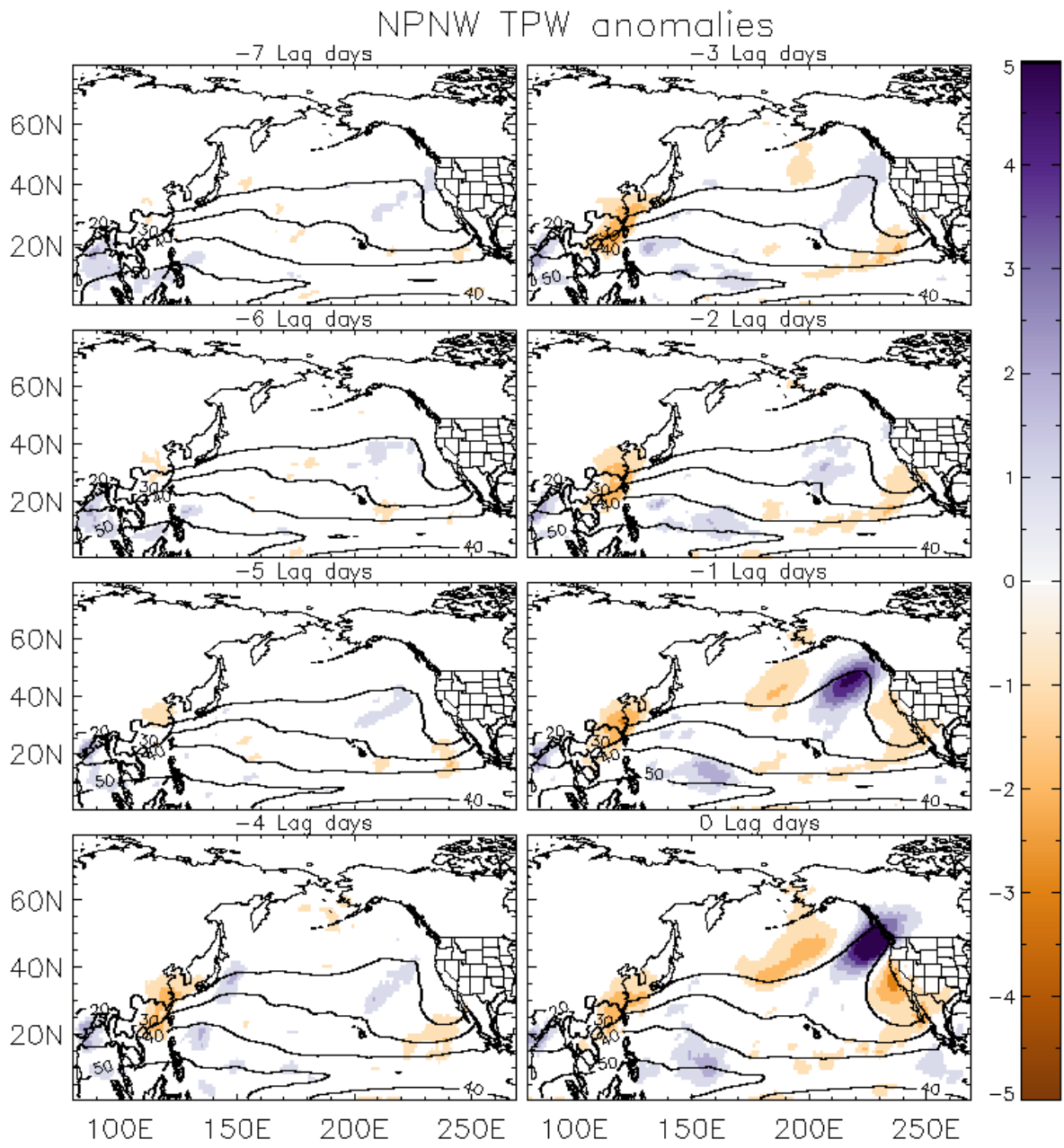
**Fig. 2.6** Same as Fig. 2.3, but for ARs affecting NPNW

Prior to landfall (Lag -7 to -1 days), ARs are associated with a buildup of moisture above the eastern Pacific Ocean that occurs a few days earlier (Fig. 2.3-2.6), characterizing ARs as synoptic scale phenomena. As composites are averages of group events, weak or no statistically significant anomalies indicate case-to-case variability and suggest that SCA ARs have greater consistency among events due to statistically significant anomalies, whereas ARs landfalling farther north show more variability in the days prior to AR landfall. In other words, statistically significant anomalies resulting from the composites of these fields do not properly characterize the narrow zones with high TPW anomalies associated with ARs landfalling farther north. This is because of the spatial characteristics of the ARs and the large case-to-case variability of the moisture plumes. In terms of orientations, leading edges for SCA AR moisture plumes initialize farther eastward as well as equatorward with their trailing ends extending to the eastern Pacific (Fig. 2.3) whereas leading edges for ARs landfalling farther north initialize farther westward and poleward as well as have trailing ends extending farther westward (Fig. 2.4-2.6). These orientation differences are as anticipated, and suggest that SCA ARs vary in terms of manifestation as well as possible moisture sources from ARs landfalling farther north.

Composites of h500 anomalies (Fig. 2.7a-d) on AR landfall days display trough-ridge couplets with an offshore trough and onshore ridge leading to overall southwesterly flow for all landfall regions (Neiman et al. 2008a). SCA ARs exhibit the lowest positive h500 anomalies (maximum +34 m SCA, Fig. 2.7a) as well as the strongest negative anomalies (minimum -159 m) corresponding to the onshore ridge and offshore trough, respectively. These differences result in a shifting of the trough and ridge axes, guiding AR moisture farther south along the coastline. The other landfall regions have weaker negative h500 anomalies (minimum -118 m NCA, Fig. 2.7b; -107 m SPNW, Fig. 2.7c; -87 m NPNW, Fig. 2.7d) as well as stronger positive anomalies (maximum +49 m NCA; +72 m SPNW; +123 m NPNW), guiding wind and moisture farther northward

along the coast. Additionally, SCA ARs are associated with negative h500 anomalies over Oregon, Washington, and southern British Columbia that are closer to the coast as well as positive anomalies to the south and southeast (Fig. 2.7a). These anomalies shift for ARs landfalling farther north with NPNW ARs displaying positive h500 anomalies over Oregon, Washington, and southern British Columbia with weaker negative anomalies directly to the south and west and additional positive anomalies off the coast of Hawaii (Fig. 2.7d). These h500 anomaly wave train patterns resemble the two phases of the Pacific/North American Teleconnection Pattern (PNA), with SCA ARs most closely resembling the negative PNA (PNA-) phase and NPNW resembling the positive PNA (PNA+) phase (Wallace and Gutzler 1981). PNA- involves a westward retraction of the jet stream along with cooler, wetter weather over western North America while PNA+ indicates an eastward extension of the jet stream along with warm, drier conditions over southwestern North America (Leathers et al. 1991).
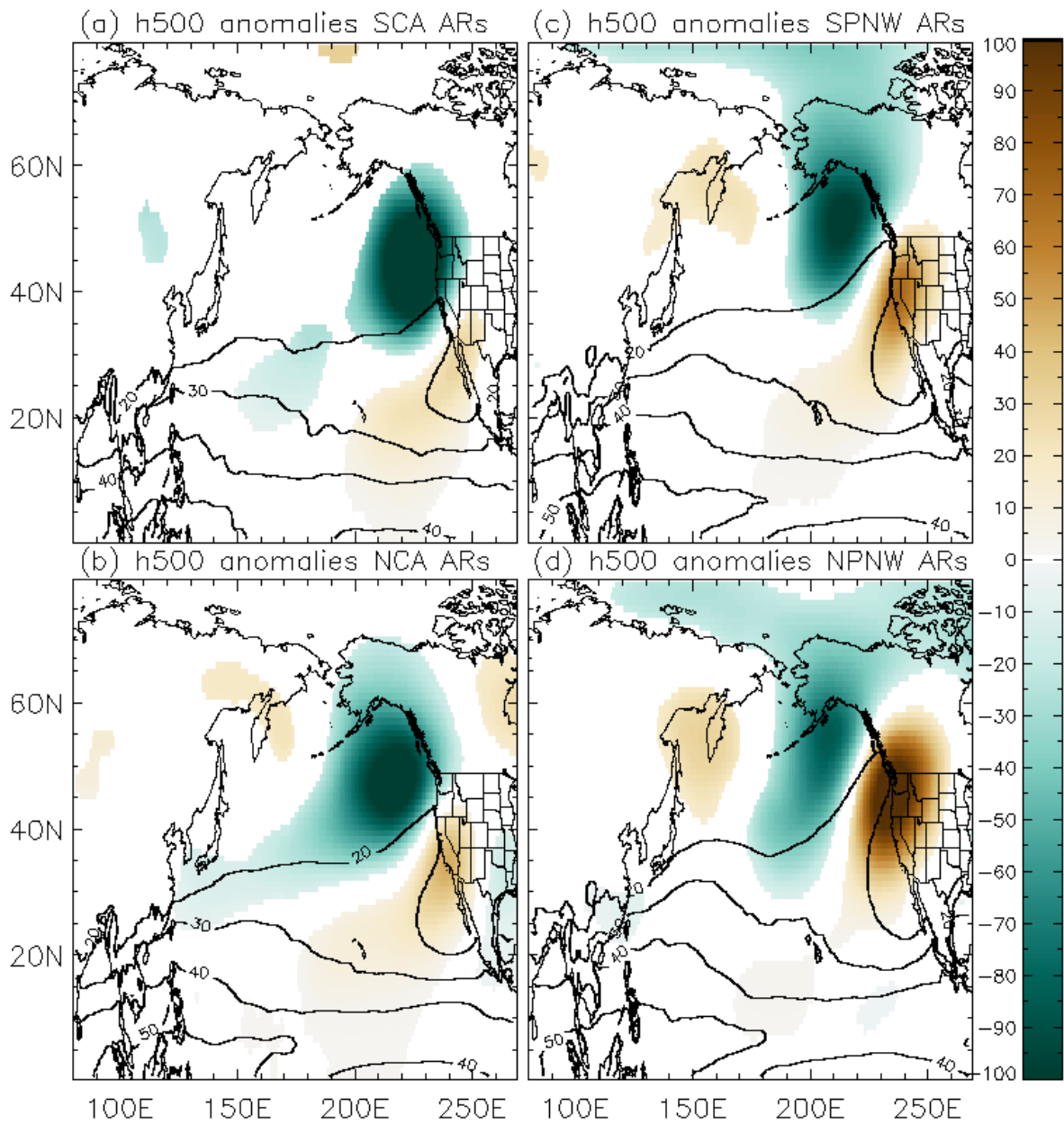
**Fig. 2.7** Composites of h500 anomalies (colored shading; m) on the day of AR landfall (0 Lag days) for ARs affecting **a** SCA, **b** NCA, **c** SPNW, and **d** NPNW. Anomalies are calculated at the 95% level using a Student's t-test. TPW contours are overlaid to help visualize AR plume location and begin at 20 kg m$^{-2}$ with a contour interval of 10

A daily PNA record from NOAA's Climate Prediction Center (CPC) reveals a neutral trend in PNA occurrences during Oct-Mar 1979-2013 (not shown) with a slightly higher proportion of PNA+ events at or greater than 1 standard deviation and an analysis of AR frequencies corresponding with PNA phases at or greater (less) than +1 (-1) standard deviation (Table 2.2) reveals greater AR incidences during PNA+ for all four landfall regions. However, according to a test of proportions at a 95 percent confidence interval, the frequency of SCA ARs during PNA+ is not significantly greater than that during PNA-, whereas ARs during PNA+ are significantly more frequent for all other landfall areas. A previous study by Guan et al. (2013) concludes that from Nov. 1997 to Mar. 2011, ARs affecting the Sierra Nevada are more frequent during PNA-. Although our results do not support this finding, it is important to note that Guan et al.'s (2013) study focuses on a smaller, mountainous area within eastern California and covers a shorter time span (1997-2011) during which the PNA was predominantly negative. In a different study, Payne and Magnusdottir (2014) determine that from 1979 to 2011 ARs affecting North America's west coast between 20.0°-60.0°N are associated with a westward retraction of the jet stream which coincides with changes in the potential vorticity gradient resulting in Rossby wave breaking. Fig. 2.8(a-d) shows composites of 200mb winds on AR landfall days for each location. Only wind speeds meeting or exceeding a 40ms$^{-1}$ threshold are shown in order to visualize the upper level jet core. These composites show an eastward extension of the jet core for SCA ARs (Fig. 2.8a) whereas the jet core retracts farther westward for ARs landfalling farther north (Fig. 2.8b-d). Particularly, SCA ARs show more intense jets east of 180°E compared to SPNW and NPNW, and with NCA, SCA ARs showing more intense jet east of 150°W, closer to shore. As ARs landfall farther south, the jet core is more zonally-oriented with greater concentrations of strong winds (≥60ms$^{-1}$) and shifts to a more wavelike pattern as ARs landfall farther north. This displacement of the jet core suggests that while a westward retraction of jet winds is important for

most ARs landfalling along the western coast of North America (consistent with results from Payne and Magnusdottir 2014), an eastward movement of the jet exit region plays a significant role with SCA ARs. Additionally, this retraction and extension may not be primarily determined by PNA phase.

**Table 2.2** AR frequencies according to landfall region coinciding with strong (+/- 1 standard deviation) positive and negative PNA phases

|  | no. ARs | PNA(+) | PNA(-) |
|---|---|---|---|
| SCA | 72 | 15 | 10 |
| NCA | 213 | 62 | 18 |
| SPNW | 183 | 51 | 21 |
| NPNW | 160 | 42 | 6 |
| All ARs | 719 | 201 | 63 |
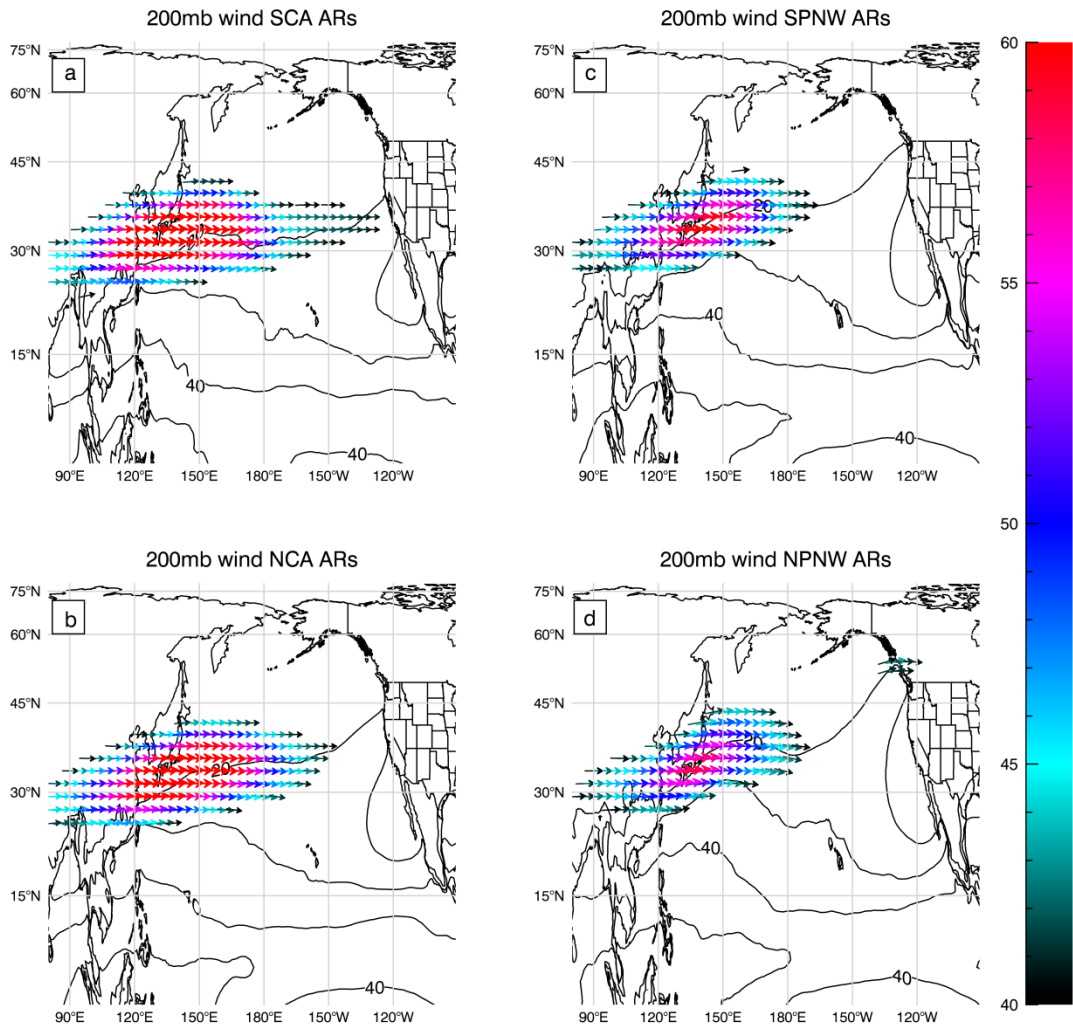
**Fig. 2.8** Composites of 200mb wind (ms$^{-1}$) on AR landfall days for ARs affecting **a** SCA, **b** NCA, **c** SPNW, and **d** NPNW. Winds below 40ms$^{-1}$ are disregarded in order to visualize the location of the jet core. TPW (contours) is overlaid to help visualize AR plume location

T2m anomaly composites (Fig. 2.9-2.12) for AR landfall days show warming within AR plumes for all landfall regions, consistent with findings that ARs have warm low-troposphere temperatures (Neiman et al. 2008a). Additionally warming is seen downstream of AR plumes confirming the presence of onshore ridges (Neiman et al. 2008a) whereas cooling is observed poleward of the plume. These patterns of temperature along with the corresponding geopotential height patterns are consistent with the baroclinic wave theory, supporting the idea that ARs are components of extratropical cyclones. Even though SCA ARs have the least amplified onshore ridge, positive t2m anomalies downstream of AR plumes are comparable to other landfall regions (+2 °C, SCA, Fig. 2.9; +2 °C, NCA, Fig. 2.10; +2 °C, SPNW, Fig. 2.11; +3 °C, NPNW, Fig. 2.12), suggesting dynamical forcing of SCA ARs.
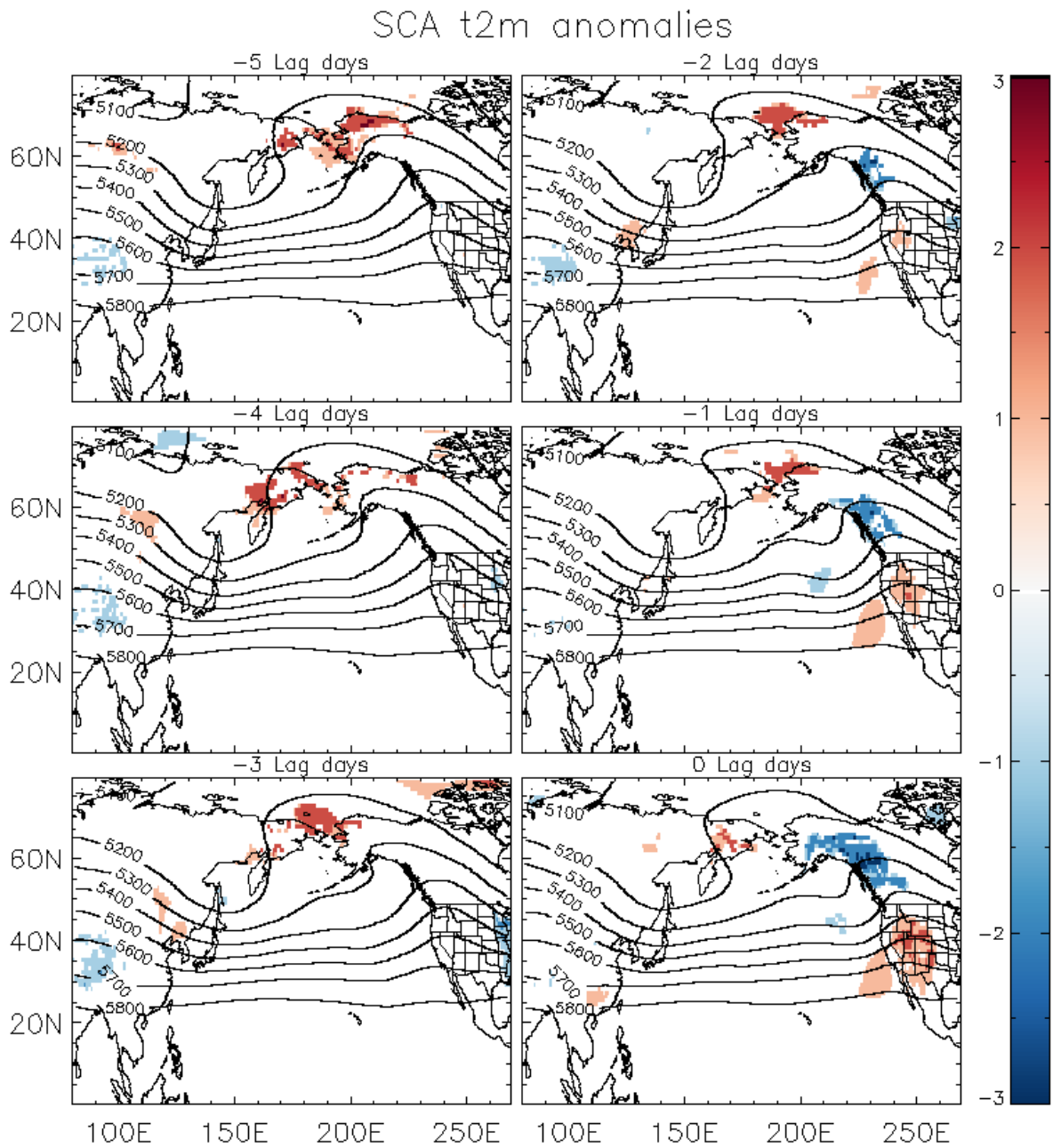
**Fig. 2.9** Composites of t2m anomalies (colored shading; °C) and h500 (contours; m) starting five days prior to AR landfall (-5 Lag days) and continuing to the day of AR landfall (0 Lag days) for ARs affecting SCA. Anomalies are calculated at the 95% level using a Student's t-test
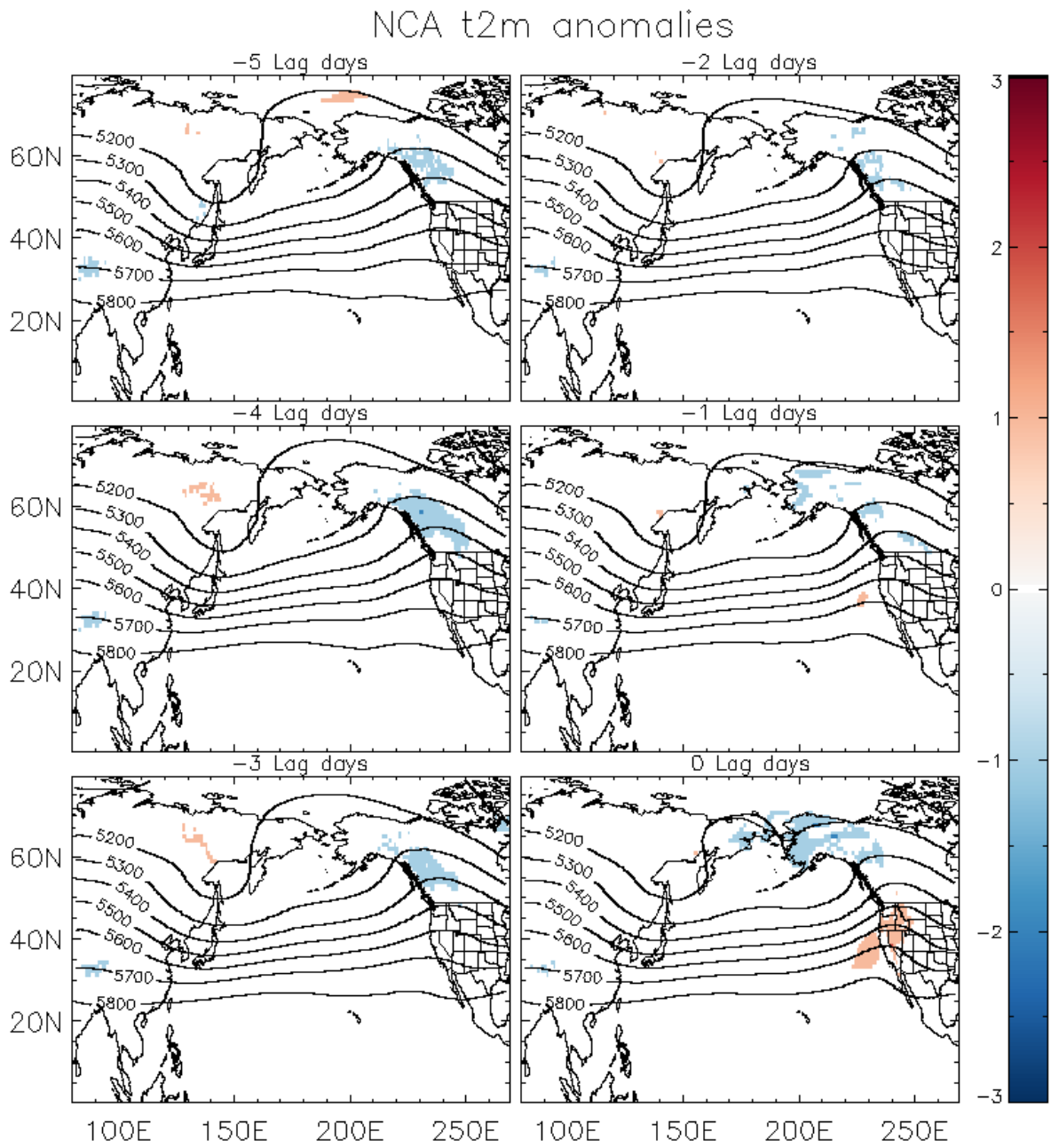
**Fig. 2.10** Same as Fig. 2.9, but for ARs affecting NCA
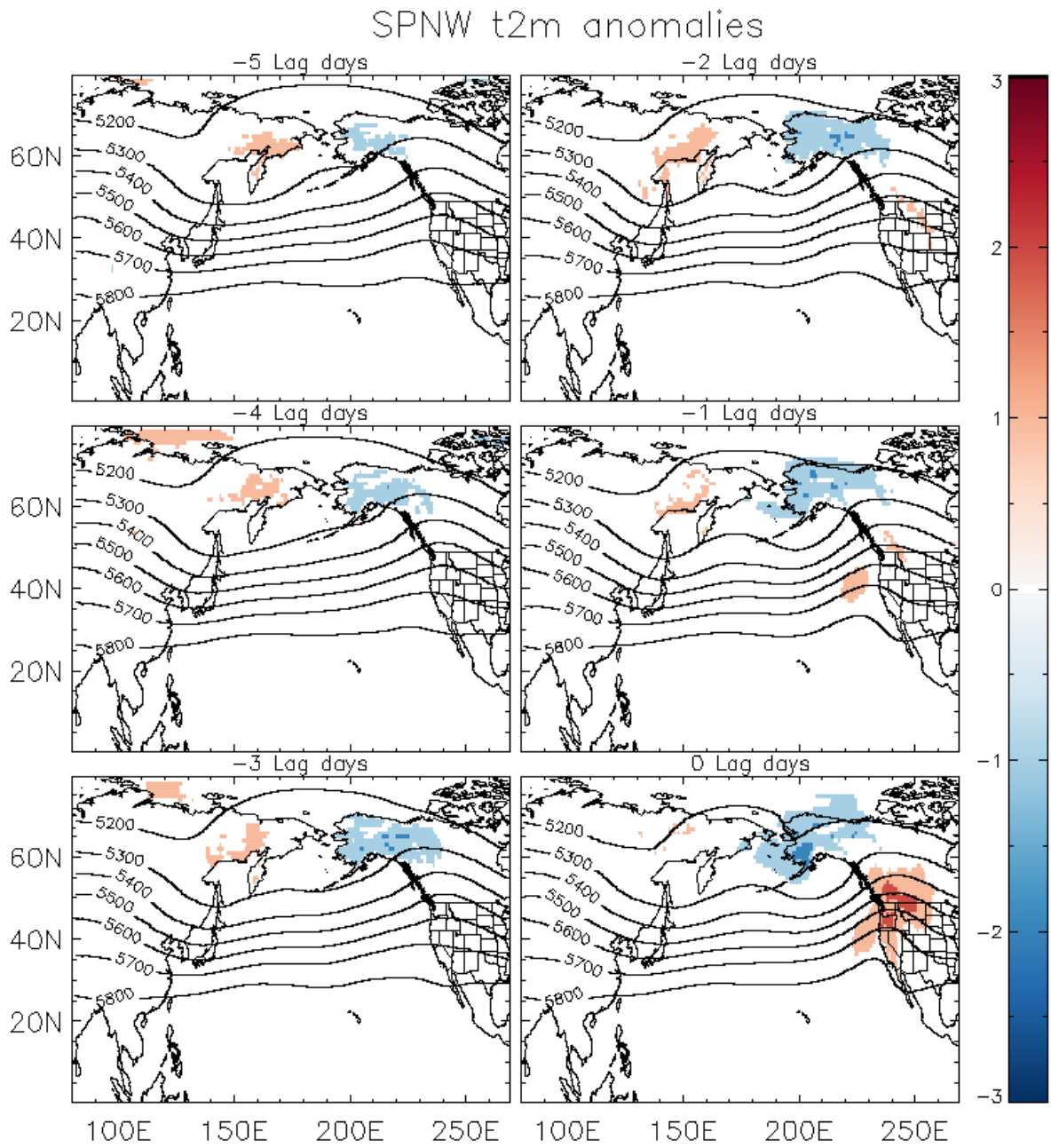
**Fig. 2.11** Same as Fig. 2.9, but for ARs affecting SPNW
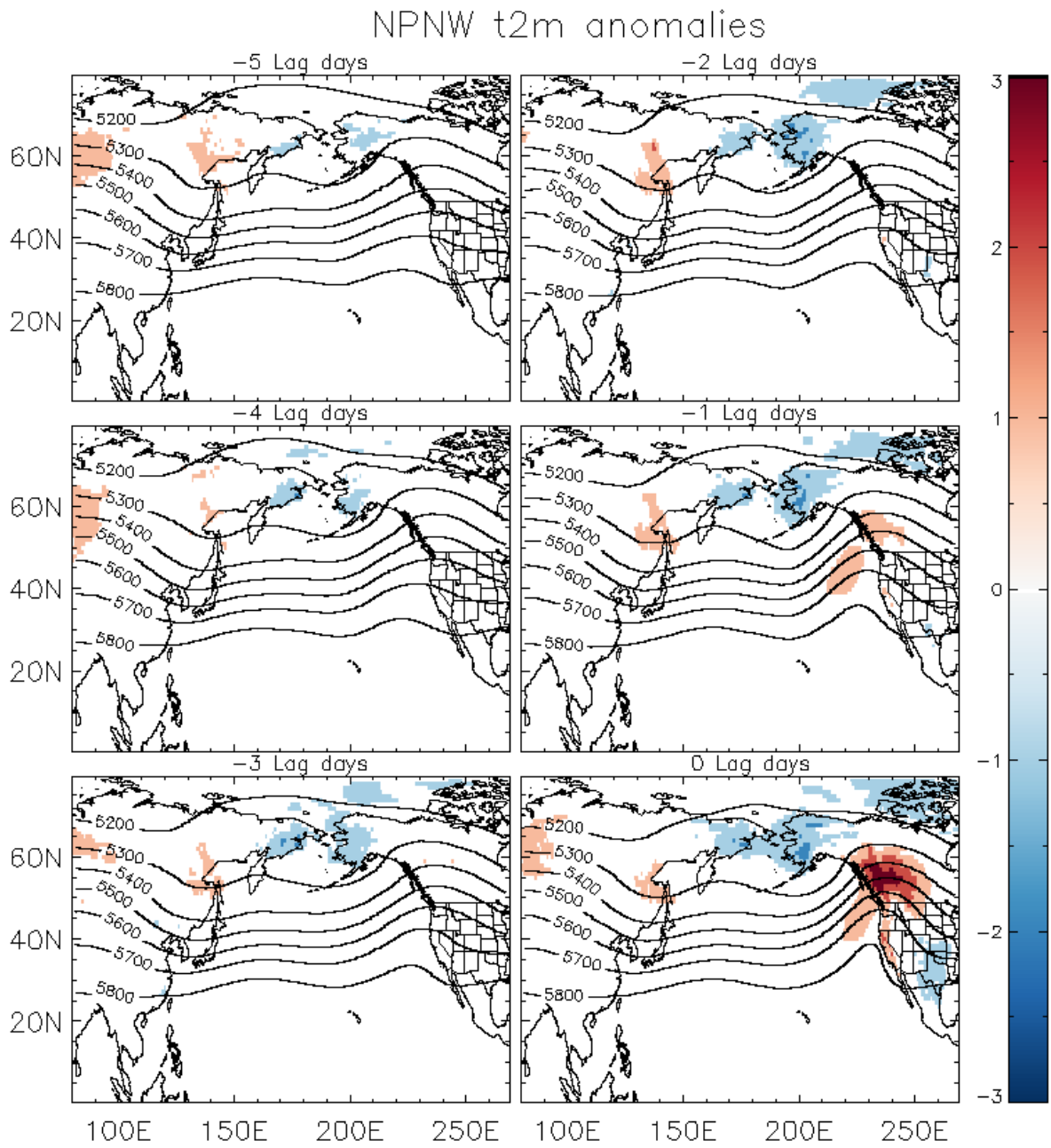
**Fig. 2.12** Same as Fig. 2.9, but for ARs affecting NPNW

Prior to landfall, h500 composites (Fig. 2.9-2.12) show differing trough-ridge patterns progressing through the Pacific. Five days prior to landfall (-5 Lag days), all regions develop a trough over the far western Pacific near the Korean Peninsula along with a ridge over Alaska. However, the trough appears most pronounced for ARs landfalling farther south with SCA ARs (Fig. 2.9) displaying the widest trough as well as the most amplified ridge. The dynamics of these systems along with the previously described extension/retraction of jet winds suggest that the amplitude of the trough developing over eastern Asia/the western Pacific along with an adjacent amplified ridge is perhaps the main mechanism responsible for the equatorward displacement of upper level jet. This leads to the eastward extension of the jet core, forcing AR associated moisture to landfall farther south, eventually landfalling in SCA.

## 2.5 MJO and ENSO Effects

AR occurrences at landfall coinciding with MJO activity are assessed using an MJO index from Jones and Carvalho (2012). This index identifies daily MJO activity including MJO phases (p1-p8) and magnitudes. A complete description of the index and its construction can be found in Jones and Carvalho (2012). Of the 6370 dates examined (Oct-Mar 1979-2013) 3873 (60.8%) align with active MJO and 2497 (39.2%) with inactive MJO. For the 719 identified AR events landfalling on North America's west coast (30.0°-55.0°N) during Oct-Mar 1979-2013, 418 (58.13%) occur during an active MJO whereas 301 (41.86%) ARs take place during an inactive MJO (Table 2.3). For the 72 ARs landfalling in SCA 40 (55.56%) occur during an active MJO and 32 (44.4%) during an inactive MJO. All landfall regions experience greater AR frequencies during active MJOs; however, for all regions except NPNW, the AR frequency differences during active and inactive MJO are not statistically significant according to a test of proportions at a 95 percent confidence interval.

This suggests that for most of western North America during Oct-Mar, ARs landfalling during active MJO may occur by chance.

**Table 2.3** AR frequencies according to landfall region during active (ac.) and inactive (in.) MJO

|  | no. ARs | MJO (ac.) | % | MJO (in.) | % |
|---|---|---|---|---|---|
| SCA | 72 | 40 | 55.56% | 32 | 44.44% |
| NCA | 213 | 133 | 62.44% | 80 | 37.56% |
| SPNW | 183 | 115 | 62.84% | 68 | 37.16% |
| NPNW | 160 | 81 | 50.63% | 79 | 49.38% |
| All ARs | 719 | 418 | 58.14% | 301 | 41.86% |

In regards to MJO phases (Table 2.4) for all landfalling ARs (30.0˚-55.0˚N) the greatest AR frequencies occur during p1 and p7 (62 dates each) with secondary peaks at p3 (58 dates) and p6 (54 dates). During p1, MJO enhanced convection manifests over the equatorial Indian Ocean with suppressed convection directly to the east over the western Pacific Ocean along with a retracted jet stream (Bell and Higgins 2005; Zhang 2005). At p3 enhanced convection has migrated eastward over the eastern Indian Ocean with suppressed convection towards the central Pacific. By p6 enhanced convection has continued to the western equatorial Pacific Ocean with suppressed convection directly to the west over the equatorial eastern Indian Ocean. At p7 enhanced convection has progressed farther towards the central Pacific Ocean and begins to dissipate, while wind and surface pressure signals normally coupled with the convection continue to propagate eastward and suppressed convection is to the west over the western Pacific Ocean (e.g., Jones and Carvalho 2012). Additionally, as the MJO enhanced convection advances towards the central

Pacific, there is an eastward extension of the Jet Stream (Bell and Higgins 2005; Zhang 2005). Overall AR activity is consistent with previous analyses such as from Guan et al. (2012) who states that SWE fractions in the Sierra Nevada from ARs increase during MJO p3 and p6. Additionally, Payne and Magnusdottir (2014) conclude that ARs affecting North America's west coast (20.0°-60.0°N) increase during MJO p3, p6, p7, and p8, with the greatest frequency increase during p6. However, our results show half the total ARs during p8. Conclusions from individual landfall regions (Table 2.4) are inconsistent with these previous findings and are also not uniform between landfall areas suggesting that MJO activity during particular MJO phases is not indicative of specific AR landfall location.

**Table 2.4** AR frequencies according to landfall region corresponding to various MJO phases

|  | p1 (phase1) | p2 | p3 | p4 | p5 | p6 | p7 | p8 |
|---|---|---|---|---|---|---|---|---|
| SCA | 4 | 9 | 6 | 2 | 7 | 3 | 6 | 3 |
| NCA | 15 | 16 | 16 | 16 | 12 | 19 | 28 | 11 |
| SPNW | 21 | 18 | 17 | 12 | 13 | 13 | 10 | 11 |
| NPNW | 15 | 6 | 11 | 13 | 10 | 12 | 11 | 3 |
| All ARs | 62 | 52 | 58 | 50 | 47 | 54 | 62 | 33 |

AR events at landfall and coinciding ENSO phases are also assessed. ENSO phases are identified from the Oceanic Niño Index (ONI) from the CPC of NOAA. A description of ONI's construction can be found at the CPC's website (www.cpc.ncep.noaa.gov). For all identified ARs (30.0°-55.0°N) during Oct-Mar 1979-2013, the greatest event frequencies occur during neutral ENSOs (315 dates, 43.8%) with roughly even numbers during warm (203 dates, 28.2%) and cold (201, 28.0%) ENSOs (Table 2.5). As neutral ENSO occurs most frequently (45.2% of Oct-Mar 1979-2013, with 29.0% warm, and 25.7% cold), this is to be expected. NCA, SPNW, and NPNW ARs also occur more frequently during neutral ENSO conditions (Table 2.5). However, SCA ARs show more even proportions of warm (25, 34.72%), cold (25, 34.72%), and neutral (22, 30.56%) ENSOs (Table 2.5) that is significant according to a test of proportions at the 95 percent confidence interval. This is also apparent in Fig. 2.13 that shows AR interannual variability by water year for each landfall location. The increased frequencies of ARs during ENSO neutral conditions for NCA, SPNW, and NPNW are consistent with previous findings from Bao et al. (2006). Payne and Magnusdottir (2014) conclude that during warm ENSOs AR landfalling latitudes shift southward, in part explaining the increase of AR frequencies in SCA during warm ENSOs but not the frequency increase during cold ENSOs. These results indicate that the ENSO neutral phase may provide the background atmospheric conditions required for AR occurrence in western North America but may not play a direct role in the development and/or modulation for ARs occurring farthest south.

**Table 2.5** AR frequencies according to landfall region corresponding to ENSO phases

|  | no. ARs | warm | % | cold | % | neutral | % |
|---|---|---|---|---|---|---|---|
| SCA | 72 | 25 | 34.72% | 25 | 34.72% | 22 | 30.56% |
| NCA | 213 | 53 | 24.88% | 60 | 28.17% | 100 | 46.95% |
| SPNW | 183 | 51 | 27.87% | 53 | 28.96% | 79 | 43.17% |
| NPNW | 160 | 48 | 30.00% | 42 | 26.25% | 70 | 43.75% |
| All ARs | 719 | 203 | 28.23% | 201 | 27.96% | 315 | 43.81% |
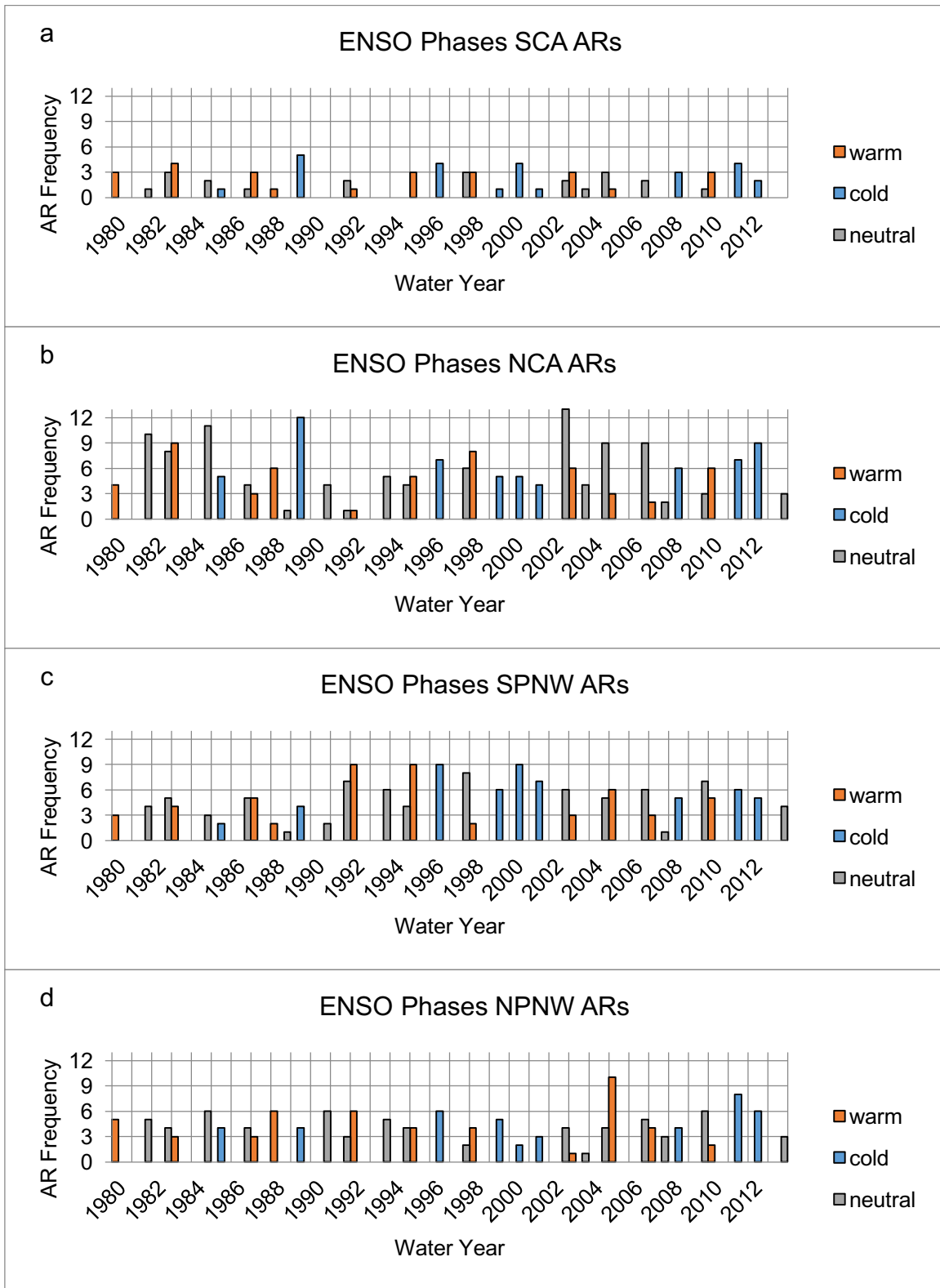
**Fig. 2.13** Seasonal Oct-Mar AR frequencies for water years 1980-2013 and corresponding ENSO phase during landfall for **a** SCA, **b** NCA, **c** SPNW, and **d** NPNW

**2.6 Conclusions**

Understanding the characteristics and atmospheric conditions behind SCA AR events is imperative for proper forecasting, hazard mitigation, as well as water resources management. This study uses an algorithm to identify ARs affecting western North America within CFSR TPW fields spanning from 1979 to 2013 and then classifies ARs according to region of landfall. The current identification method modifies of a previous algorithm established by Jiang and Deng (2011) as well as Jiang et al. (2014) and most notably uses a fit ellipse approach to detect individual AR events. The algorithm identifies 719 ARs landfalling between 30.0°-55.0°N with 72 landfalling in SCA, 213 in NCA, 183 in SPNW, and 160 in NPNW. Composites of TPW, TPW anomalies, h500, h500 anomalies, 200-mb winds, as well as t2m anomalies are investigated for ARs affecting each individual landfall region on the day of, prior to, and after AR landfall in order to differentiate characteristics of ARs landfalling in different areas. In general, ARs landfalling along the North American west coast are characterized by baroclinic midlatitude wave trains progressing through the Pacific resulting in northeastward oriented moisture plumes extending from low-to midlatitudes that appear to culminate along coastal mountain ranges. On landfall days ARs are characterized by an offshore trough and onshore ridge as well as localized low-tropospheric warming.

Although SCA ARs display similar features to ARs landfalling farther north along the western coast of North America, differences arise in their progression and landfall. Anomalously high moisture associated with AR plumes appears farther eastward as well as equatorward for SCA ARs and in addition, materialize days earlier suggesting that SCA AR moisture plume patterns have less case-to-case variability. Several days prior to landfall, SCA ARs display a wide trough off the eastern coast of Asia along with an amplified ridge over Alaska leading to the displacement and possible merger of the upper level jets and subsequent eastward extension of the jet core with

winds at or greater than 60ms$^{-1}$ close to shore. In combination with an offshore trough and weak onshore ridge on the day of landfall, there is increased zonal flow of wind and moisture suggesting that the region of landfall depends on the phase, position, and amplitude of the wave-train.

ARs occurring during and throughout various phases of the PNA, MJO, and ENSO are also investigated with SCA ARs again exhibiting differing relationships than that of ARs landfalling farther north. H500 anomalies for SCA ARs most closely resemble PNA- whereas ARs landfalling farther north resemble PNA+. However, an analysis of ARs with the PNA index indicates that ARs occur more frequently during PNA+ for all landfall regions but that the frequencies of SCA ARs during PNA+ and PNA- is not significantly different. All other landfall regions show significantly increased AR activity during PNA+. This finding is contradicted by the eastward extension of the jet core seen with SCA ARs, a feature associated with PNA+, suggesting that other mechanisms may be more relevant in modifying the position of the jet. Additionally, as ARs landfall farther north, there is a westward retraction of the jet core, a feature more common to the PNA- phase. This indicates that the PNA may not be the main driver of AR activity for the western coast of North America.

The frequencies of SCA, NCA, and SPNW ARs reveal no statistically significant differences of proportions for active or inactive MJO whereas NPNW ARs occur more evenly between active and inactive MJO, inconsistent with overall MJO activity. Furthermore, while ARs in general occur more frequently during MJO phases 1, 3, 6, and 7, when separated into landfall regions there is no discernible pattern. In regards to ENSO, SCA ARs occur evenly between warm, cold, and neutral ENSOs whereas NCA, SPNW, and NPNW see greater AR frequencies during ENSO neutral conditions in accordance with ENSO proportions. These results hint at the complexity of SCA ARs, as the dominant mechanisms affecting ARs along the North American western coast do not appear to affect SCA ARs the same way.

47

**Acknowledgements**

# Chapter 3

## Backward Trajectories Analysis of Southern California Atmospheric Rivers

**Abstract**

Atmospheric rivers (ARs) are filamentary channels of high water vapor flux that transfer moisture horizontally through the atmosphere at low-levels. These features form over the oceans with limited losses of moisture through precipitation until landfall. For areas with extensive topographical variations, particularly along coastlines, ARs are often responsible for large annual rainfall totals as well as high-intensity storms due to orographic forcing. ARs are important factors when predicting hazardous events such as flooding and are vital components of many regional water budgets. This is especially true for drought-prone areas such as Southern California (SCA) which experiences relatively few storms per season, many of which are AR events. While extensive research has been developed to investigate AR events affecting the west coast of the U.S, few focus on southern latitudes. Additionally, apart from case studies, limited research has addressed the climatology of AR lifecycles.

We use a Lagrangian model to create backward air parcel trajectories of 159 AR events that made landfall on the U.S. west coast from December 2004 to December 2015. Trajectories are used to examine the lifecycles and movements of these ARs and to differentiate SCA ARs from ARs landfalling farther north. We compare hourly trajectories for the hour of and 72 hours before landfall. Prior to landfall, SCA ARs share similarities but also have distinct differences from other ARs. At 1000 m above mean sea level (MSL) SCA AR trajectories are shorter than trajectories for ARs landfalling farther north. Additionally, along trajectory measurements for SCA ARs tend to be warmer and have higher specific humidity values. This applies to both the 1000 m

and 2000 m MSL levels. These results imply that SCA ARs move slower and have the potential to produce higher-intensity storms at landfall.

## 3.1 Introduction

Few studies have examined AR trajectories and lifecycles (e.g. Ramos et al. 2016; Rutz et al. 2015; Sodemann and Stohl 2013) and are often limited to singular case study events (e.g. Moore et al. 2012). Those that did examine AR trajectories often focused on ARs landfalling farther north along North America's western coast (e.g. Neiman et al. 2013). While use of trajectory models is often limited to case studies, these tools can provide us with valuable information about the characteristics of AR events in the days leading up to landfall. This research aims to examine the trajectories and lifecycles of ARs affecting the western coast of North America with a focus on ARs affecting SCA. The main goal of this work is to determine the differences of SCA ARs from ARs landfalling farther north using trajectory locations and distances, as well as along trajectory characteristics before and during landfall. This will be achieved by describing in detail the climatology of the trajectories and respective environmental conditions along the trajectories. The backward trajectory analysis is beneficial for this study as it provides hourly outputs of location as well as several along trajectory characteristics important to AR progression including pressure, specific humidity values, among others. This paper is organized as follows. Section 3.2 describes datasets and methods used. Section 3.3a discusses trajectory model locational results. Section 3.3b discusses along trajectory characteristic results. Section 3.4 presents a case study analysis. Section 3.5 conclusions.

**3.2 Datasets & Methods**

Two gridded datasets from the National Centers for Environmental Prediction (NCEP) at the National Oceanic and Atmospheric Administration (NOAA) provide synoptic-scale conditions for these analyses: 1) the Climate Forecast System Reanalysis (CFSR), used for AR identification as well as determining AR landfall locations, and 2) the Global Data Assimilation System (GDAS), used for backward trajectories. We use daily CFSR (Saha et al. 2010) fields of total precipitable water (TPW) from 1979 to 2015 available at a 0.5° × 0.5° horizontal resolution and calculate daily anomaly fields at each grid point by removing the smoothed annual cycle. TPW (in kg m$^{-2}$) is an equivalent to integrated water vapor as it reflects the water total within an atmospheric column (vertically integrated, surface – 200mb) if all water vapor condenses into liquid water with 1 kg m$^{-2}$ equal to 1 mm (Campmany et al. 2010). We use daily GDAS (Kanamitsu 1989) analyses available at a 1.0° × 1.0° horizontal resolution with a vertical resolution of 25 hPa between 1000 and 900 hPa and 50 hPa available from December 2004 until December 2015.

We use an AR identification algorithm to identify events and their landfall locations for ARs affecting the western coast of North America during the wet season months of October through March within 0.5° × 0.5° TPW fields using a fit ellipse approach. More information about the algorithm can be found in Harris and Carvalho (2017). We then designate ARs according to regions of landfall and create backward air parcel trajectories of 159 AR events (Table 3.1) using the HYbrid Single-Particle Lagrangian Integrated Trajectory (HYSPLIT) model (Draxler and Hess 1997, 1998) from the Air Resources Laboratory at NOAA. HYSPLIT uses a Lagrangian methodology along with 3D meteorological fields of horizontal wind, temperature, pressure and/or heights, along with surface pressure to create forward and backward trajectories.

We use the TPW anomaly fields to determine locations of the maximum positive TPW anomaly overland for each AR event affecting North America between 34.0°-49.0°N and within 2° of the coastline. This is the main starting location (latitude, longitude), i.e. the first and center grid cell, for the backward trajectories. In HYSPLIT one backward trajectory is calculated from this grid cell. Additionally, we build a box of eight other grid cells each offset by 1.0° longitude/latitude surrounding the original cell with a backward trajectory calculated at each cell to create a 3° latitude × 3° longitude box centered over the landfall location grid cell. This group of nine cells/trajectories is obtained for each of the ending levels, 1000 m, 2000 m, and 3000 m above mean sea level (MSL), consistent with previous backward trajectories analyses of ARs using HYSPLIT (e.g. Moore et al. 2012) resulting in 27 calculated trajectories for each AR. Backward trajectories run hourly for the previous 72–h, consistent with Moore et al. (2012), with GDAS providing the 3D atmospheric conditions for the events including vertical motion fields. We use GDAS as it is already converted into a HYSPLIT ready format and is used in previous AR HYSPLIT analyses (e.g. Neiman et al. 2013; Moore et al. 2012). It is important to note that AR lifecycles range temporally. The designated 72–h is a framework to understand the selected AR events and their synoptic conditions. Longer or shorter temporal trajectories may be more appropriate depending on individual events. Since the main goal of this study is to provide a climatology of all AR events we use 72–h as a guideline to evaluate properties that are consistent among ARs that landfall in coastal North America. Our analyses indicate that longer trajectories are normally subject to a number of distinct processes, increasing the variance among events (not shown).

HYSPLIT computes trajectory advection using 3D velocity vectors ($V$) averages for initial, $P(t)$, as well as first guess, $P'(t+\Delta t)$, positions, where the advection distance per time step ($\Delta t$) is

less than the grid spacing and the velocity vectors are linearly interpolated in time and space. The first guess position is calculated as

$$P'(t + \Delta t) = P(t) + V(P, t)\Delta t \qquad \text{(Eq. 3.1)}$$

And the final position is calculated as

$$P(t + \Delta t) = P(t) + 0.5[V(P, t) + V(P', t + \Delta t)]\Delta t \qquad \text{(Eq. 3.2)}$$

HYSPLIT is terrain following (normalized $\sigma$ coordinate) with

$$\sigma = (Z_{top} - Z_{msl})/(Z_{top} - Z_{gl}) \qquad \text{(Eq. 3.3)}$$

Where $Z_{top}$ is the height of the top of the model, $Z_{msl}$ is the height of mean sea level, and $Z_{gl}$ is the height of ground level, so that $\sigma$ is normalized to be a fraction of the total model depth. If a trajectory leaves the top of the domain during the sequence, that trajectory is terminated whereas if the trajectory contacts the ground during the run, it continues. When describing trajectories and along trajectory characteristics, the term 'parcel' is sometimes used as a frame of reference for understanding environmental conditions during a trajectory, consistent with other HYSPLIT AR studies (e.g. Moore et al 2012; Neiman et al. 2013). Parcels are best thought of as points with constant volumes following the course of the trajectory that do not interact with the environment. Please see Draxler and Hess (1997) regarding HYSPLIT's construction and/or additional formulas used within the model.

**Table 3.1** Landfall regions, information, and numbers of identified landfalling ARs with backward trajectories calculated by means of HYSPLIT for Oct-Mar seasons from Dec. 2004 to Dec. 2015. Trajectory numbers are the number of individual trajectories calculated at each level

| Name | Abbr. | Lat. Covered (°N) | Landfalling ARs | Trajectories per Level |
|---|---|---|---|---|
| Southern California | SCA | 32.0 °-37.0 ° | 30 | 270 |
| Northern California | NCA | 38.0 °-43.0 ° | 70 | 630 |
| Pacific Northwest | PNW | 44.0 °-49.0 ° | 59 | 531 |
| All ARs | - | 32.0 °-49.0 ° | 159 | 1431 |

## 3.3 HYSPLIT results

We find differences in trajectory distances as well as along trajectory parcel measurements between the three landfall regions. Differences are most pronounced at the 1000 m MSL level although we also discuss the 2000 m and 3000 m MSL levels when applicable. Figs. 3.1-3.12 depict variables at 1000 m and 2000 m MSL only as AR cores tend to occur below 2500 m and various studies show the bulk of moisture flux around 1000 m (e.g. Ralph et al. 2005). We calculate differences between landfall area groups using a Sign-Test (Anderson and Finn 1996) which compares the distributions of two groups based on medians. The Sign-Test involves merging together the two groups of interest, determining the median of the combined group (M), and then using a 2–Proportion Z-Test calculated as

$$z = \frac{\hat{p}_1 - \hat{p}_2}{\sqrt{\hat{p}\hat{q}\left(\frac{1}{n_1} + \frac{1}{n_2}\right)}}$$

(Eq. 3.4)

Where $\hat{p}_1$ ($\hat{p}_2$) is the proportion of the first (second) sample group that is greater than M from the combined group. Value $\hat{p}$ ($\hat{q}$) is the proportion of the combined group that is greater (less) than

M (as M is the median value of the combined group, by definition these proportions must be ½ and ½), with $n_1$ ($n_2$) as the number in the first (second) sample group. The test is two-tailed with larger z values indicating distributions that have greater differences from one another with critical values of ±1.96 at the 95% ($\alpha$=0.05) significance level (Anderson and Finn 1996).

### 3.3a Trajectory pathways and distances

We calculate median trajectory pathways along with interquartile ranges for all ARs landfalling within specified regions to determine overall movements of these AR events. For trajectories ending at 1000 m MSL (Fig. 3.1), median trajectories for all regions are quasi-zonal and exhibit cyclonic curvature. Trajectories become less zonal with less cyclonic curvature at 2000 m (Fig. 3.1) and 3000 m MSL (not shown) and extend in a northeastward direction. Qualitatively, ARs landfalling farther south appear to have the most cyclonic curvature at 1000 m MSL, although they display the most 'zonal' orientations at 2000 m MSL which is consistent with previous North American AR studies (e.g. Harris and Carvalho 2017). SCA AR trajectory locations 72 hours before landfall are farther eastward than for comparable trajectories of ARs landfalling farther north and, as expected, SCA AR trajectories also appear farther south (Harris and Carvalho 2017). Over the course of 72 hours, all trajectories remain north of 25°N with only a few trajectories in the 25th quartile traveling south of 30°N. As moisture within an AR is from a combination of local sources, such as convergence along a cold front, as well as from horizontal transport of moisture over distances (Bao et al. 2006), this suggests that moisture sources for many of these events may not be tropical in nature within 72 hours from landfall.
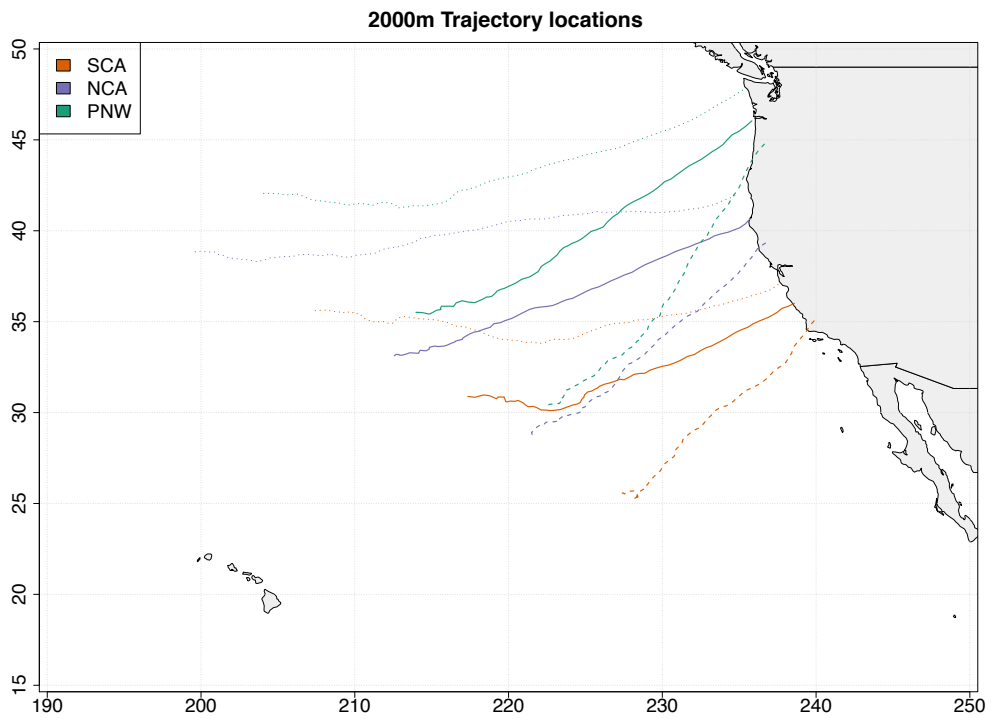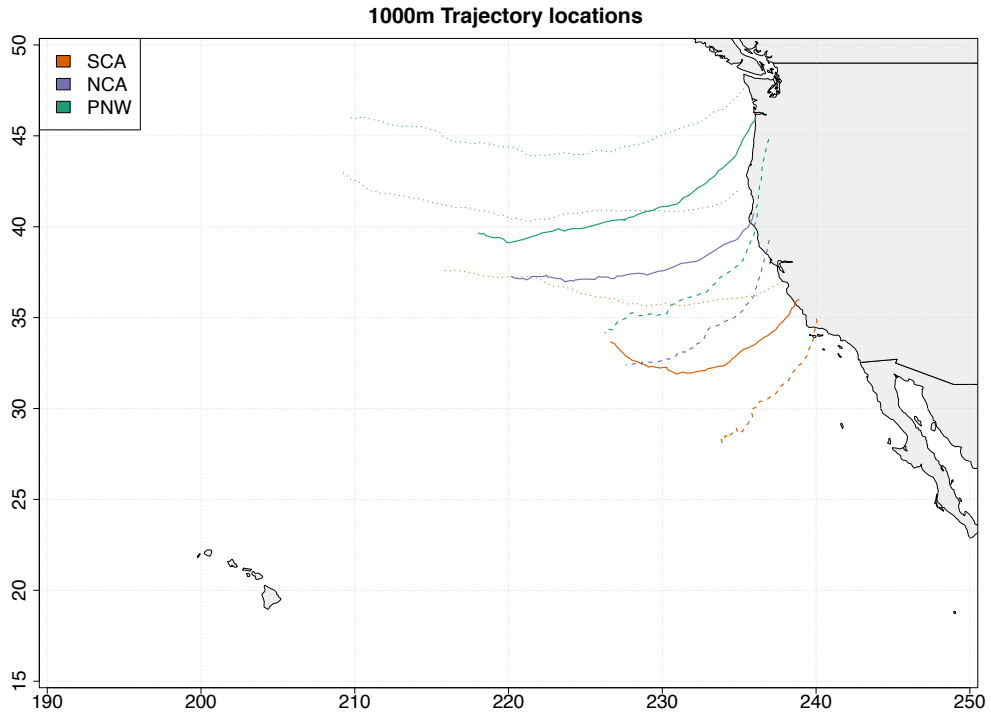
**Fig. 3.1** Median (solid lines), 25th (dashed lines), and 75th (dotted lines) quartile trajectories over 72–h according to landfall region and level. 3000 m MSL plot not shown

At all levels SCA ARs have the shortest median trajectories but the interquartile range (Fig. 3.2) indicates that trajectory distances vary. For trajectories ending at 1000 m MSL (Fig. 3.2), SCA (median=1877.79km IQR=1275.58km) AR trajectories are significantly shorter than both NCA (median=2328.45km IQR=1233.11km) and PNW (median=2497.10km IQR=1131.29km) ARs but they have the highest interquartile range. At 2000 m MSL (Fig. 3.2), SCA (median=2625.03km IQR=1420.74km) ARs are significantly shorter than both NCA (median=2897.58km IQR=1423.41km) and PNW (median=2955.83km IQR=1296.97km) ARs with similar dispersions between SCA and NCA ARs. For trajectories ending at 3000 m MSL (not shown), SCA (median=3324.98km IQR=2220.235km), NCA (median=3588.85km IQR=1886.13km), and PNW (3497.14km IQR=1601.92km) ARs are not significantly different from one another, although SCA ARs still have the shortest median trajectories. Since over the course of 72–h SCA ARs do not travel as far as their northern counterparts, they are slower moving. This difference in speeds implies that extratropical cyclones are not likely to affect SCA ARs in the same manner as NCA and PNW ARs. For example, SCA ARs may tend to be more stationary and thus, several extratropical cyclones may affect a single SCA AR event such as with the case study event discussed in section 3.4.

**AR trajectory distances 1000m**

**AR trajectory distances 2000m**
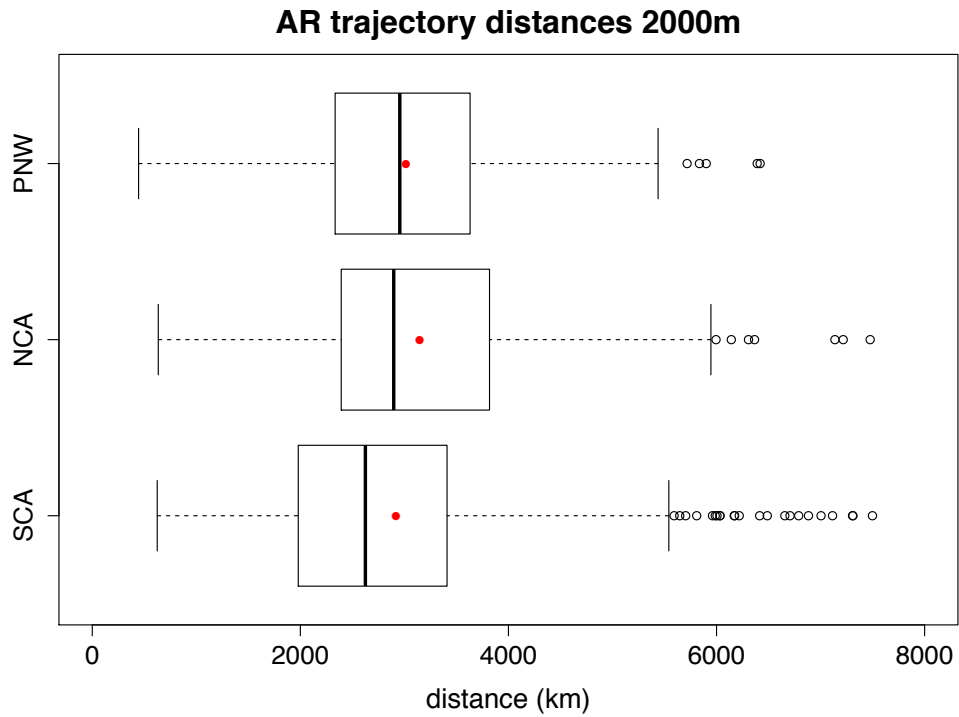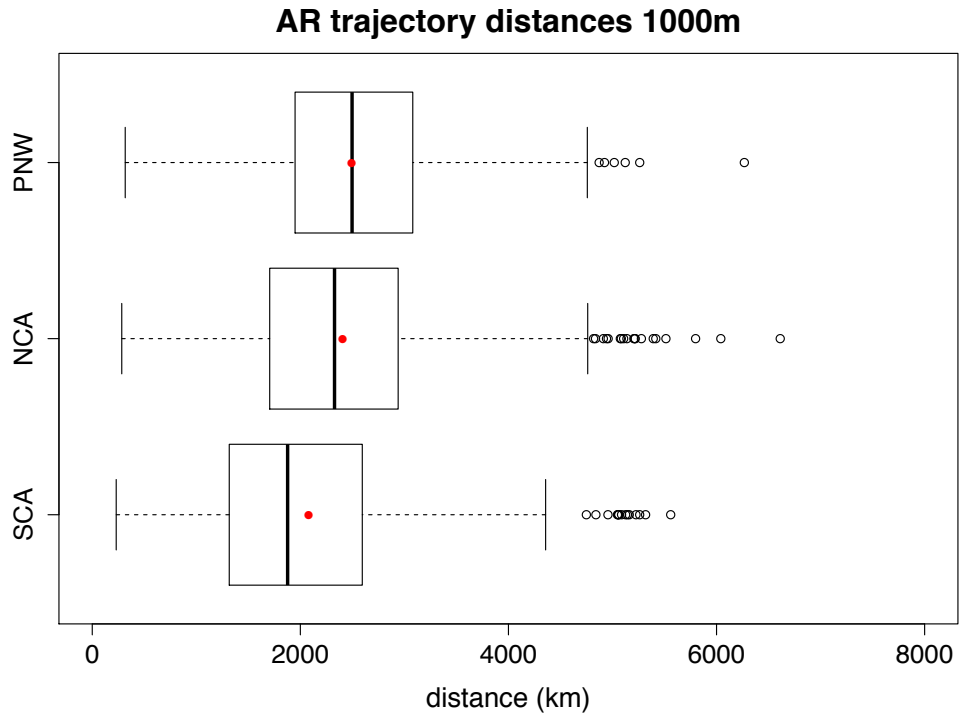
**Fig. 3.2** Boxplots depicting AR trajectory distances (km) according to landfall region and level. Box depicts interquartile range (IQR) (25th-75th percentile) and whiskers depict values within 1.5×IQR of the IQR with median (black lines) and mean (red dots) distances. Outliers are depicted as open circles. 3000 m MSL not shown

**3.3b Along trajectory characteristics**

We calculate median and interquartile along trajectory values for all ARs landfalling within specified regions to gain insight into the conditions present during AR progression. All trajectories ending at 1000 m and 2000 m MSL experience either some parcel moistening (1-3 g kg$^{-1}$) or moisture holds constant (Fig. 3.3), except for the hours directly before (0-15 hours) landfall. Moistening tends to occur at higher rates in the earlier trajectory hours, farther from landfall. Additionally, at all levels most trajectories experience subsidence ($\leq$1.75hPa hr$^{-1}$) before landfall (Fig. 3.4) (15-72 hours). This increase of moisture along with subsidence can be explained by either evaporation (e.g., from the ocean surface or from precipitation) or moisture advection by the winds (Trenberth 1999). With temperatures (Fig. 3.5), for parcels ending at 1000 m MSL we see warming (1-3 K) over the course of the trajectory, most likely due to subsidence (Fig. 3.4), whereas at 2000 m MSL temperatures stay nearly constant until the hours before landfall. Additionally, we see a gradual rise of relative humidity (Fig. 3.6) over the course of the trajectories. Towards landfall for all regions, specific humidity levels drop and air rises with corresponding drops in temperature as well as rises in relative humidity values to greater than 70% indicating orographic uplift resulting in condensation and precipitation.
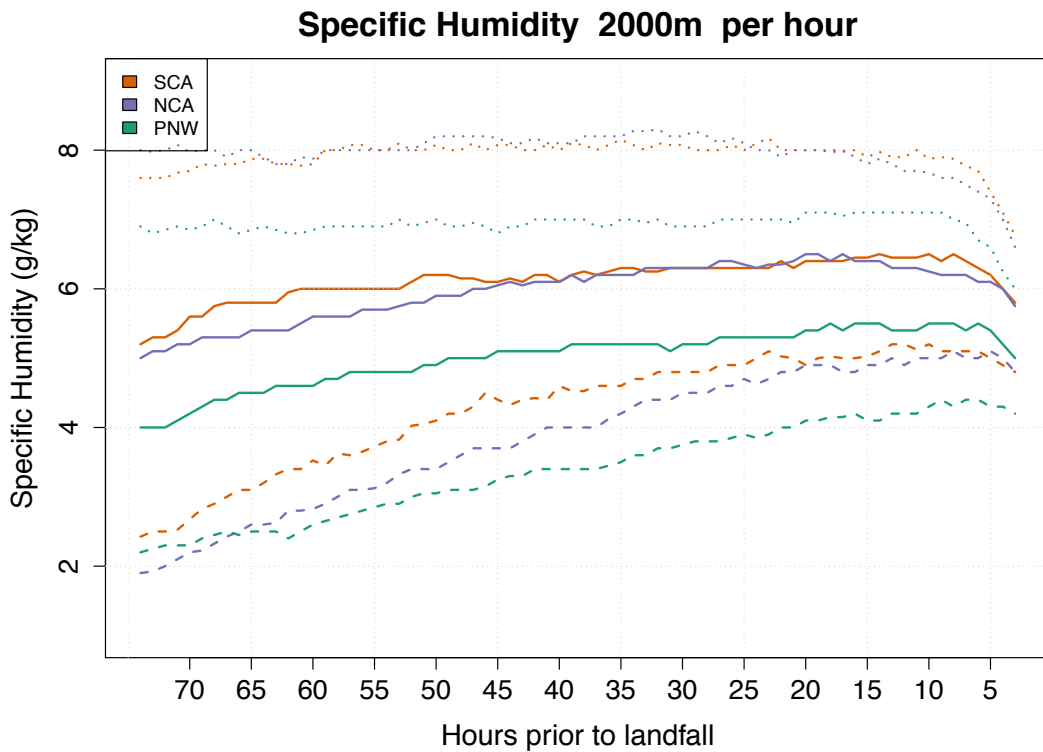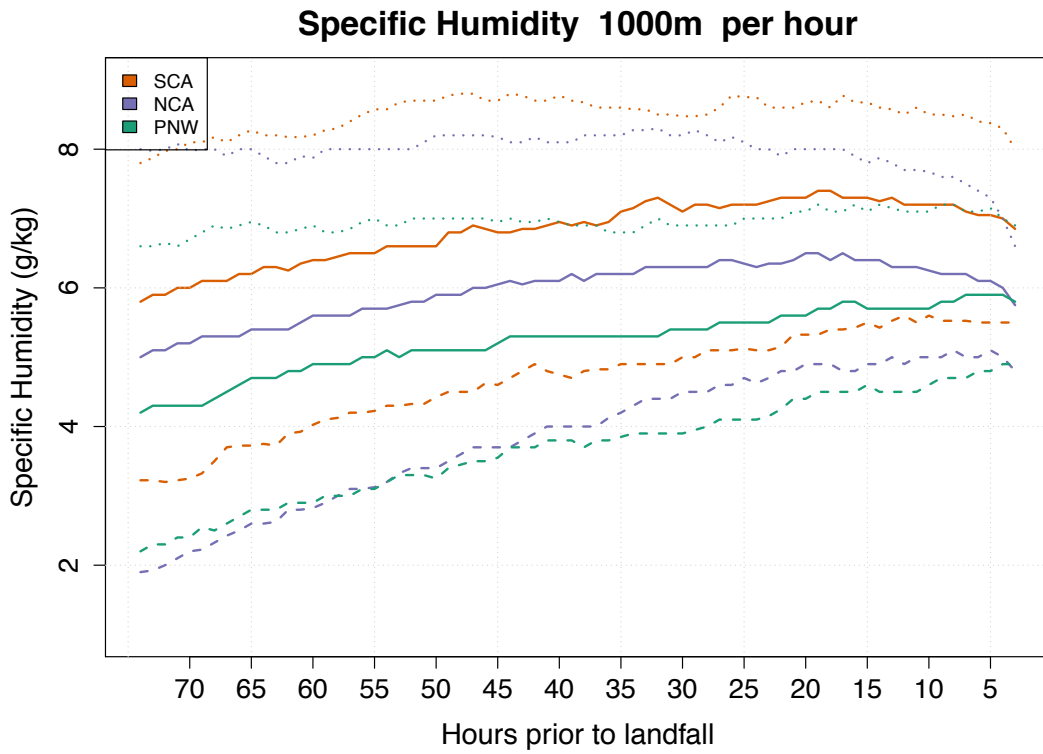
**Fig. 3.3** Time series of median (solid lines), 25th (dashed lines), and 75th (dotted lines) quartile values of hourly specific humidity (g kg^{-1}) according to landfall region and level. 3000 m MSL plot not shown.
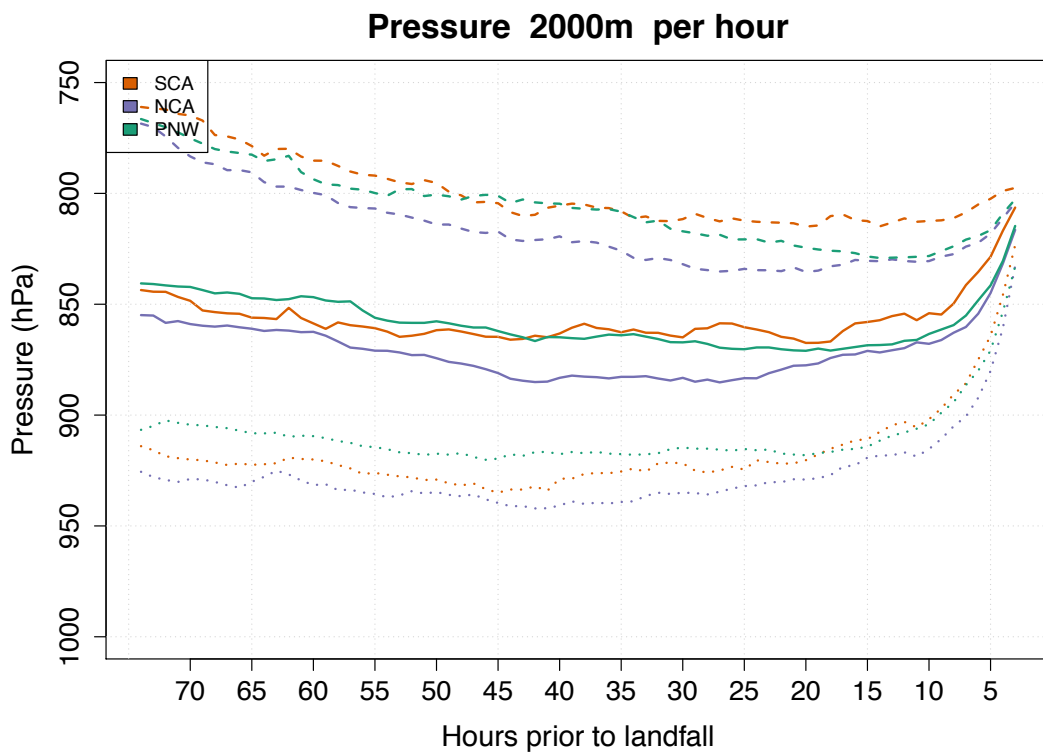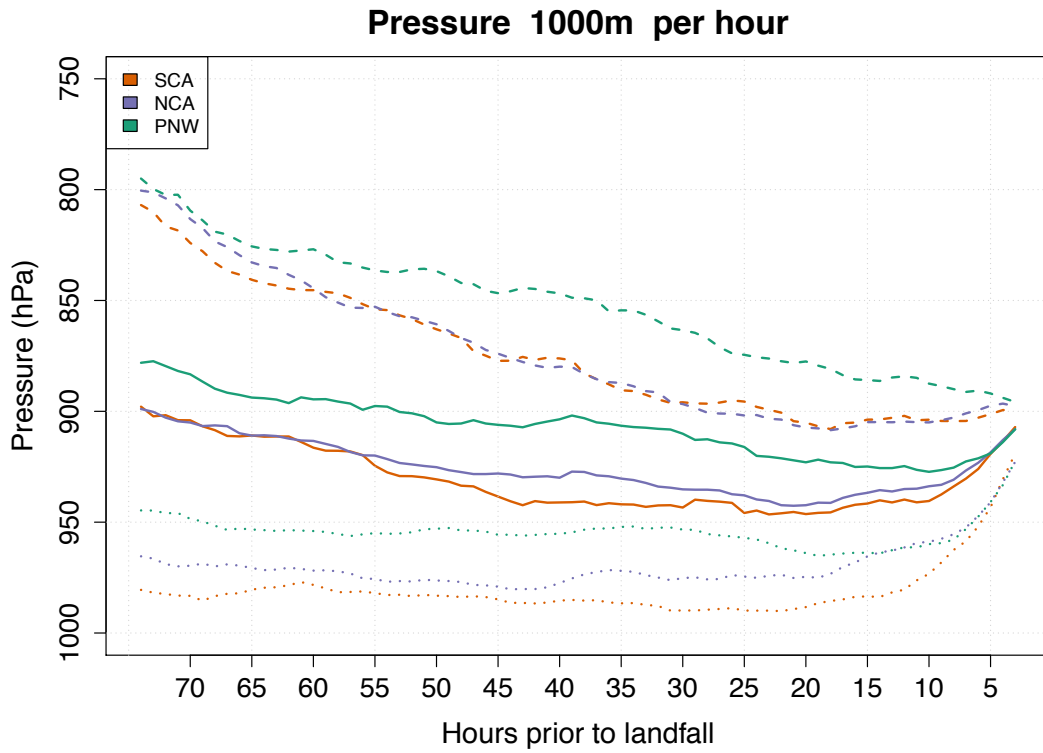
**Fig. 3.4** Same as Fig. 3.3, but for pressure (hPa). 3000 m MSL plot not shown
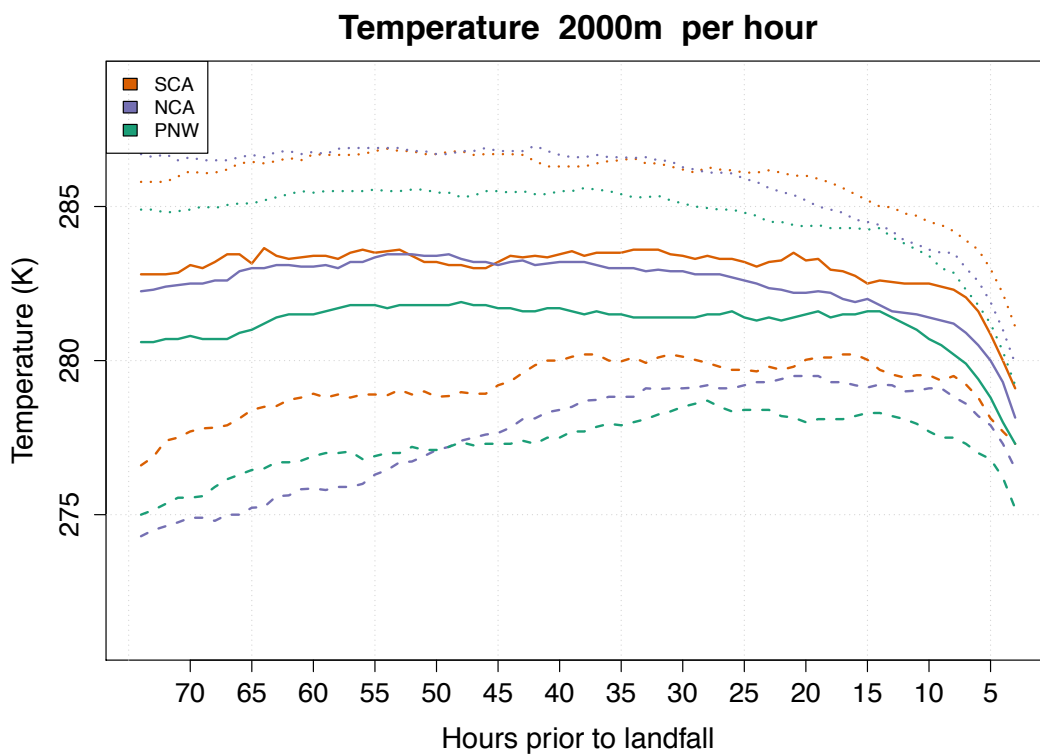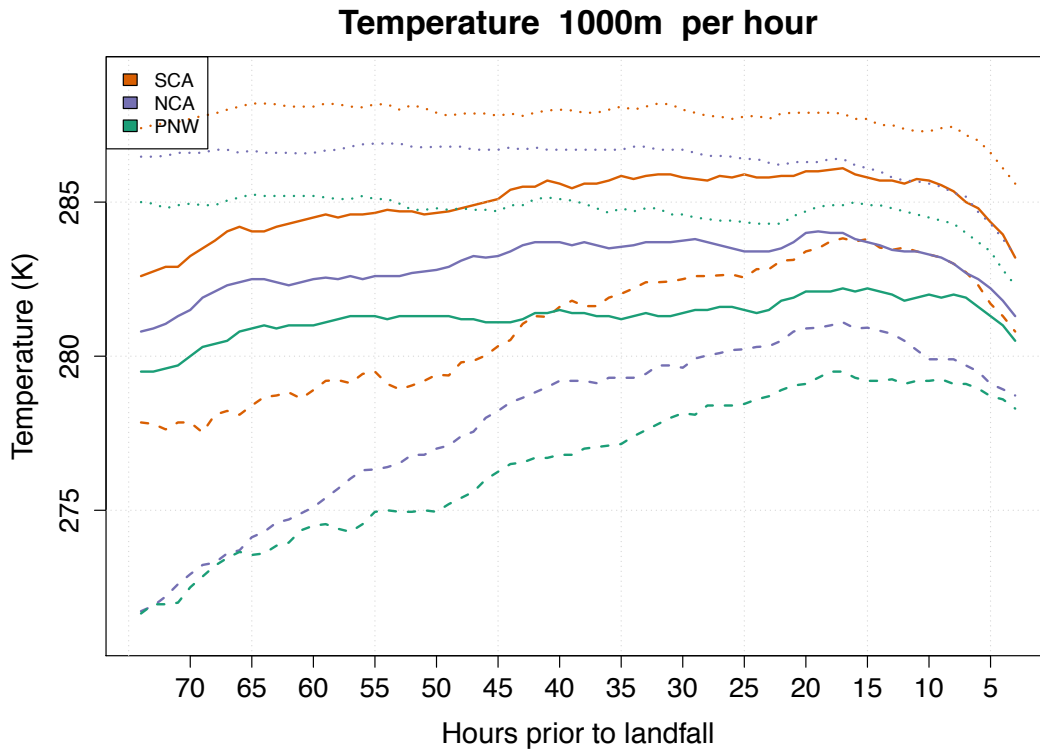
**Fig. 3.5** Same as Fig. 3.3, but for temperature (K). 3000 m MSL plot not shown
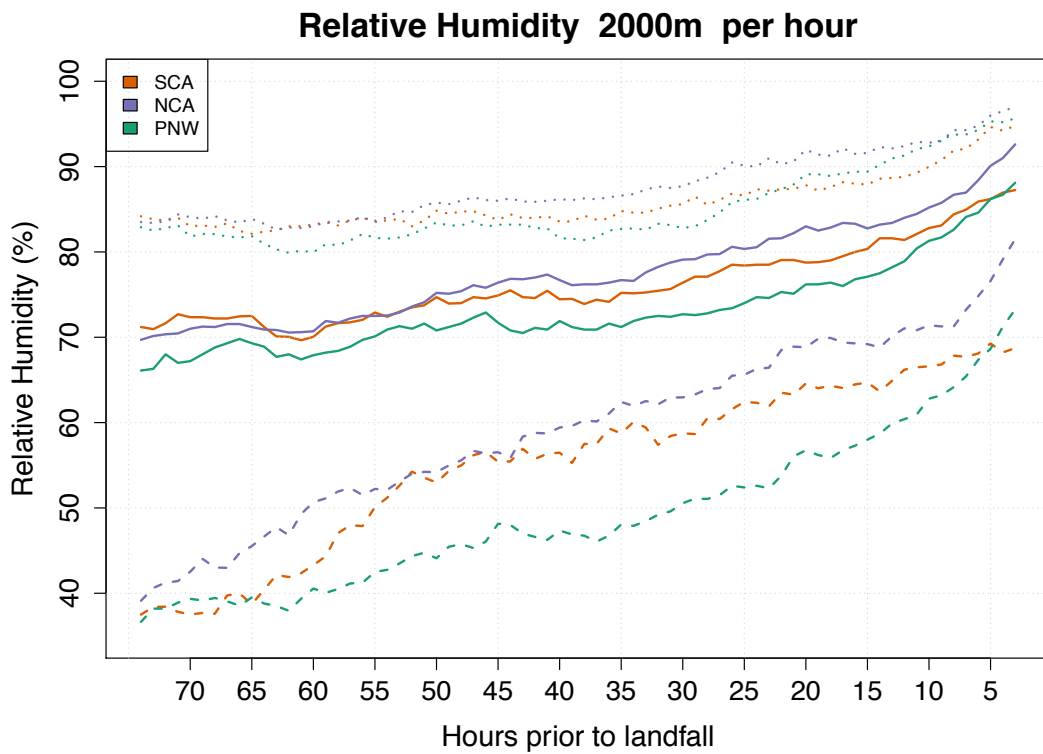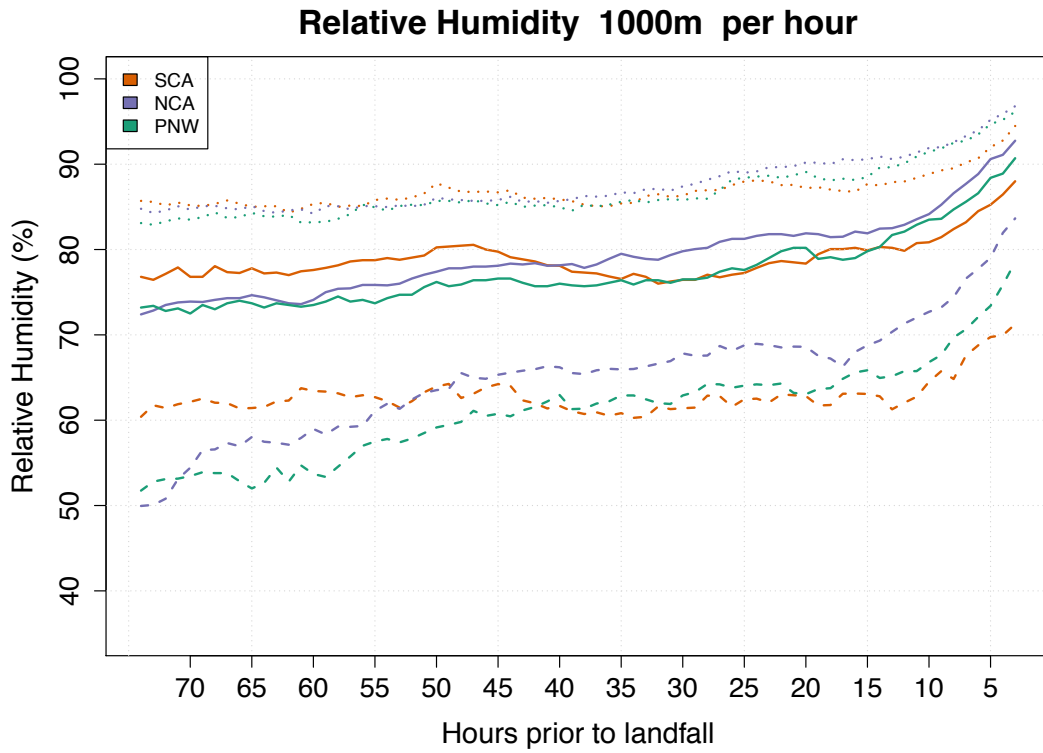
**Fig. 3.6** Same as Fig. 3.3, but for relative humidity (%). 3000 m MSL plot not shown

Boxplots show differences in along trajectory measurements of temperature and specific humidity between different landfall regions. For parcels ending at 1000 m MSL, the maximum temperatures recorded along trajectories (tmax) (Fig. 3.7) are significantly higher with a smaller interquartile range for SCA (median=288.1K IQR=4.8K) than either NCA (median=286.3K IQR=5.6K) and PNW (median=285.0K IQR=5.6K) ARs. For trajectories ending at 2000 m MSL, there are no statistically significant differences in tmax values between SCA (median=286.4K IQR=5.1K) and NCA (median=285.9K IQR=6.5K) ARs, although both SCA and NCA ARs are significantly warmer than PNW (median=284.5K IQR=5.8K) ARs. This signifies that at lower levels, SCA ARs tend to reach temperatures that are warmer than both NCA and PNW ARs and that temperatures vary the least but that differences diminish higher in the atmosphere. SCA ARs also have significantly higher temperatures recorded at landfall (tland) (Fig. 3.8) at both 1000 m and 2000 m MSL with SCA ARs having median values of 283.2K (IQR=4.8K) (min.=274.1K) at 1000 m MSL with no values below freezing (273K) and 279.1K (IQR=3.8K) at 2000 m MSL. NCA ARs have median tland values of 281.3K (IQR=4.6K) (min.=265.5K) as well as 278.2K (IQR=3.4K) and PNW with 280.5K (IQR=4.0K) (min.=269.8K) and 277.3K (IQR=4.0K), at 1000 m and 2000 m MSL respectively. At both levels, NCA ARs are also significantly warmer than PNW ARs for both tmax as well as tland. This is somewhat as expected, as SCA is closer to the equator and the environment in which ARs evolve is generally warmer. This increase in temperature with decrease in latitude is also an indicator that SCA ARs are more likely to originate/travel through warmer latitudes. Furthermore, warmer temperatures indicate events that are more likely to lead to precipitation rather than snow. While AR-induced events with temperatures below freezing (273K) are more common farther north and provide integral inputs to water budgets (e.g. Guan et al. 2013), warmer ARs have been linked to several extreme events resulting in flash flooding (e.g. Ralph et al. 2006) throughout much of the U.S.'s west coast.
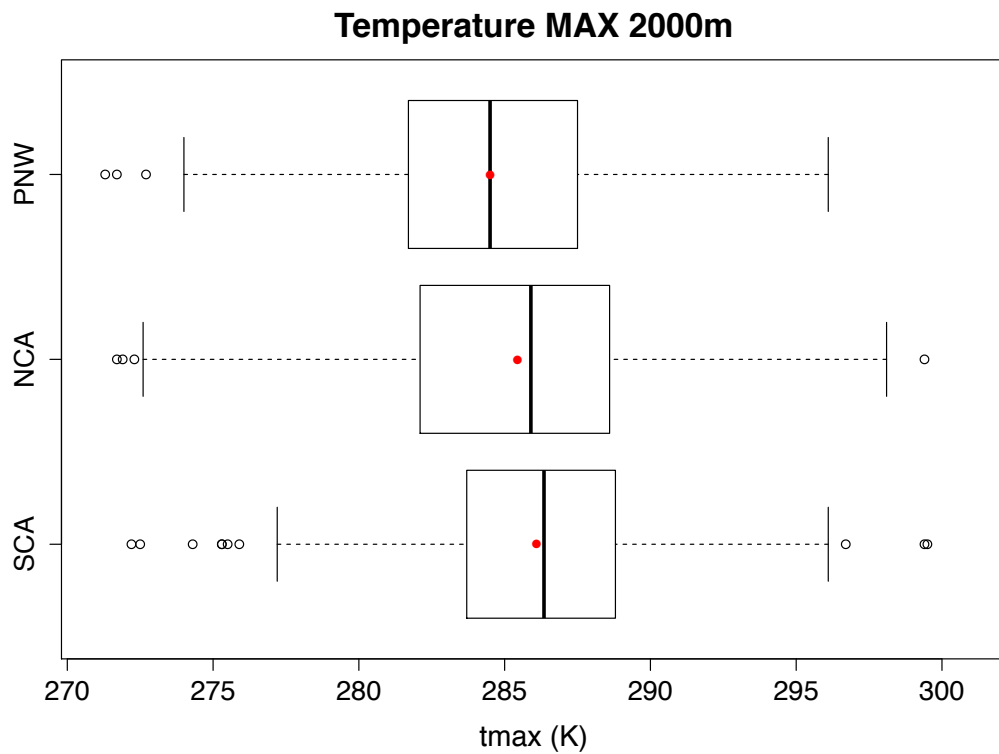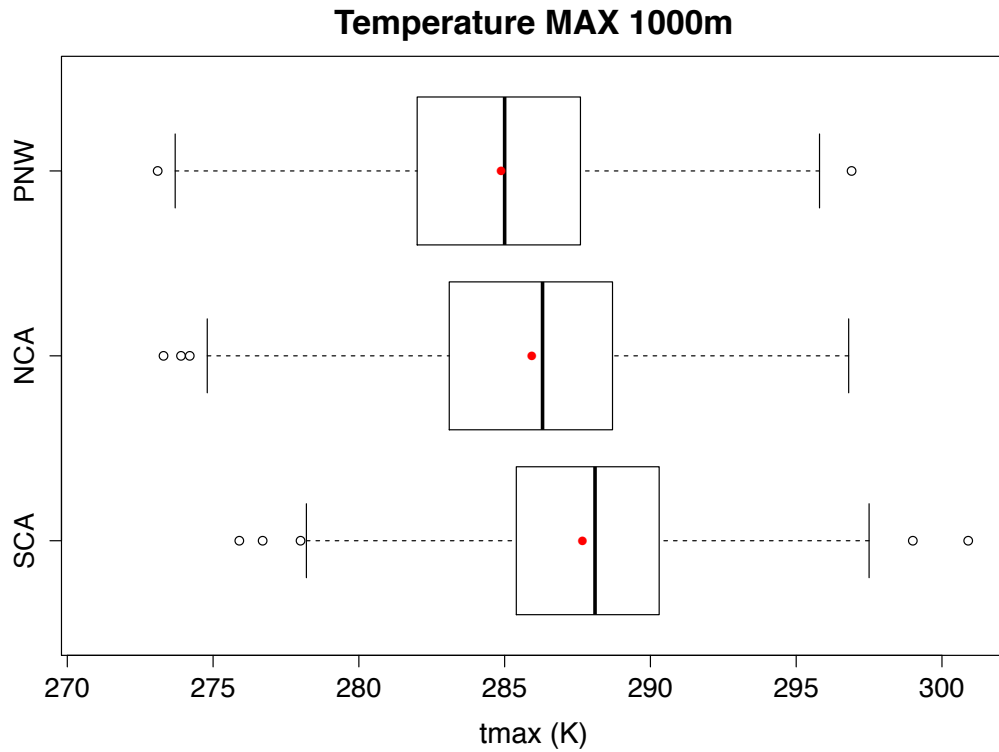
**Fig. 3.7** Boxplots depicting maximum along-trajectory temperature (tmax) (K) values for ARs according to landfall region and level. Box depicts interquartile range (IQR) (25th-75th percentile) and whiskers depict values within 1.5×IQR of the IQR with median (black lines) and mean (red dots) values. Outliers are depicted as open circles. 3000 m MSL not shown
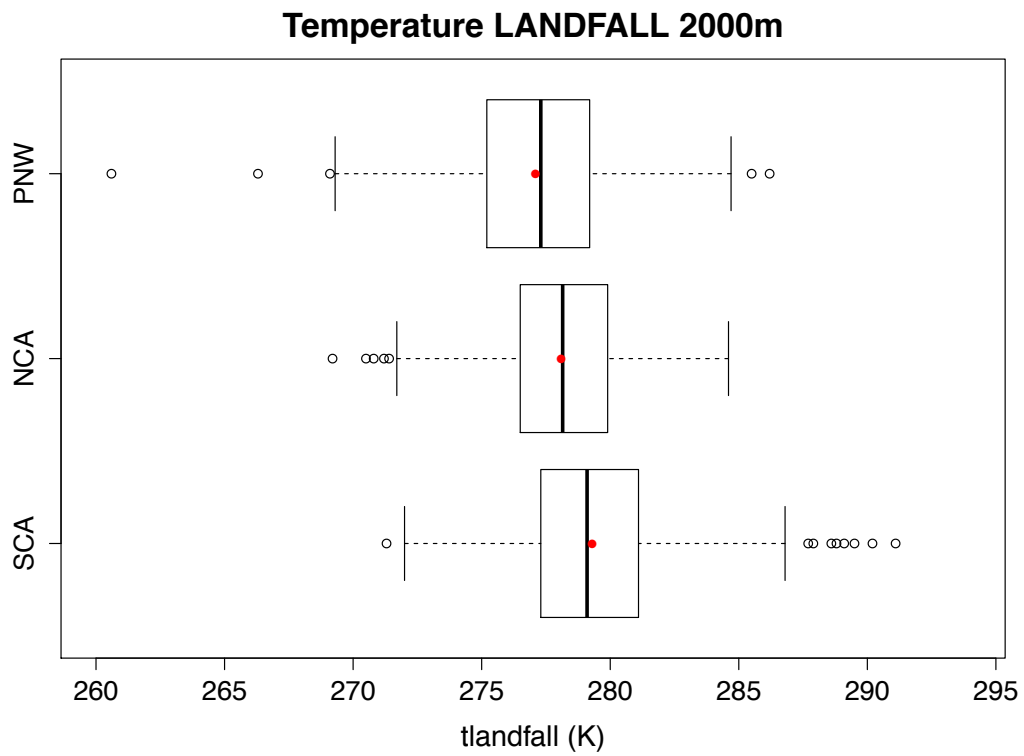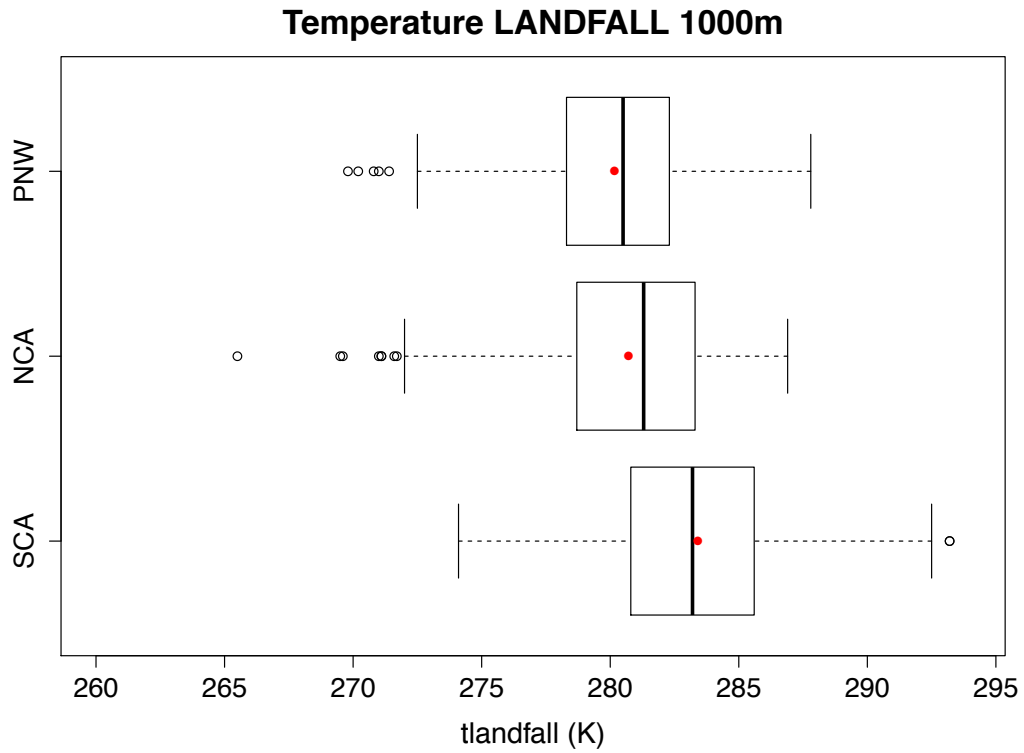
**Fig. 3.8** Same as Fig. 3.7 but for landfall temperatures (tland) (K)

To understand changes of along trajectory characteristics, we calculate differences between each trajectory's maximum measurement and their respective landfall measurement (i.e. delta = max – land). With the differences of temperature (tdelta) (Fig. 3.9), at 1000 m MSL statistically significant differences exist between SCA (median=4.1K IQR=4.3K) and NCA (median=4.6K IQR=4.6K) ARs as well as NCA and PNW (median=4.2K IQR=4.2K) ARs but not between SCA and PNW ARs. At 2000 m MSL tdelta for SCA (median=6.9K IQR=5.6K), NCA (median=7.2K IQR=5.3K), and PNW (median=7.0K IQR=4.7K) ARs are not significantly different. This indicates that SCA and PNW ARs at 1000 m MSL experience less cooling over the course of their trajectories than NCA ARs which experience more cooling. For trajectories ending at 2000 m MSL all ARs regardless of landfall location experience similar temperature changes. The higher values for tmax and tland at low levels as well as lower cooling values throughout the trajectory give SCA ARs the potential to hold more moisture, particularly at landfall.

**DELTA Temperature 1000m**

**DELTA Temperature 2000m**
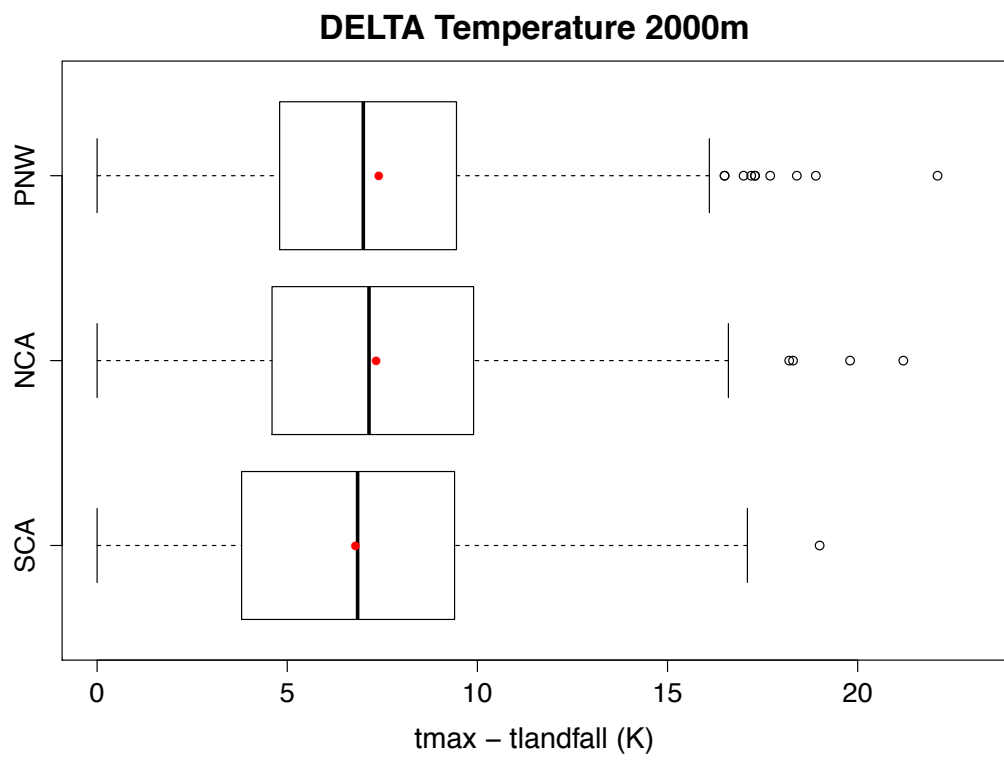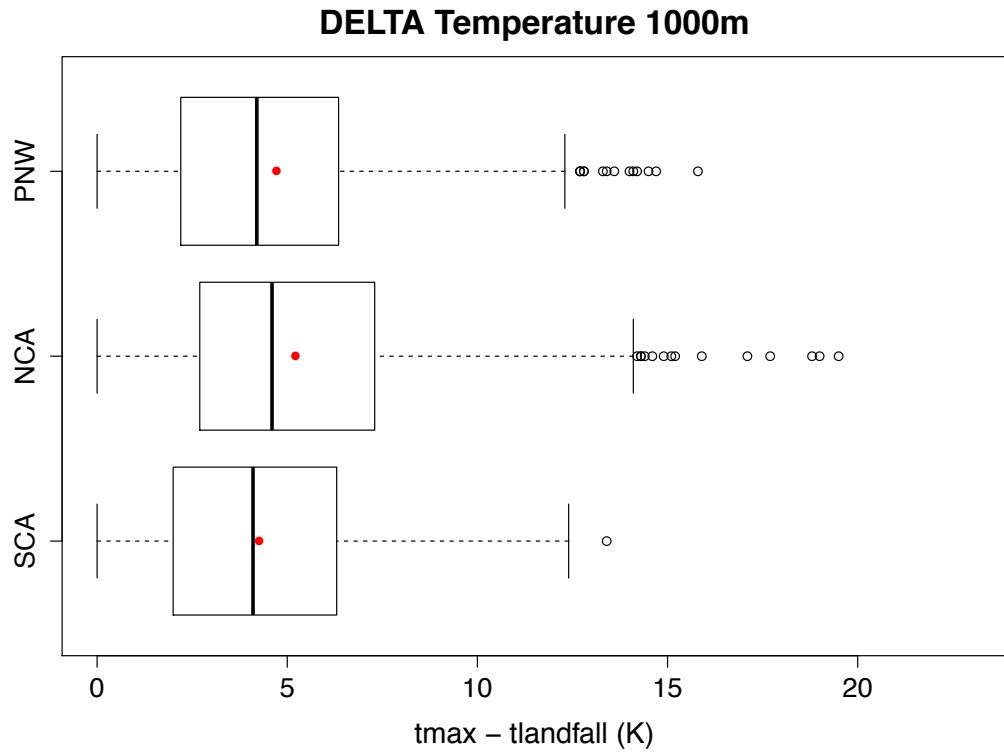
**Fig. 3.9** Same as Fig. 3.7 but for differences of temperature (tdelta) (K). Where tdelta = tmax – tland

In regards to specific humidity, differences between regions are most prominent for trajectories ending at 1000 m MSL. SCA ARs at this level have significantly higher maximum along trajectory specific humidities ($q_{max}$) (Fig. 3.10) (median=8.4gkg$^{-1}$ IQR=3.0gkg$^{-1}$) as well as specific humidities at landfall ($q_{land}$) (Fig. 3.11) (median=6.9gkg$^{-1}$ IQR=2.5gkg$^{-1}$) than both NCA ($q_{max}$ median=7.7gkg$^{-1}$ IQR=2.9gkg$^{-1}$; $q_{land}$ median=6.5gkg$^{-1}$ IQR=2.3gkg$^{-1}$) and PNW ($q_{max}$ median=6.9gkg$^{-1}$ IQR=2.7gkg$^{-1}$; $q_{land}$ median=5.8gkg$^{-1}$ IQR=2.0gkg$^{-1}$) ARs. These higher moisture values may be partially explained by the corresponding higher temperatures (Figs. 3.7-3.9) as warmer temperatures increase air's capacity to hold water vapor. At 2000 m and 3000 m MSL (not listed), SCA ($q_{max}$ median=7.8gkg$^{-1}$ IQR=3.1gkg$^{-1}$; $q_{land}$ median=5.8gkg$^{-1}$ IQR=2.0gkg$^{-1}$) and NCA ($q_{max}$ median=7.7gkg$^{-1}$ IQR=3.4gkg$^{-1}$; $q_{land}$ median=5.8gkg$^{-1}$ IQR=1.8gkg$^{-1}$) ARs have significantly higher $q_{max}$ and $q_{land}$ values than PNW ($q_{max}$ median=6.7gkg$^{-1}$ IQR=3.2gkg$^{-1}$; $q_{land}$ median=5.0gkg$^{-1}$ IQR=1.8gkg$^{-1}$) ARs but SCA and NCA ARs are comparable to one another.

**Specific Humidity MAX 1000m**



qmax (g/kg)

**Specific Humidity MAX 2000m**
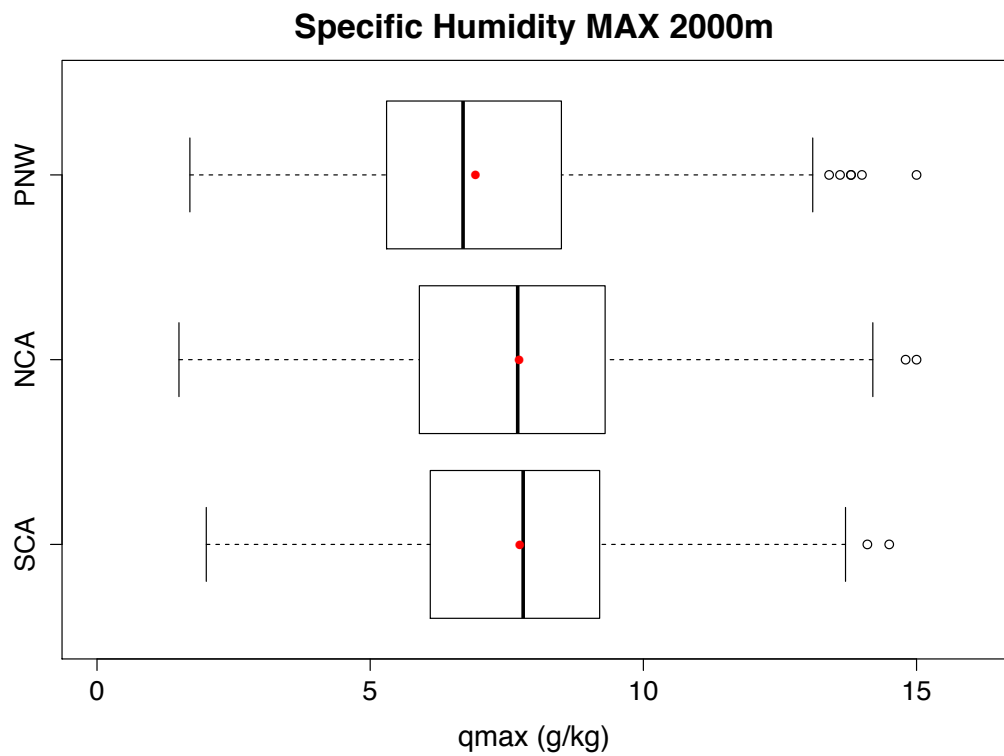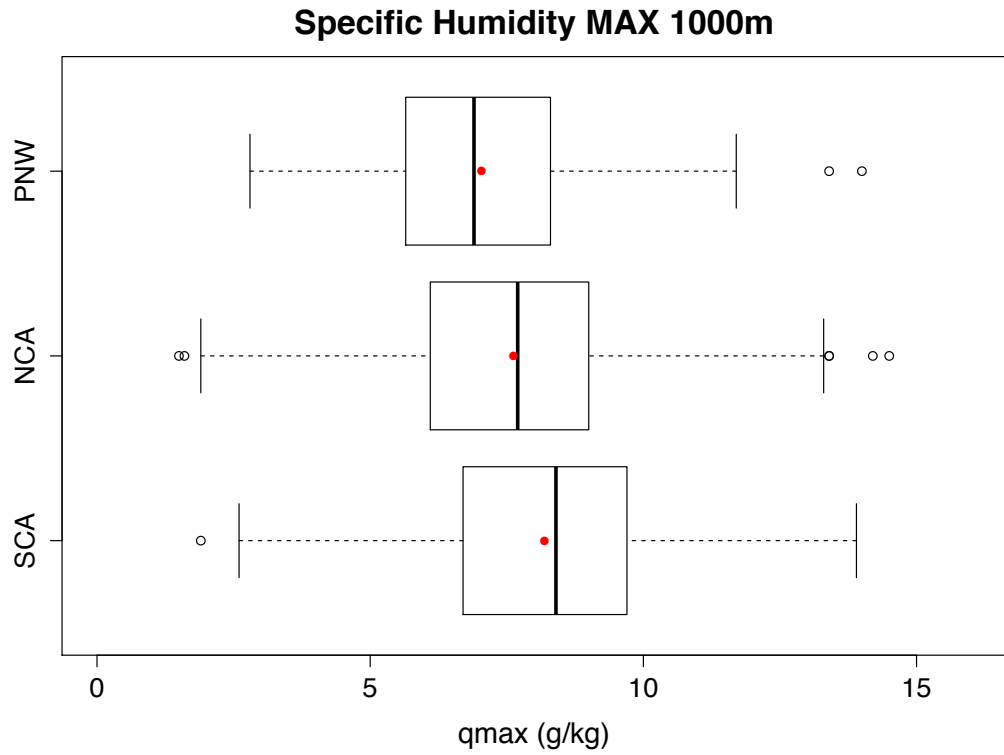


qmax (g/kg)

**Fig. 3.10** Same as Fig. 3.7 but for maximum specific humidity (qmax) (g kg$^{-1}$)

70
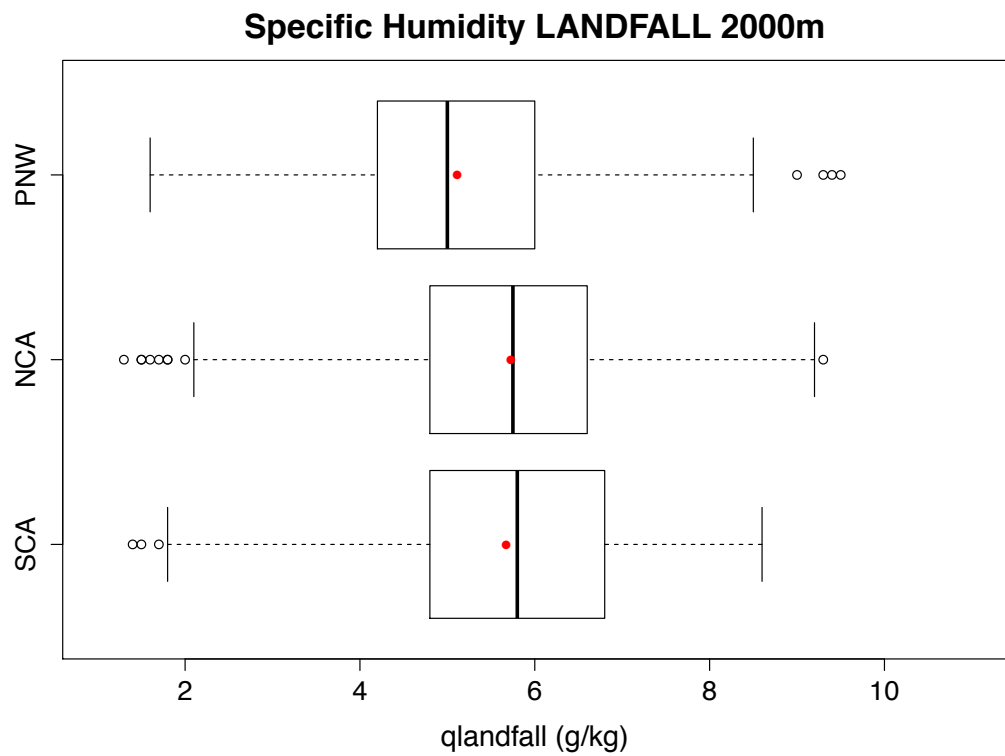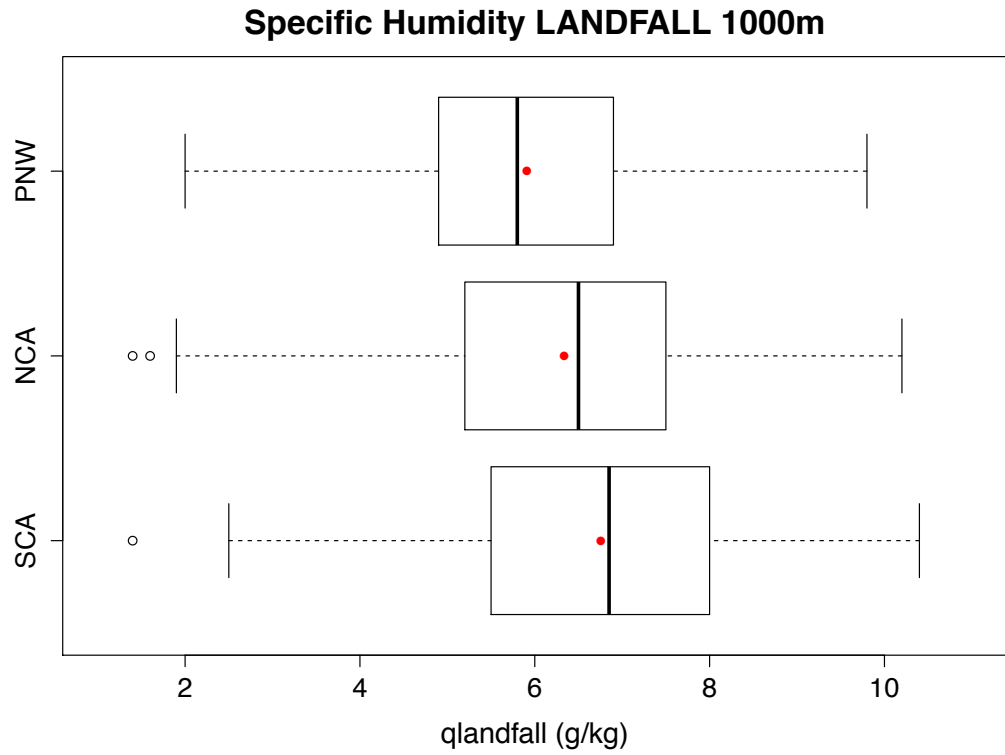
**Fig. 3.11** Same as Fig. 3.7 but for landfall specific humidity (qland) (g kg$^{-1}$)

With the differences of maximum and landfall specific humidity values along trajectories (i.e. qdelta = qmax – qland) (Fig. 3.12), for trajectories ending at 1000 m MSL, SCA (median=1.0gkg$^{-1}$ IQR=2.0gkg$^{-1}$) ARs have the highest median values and IQR but are not statistically different from NCA (median=0.9gkg$^{-1}$ IQR=1.6gkg$^{-1}$) or PNW (median=0.8gkg$^{-1}$ IQR=1.5gkg$^{-1}$) ARs. There are also no significant differences of qdelta at 2000 m MSL (not listed). This indicates that for trajectories ending at 1000 m and 2000 m MSL, ARs regardless of landfall region are experiencing similar losses of moisture along the course of their trajectories. As SCA ARs often have high qmax and qland values, they are capable of transporting large amounts of moisture to an area resulting in high-intensity storms.

## DELTA Specific Humidity 1000m



qmax – qlandfall (g/kg)

## DELTA Specific Humidity 2000m



qmax – qlandfall (g/kg)
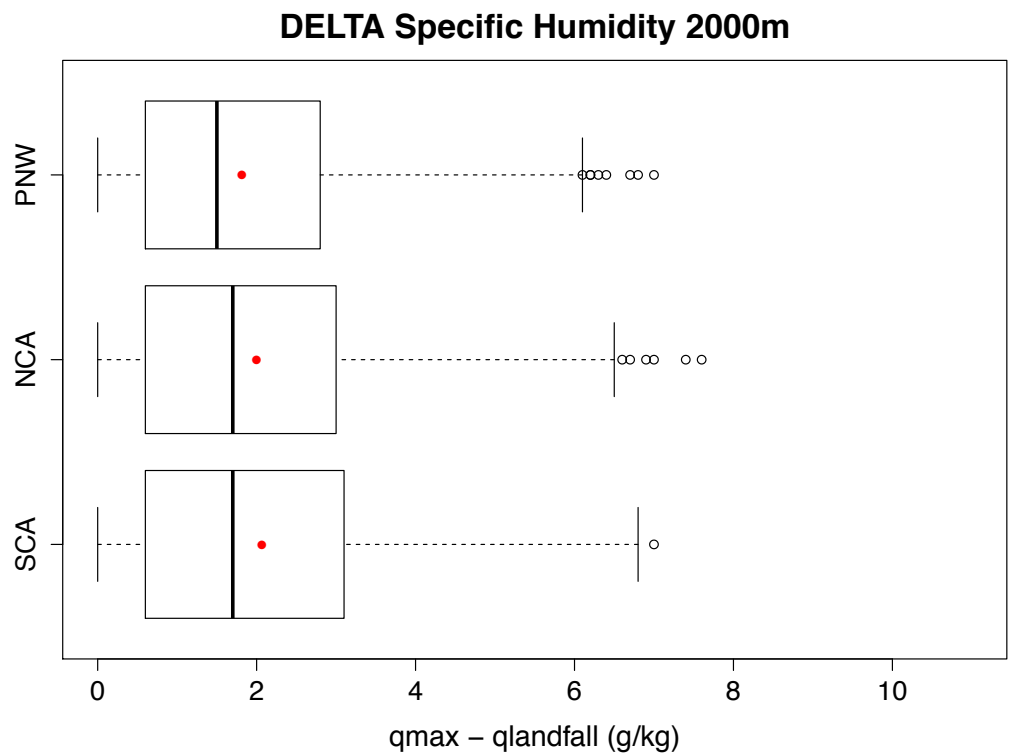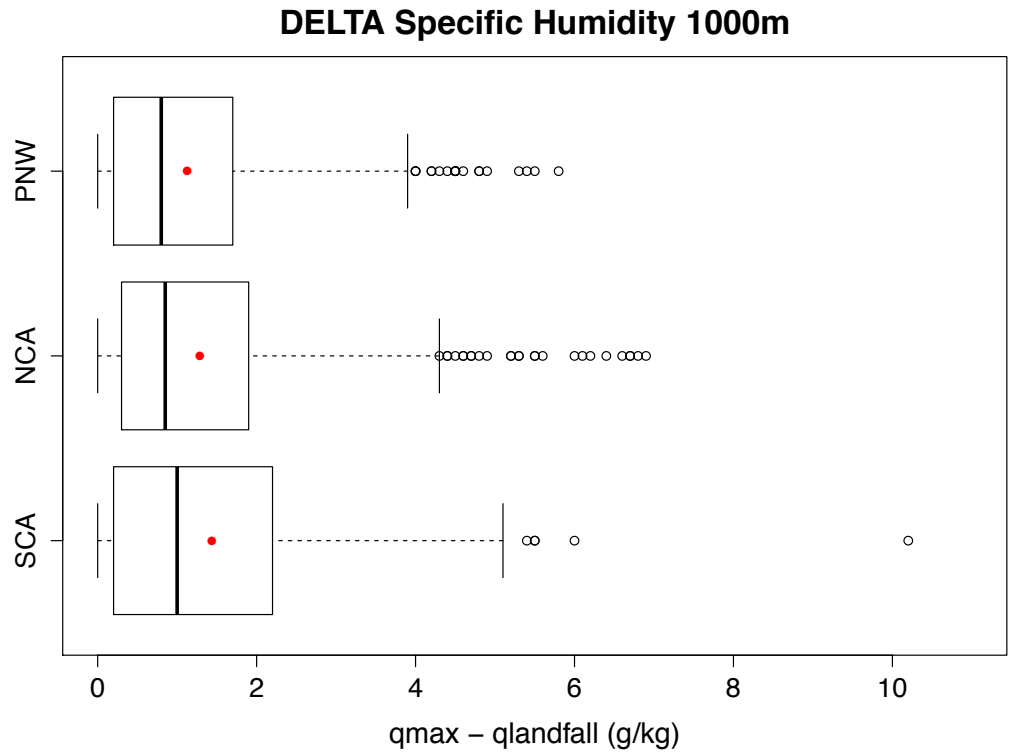
**Fig. 3.12** Same as Fig. 3.7 but for differences of specific humidity (qdelta) (g kg$^{-1}$). Where qdelta = qmax – qland

73

In an attempt to differentiate the atmospheric characteristics of SCA AR events compared to ARs landfalling farther north, we create day of landfall composites using additional CFSR fields for each landfall region. To determine if events with high specific humidity values differ in their atmospheric qualities, composites are created for events exceeding the 75th percentile for both $q_{max}$ and $q_{land}$ at 1000 m and 2000 m MSL. Figure 3.13 show composites for events exceeding the $q_{land}$ 75th percentile for trajectories ending at 1000 m MSL. Composites for events exceeding the $q_{max}$ 75th percentile (not shown) as well as trajectories ending at 2000 m MSL (not shown) show similar results.

Overall for all regions, on the day of landfall there is a plume of enhanced TPW ($\geq$20mm) extending to the coast from lower latitudes, between areas of low and high sea level pressure (SLP) (Fig. 3.13). There is an offshore trough and onshore ridge with strong winds funneling moisture towards the coast. Yet, for SCA ARs there is a continuous track of higher ($\geq$25mm) TPW values extending from south of 30°N compared to ARs landfalling farther north which have lower and/or discontinuous TPW values. Along with a weaker SLP gradient and a shallow onshore trough, there is increased zonal flow for SCA ARs. Whereas the SLP gradient is strongest and the onshore ridge most amplified for PNW ARs. All of this is consistent with the median AR trajectory orientations discussed earlier (Fig. 3.1).
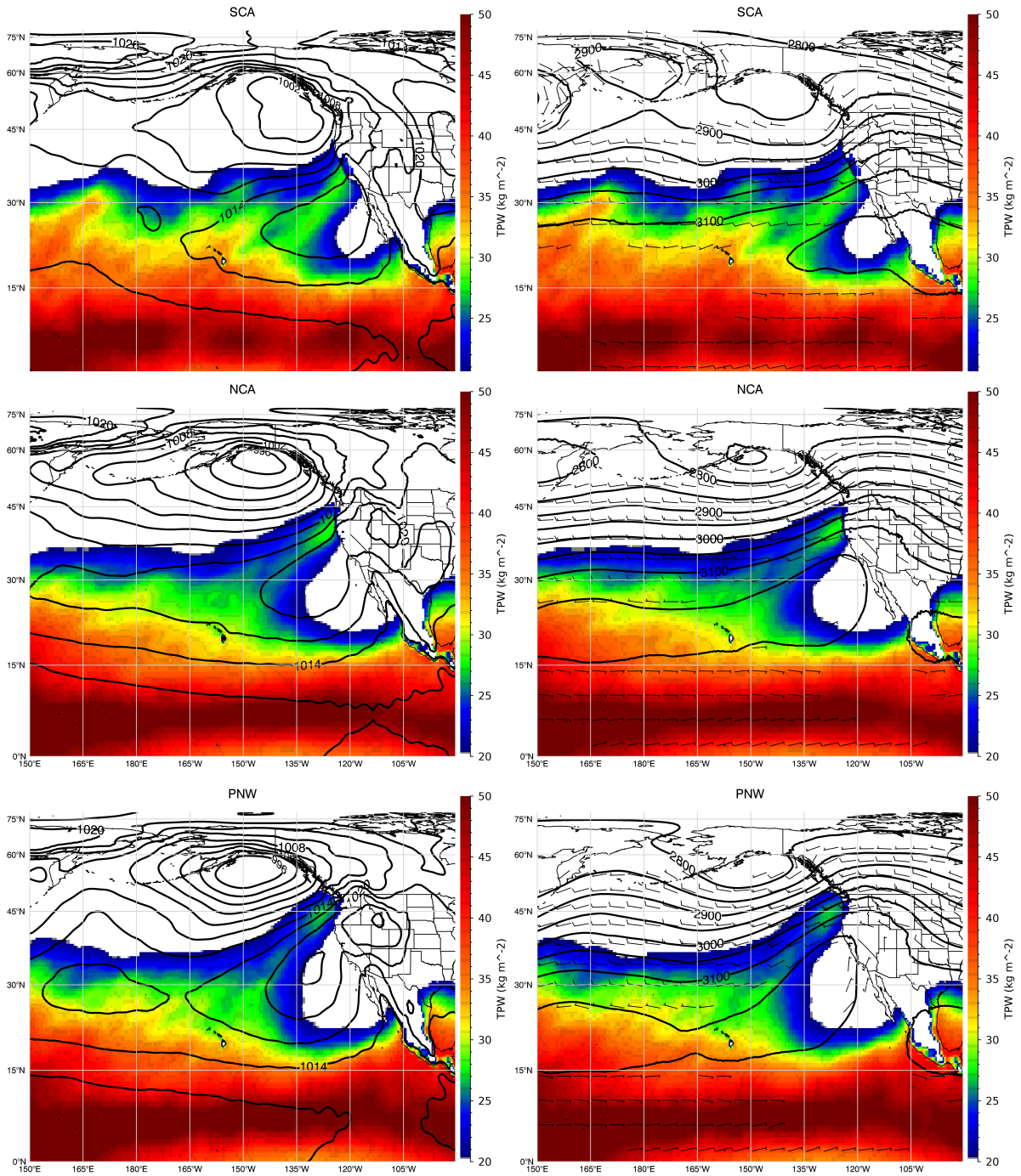
**Fig. 3.13** Composite atmospheric conditions for AR landfall days according to landfall region. (Left) Sea level pressure (hPa) (contours) and total precipitable water (kg m$^{-2}$) (fill). (Right) 700mb geopotential heights (gpm) (contours), total precipitable water (fill), and winds (m s$^{-1}$) (barbs). Note that the minimum value for total precipitable water is 20 and wind is 5, with smaller values not shown.

## 3.4 Case Study Analysis

In this section, we describe a powerful AR event to affect SCA on February 17, 2017 (021717). After years of persistent drought, the 2016-2017 water season brought significant precipitation to California. The 021717-event delivered torrential rainfall and strong winds to several coastal SCA cities including Santa Barbara, Ventura, and Los Angeles leading to flooding of low lying areas (dailynews.com[3]) as well as tree and structural damage (ktla.com[4]) costing the state millions in reported repairs (fortune.com[5]). This event was a well forecasted AR that by the time of landfall in SCA, had strengthened from initial forecasts. Additionally, this event occurred during a period of enhanced Madden-Julian Oscillation (MJO) activity according to NOAA's Climate Prediction Center[6]. On and days before 021717, the MJO was in phase eight[6] with the MJO signal evident in the central Pacific Ocean and into the Western Hemisphere (Zhang 2005). MJO activity is linked to high-intensity rainfall values throughout the western coast of North America (Jones and Carvalho 2012). Also, Payne and Magnusdottir (2014) conclude that higher frequencies of landfalling ARs to North America's west coast occur during phase 8 of the MJO.

We use previously described CFSR reanalysis fields to examine the synoptic conditions on the day of and in the hours leading up to 021717's landfall. We also use Global Precipitation Mission (GPM) data from the National Aeronautics and Space Administration to illustrate the event's rainfall. Specifically, we use 30-minute Integrated Multi-satellitE Retrievals for GPM (IMERG) available on a 0.1° × 0.1° spatial resolution spanning 60°N-S. Briefly, IMERG is a multi-satellite algorithm that uses estimates computed from various passive microwave sensors

---

[3] Web article at dailynews.com/general-news/20170217/chp-works-to-shut-down-5-freeway-after-chaotic-rain-floods-lanes-in-sun-valley

[4] Web article at ktla.com/2017/02/17/storm-forecast-as-strongest-of-season-prompts-flash-flood-watches-mudslide-concerns

[5] Web article at fortune.com/2017/02/25/california-storm-damage-costs

[6] NOAA CPC Update at cpc.ncep.noaa.gov/products/precip/CWlink/MJO/ARCHIVE/PDF/mjo_evol-status-fcsts-20170220.pdf

combined with microwave geo-IR fields that are then modified with monthly rain gauge surface data (Huffman et al. 2017). More information about IMERG can be found in Huffman et al. (2017). We use HYSPLIT to create backward trajectories for this event to determine how this AR compares to average SCA ARs. Like before, we force HYSPLIT with 1° GDAS, calculating 72–h backward trajectories ending at February 17, 2017 1800 UTC. We choose 1800 UTC as this hour aligns well with the precipitation and synoptic conditions discussed below. We calculate nine backward trajectories at each level for three levels, 1000 m, 2000 m, and 3000 m MSL.

### 3.4a Synoptic Conditions

IMERG precipitation data for 021717 1800 UTC (Fig. 3.14) depicts light precipitation values (≤5mm) throughout California including areas offshore. Rainfall corresponds to a comma formation typical to extratropical cyclones. A narrow band of high precipitation (≥11mm) occurs ahead of the presumed cold front location, impinging on the Santa Ynez Mountains. This area of strong rainfall is associated with the defined AR event, consistent with Dettinger et al. (2015) and Eiras-Barca et al. (in review) who state that AR moisture transport related to extratropical cyclones occurs in the pre-cold frontal area, and is separate as well as distinct from precipitation within the warm conveyor belt area closest to the center of the extratropical cyclone. These narrow bands of moisture and subsequent precipitation reach a maximum if an AR contacts an orographic barrier such as a mountain range (Eiras-Barca et al. in review) as seen with this AR and the Santa Ynez Mountains.
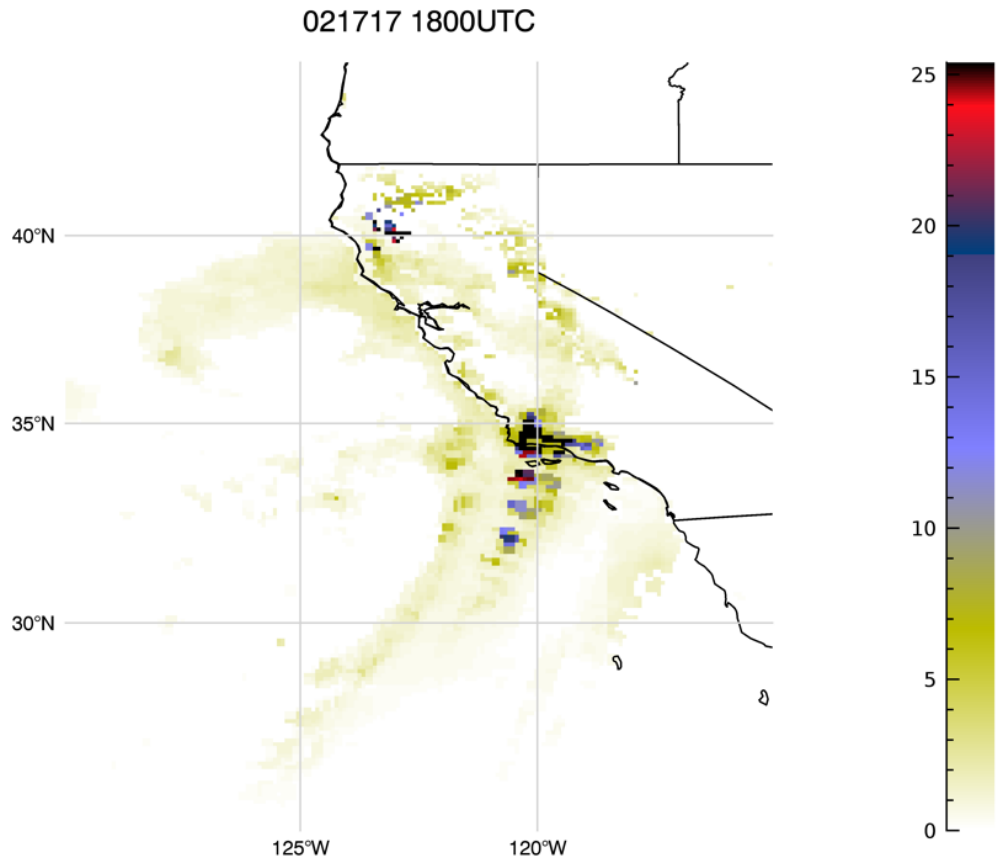
**Fig. 3.14** Gridded (0.1° × 0.1°) Global Precipitation Measurement rainfall data (in mm) for the 021717 case study event at 1800 UTC

Reanalysis (Fig. 3.15) on February 16, 2017 (021617) 0600 UTC depicts a corridor of strong westerly / southwesterly 850mb flow associated with a low-pressure system offshore from Washington / British Columbia and a corresponding TPW plume with values ≥20 mm extending from the Hawaiian Islands to northern California / southern Oregon. At 500mb there is a wide offshore trough along with vorticity maximums offshore from the Washington / Oregon coast. There are strong geopotential height gradients between both offshore troughs and onshore ridges at 850mb and 500mb. After initial AR landfall, TPW values migrate southward and weaken along

with winds. By 021617 1800 UTC we see the development of a frontal wave at 850mb. This wave strengthens on 021717 0600 and 1800 UTC and develops into a low-pressure system which can be seen in both geopotential height as well as absolute vorticity fields. This leads to the shifting in the offshore trough's axes, encouraging movement of strong wind and moisture towards SCA and it allows for the augmentation of TPW seen in 021717 0600 UTC, due to increased convergence along the cold front (e.g. Bao et al. 2006). This mesoscale frontal wave and development of a second low-pressure system are the primary reasons for this storm's high-intensity.
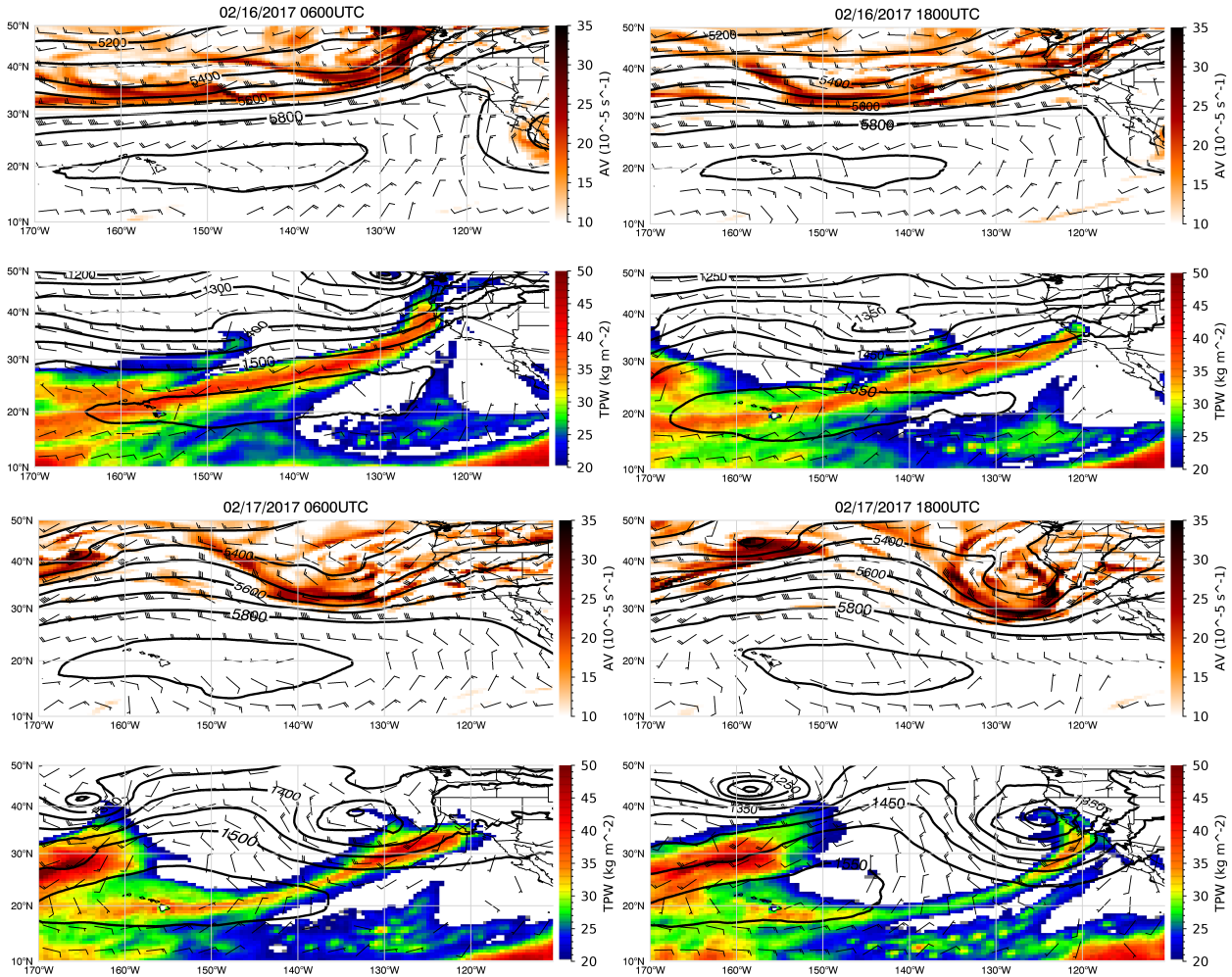
**Fig. 3.15** Atmospheric conditions for the 021717 case study event from reanalysis. Each figure consists of two images. (Top) 500mb geopotential heights (gpm) (contours), absolute vorticity ($10^{-5}$ $s^{-1}$) (fill), and winds (m $s^{-1}$) (barbs). (Bottom) 850mb geopotential heights (contours), total precipitable water (kg $m^{-2}$) (fill), and winds (barbs). Note that the minimum value for absolute vorticity is 10, wind is 5, and TPW is 20, with smaller values not shown. Titles state observation times with 021617 0600 UTC (top left), 021617 1800 (top right), 021717 0600 (bottom left), and 021717 1800 (bottom right)

### 3.4b HYSPLIT Analysis

For the variations of spatial location and temporal along trajectory characteristics, we use the medians of the nine trajectories at each level. According to the temporal characteristics (Fig.

80

3.16a–d), trajectories ending at each level are mostly consistent with the regional characteristics examined earlier. There are decreases in pressure (Fig. 3.16a) ~12 hours before and during landfall for all three levels along with increases of relative humidity (Fig. 3.16b) with values reaching over 90%, decreases of temperature (Fig. 3.16c), and increases of specific humidity (Fig. 3.16d), which are all consistent with orographic uplift and subsequent precipitation. In the 72 hours before landfall, pressure remains relatively constant whereas in the regional averages there is an increase of pressure indicative of subsidence. The trajectories ending at 1000 m MSL remain close to the sea surface until lifting begins while trajectories ending at 2000 m and 3000 m MSL remain at low altitudes (>900hPa) until lift. Relative humidity is high (>75%) in the hours before landfall with increases in relative humidity towards landfall. Temperatures before landfall stay relatively constant at each level. For specific humidity, at 1000 m and 2000 m MSL there are increases over the course of the trajectory but at 3000 m MSL specific humidity decreases.

**(a) CS Pressure per hour**
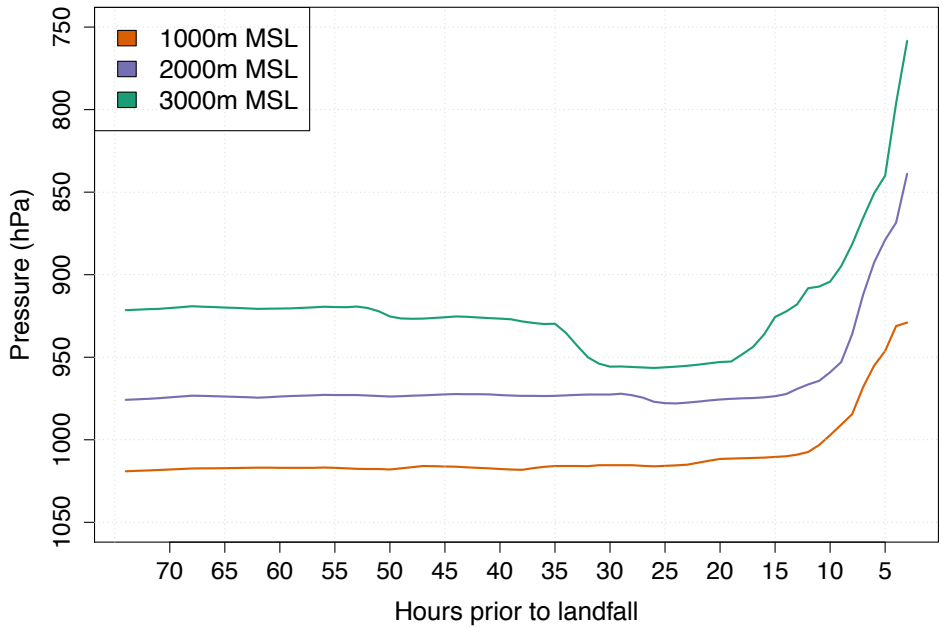
**(b) CS Relative Humidity per hour**
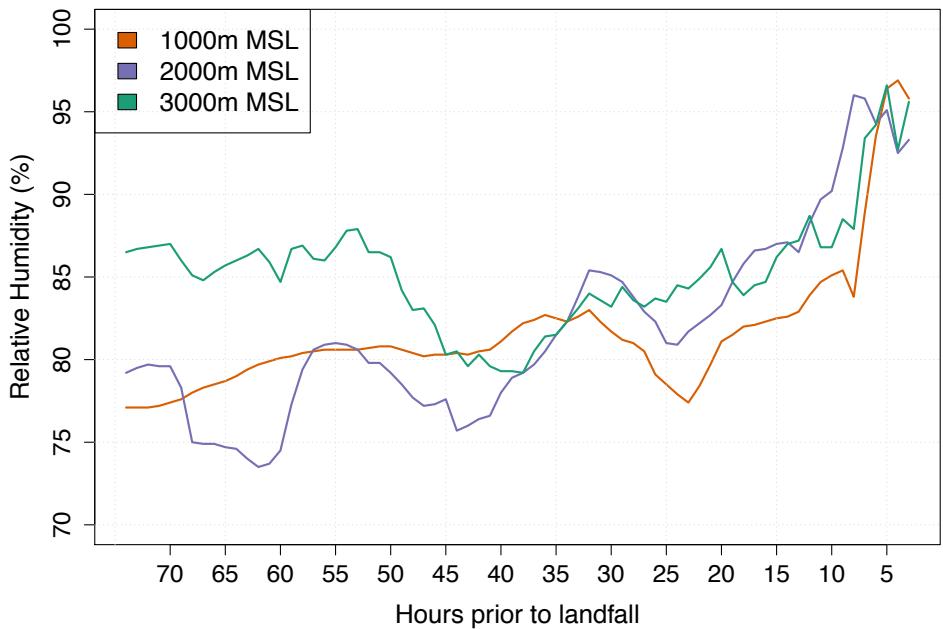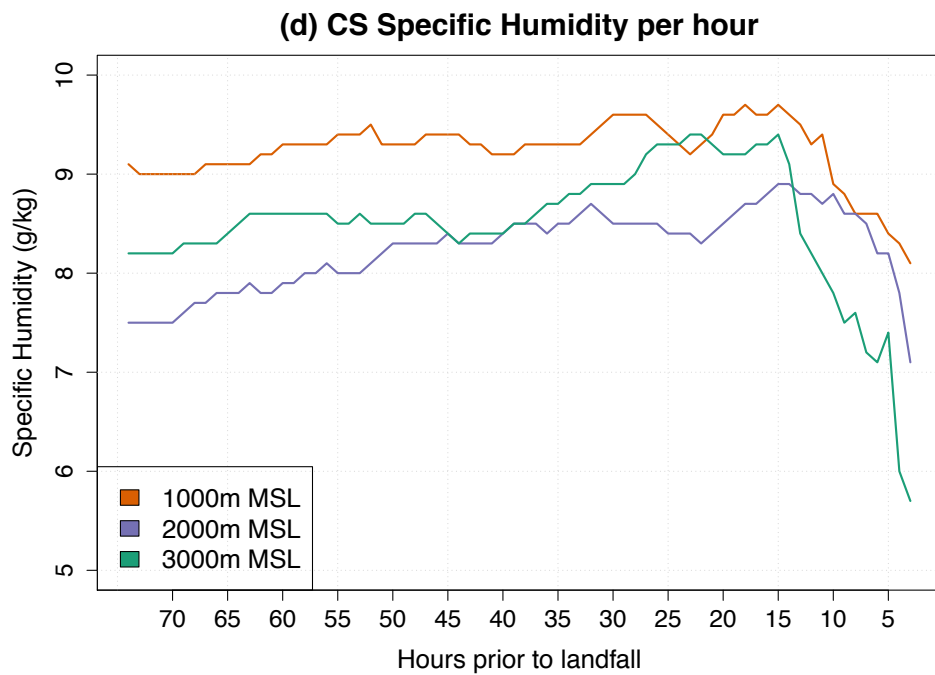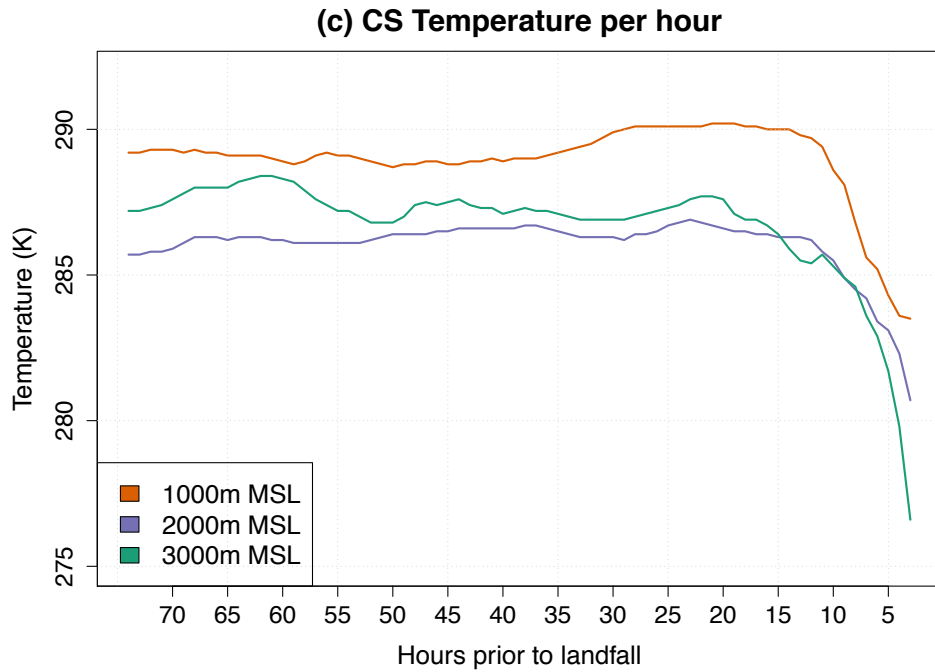
**Fig. 3.16** Hourly time series of median along-trajectory values for the 021717 case study event according to landfall level. Observed characteristics include **a** pressure (hPa), **b** relative humidity (%), **c** temperature (K), and **d** specific humidity (g kg$^{-1}$)

Overall, this AR has much higher specific humidity values and slightly higher temperatures than the previously examined ARs including those that made landfall in SCA. In terms of qmax (Fig. 3.17), this event has higher median values (9.8gkg$^{-1}$ at 1000 m MSL, 8.9gkg$^{-1}$ at 2000 m MSL, and 9.7gkg$^{-1}$ at 3000 m MSL) at all levels than all regional ARs with values surpassing SCA's 75th percentile for qmax moisture at 1000 m and 3000 m MSL. An analysis of CFSR reveals that the climatological mean specific humidity values during February (1979-2015) for (ocean) grid cells between 220°-240°E and 20°-35°N at 925mb is 6.6gkg$^{-1}$, 3.6gkg$^{-1}$ at 850mb, and 1.8gkg$^{-1}$ at 700mb (not shown). Thus, specific humidity for this event was far above regional moisture averages for the season. At all levels this AR has the highest qland values (Fig. 3.17) (qland medians: at 1000 m MSL 8.1gkg$^{-1}$, 2000 m MSL 7.1gkg$^{-1}$, and 3000 m MSL 5.7gkg$^{-1}$) and surpasses the 75th percentile for qland measured moisture for SCA ARs at all levels as well. Additionally, this AR also has higher tmax values (Fig. 3.18) (medians: at 1000 m MSL 290.2K, 2000 m MSL 287.3K, and 3000 m MSL 289.1K) at all levels but, median tland temperature values (Fig. 3.18) (medians: at 1000 m MSL 283.5, 2000 m MSL 280.7K, and 3000 m MSL 276.6K) are comparable to other SCA ARs (Figs. 3.7–3.8). This may be due to this event originating from much lower in the troposphere (Fig. 3.16a) and unlike regional averages, these trajectories do not experience long duration subsidence. These very high specific humidity values and high temperatures account for the high-intensity rainfall (Fig. 3.15) seen during this event. We also see that over the course of 72-h these trajectories have shorter trans-Pacific pathways (Fig. 3.19) indicating a very slow-moving system, but are consistent with previous results in that 1000 m MSL (median=1282.85km) trajectories are the shortest followed by 2000 m (median=1478.51km) and then 3000 m MSL (median=2122.66km) trajectories (Fig. 3.20). Although, in the 72 hours before landfall these trajectories travel from south of 30°N, indicating more tropical sources of moisture and high overall temperatures.
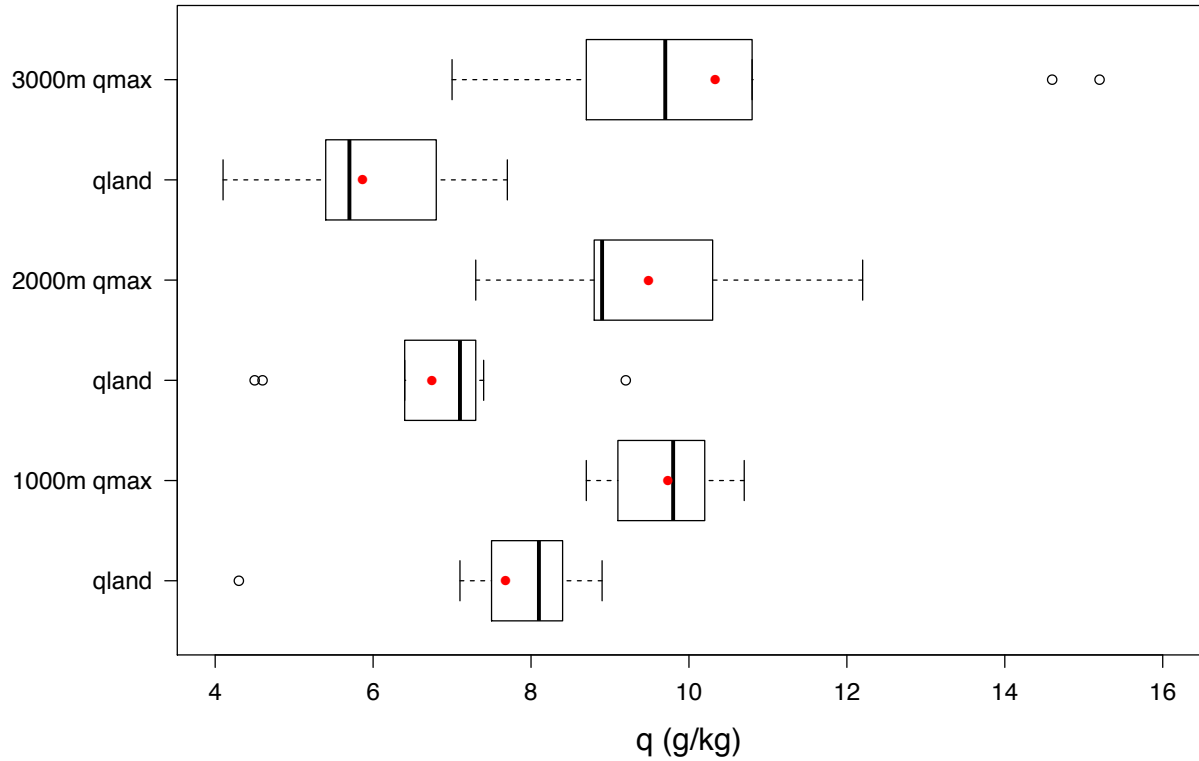
**Fig. 3.17** Boxplots of trajectory maximum (qmax) and landfall (qland) specific humidity values for the 021717 case study event according to landfall level. Box depicts interquartile range (IQR) (25th–75th percentile) and whiskers depict values within 1.5×IQR of the IQR with median (black lines) and mean (red dots) values. Outliers are depicted as open circles
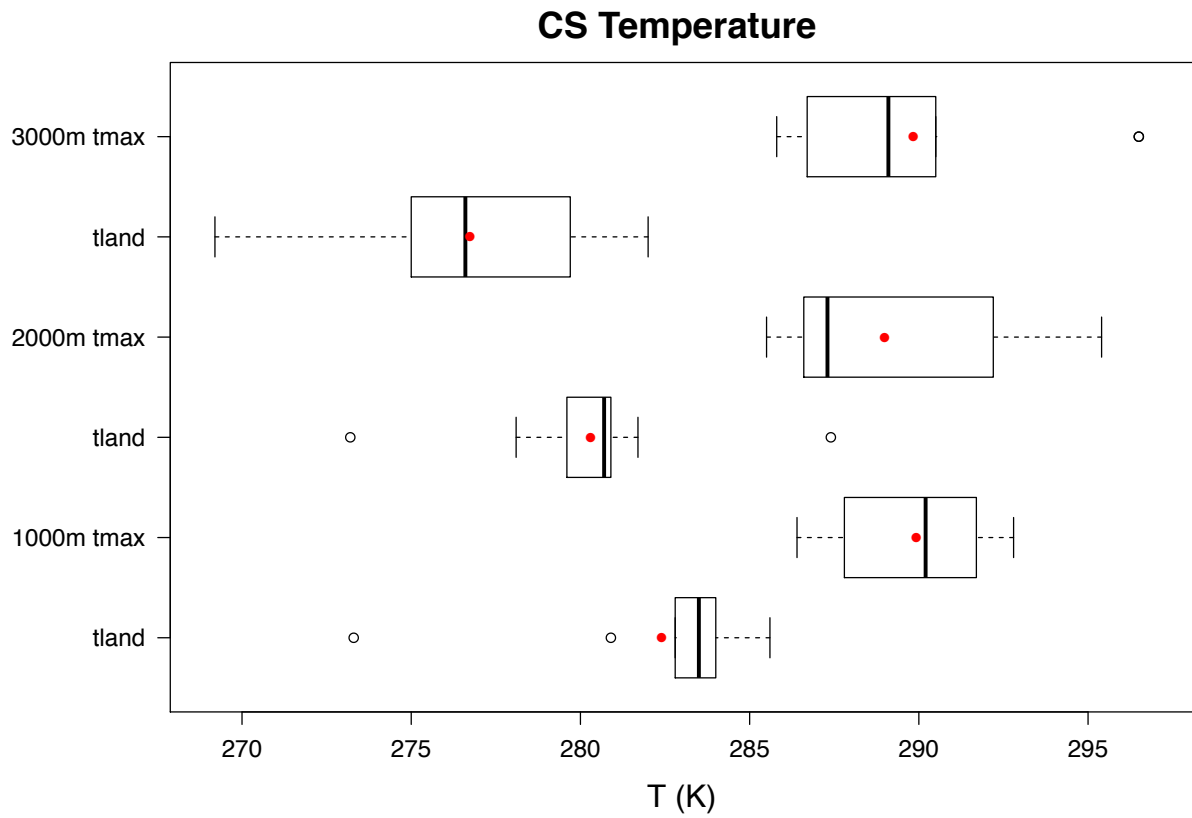
**Fig. 3.18** Same as Fig. 3.17, but for maximum (tmax) and landfall (tland) temperatures
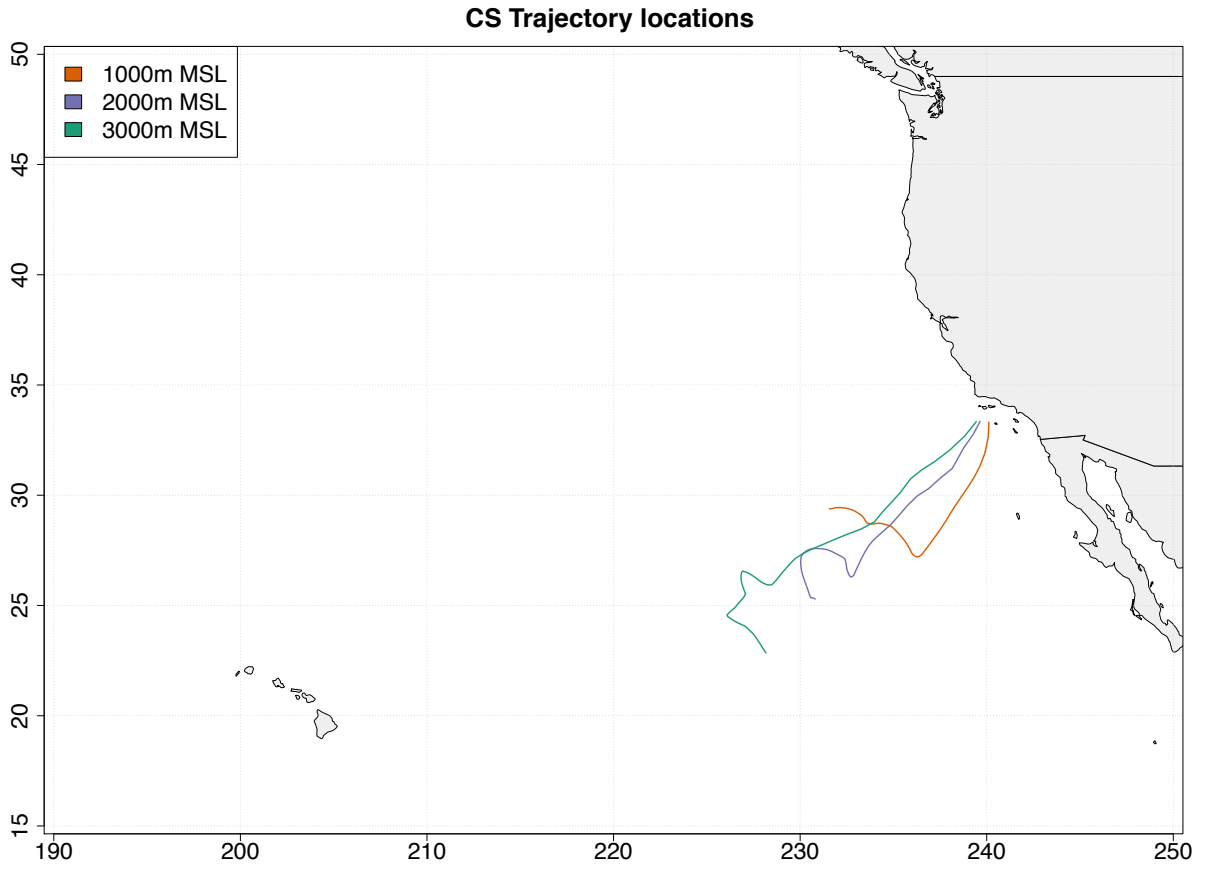
**Fig. 3.19** Median trajectories over 72–h for the 021717 case study event according to landfall level

## CS trajectory distances
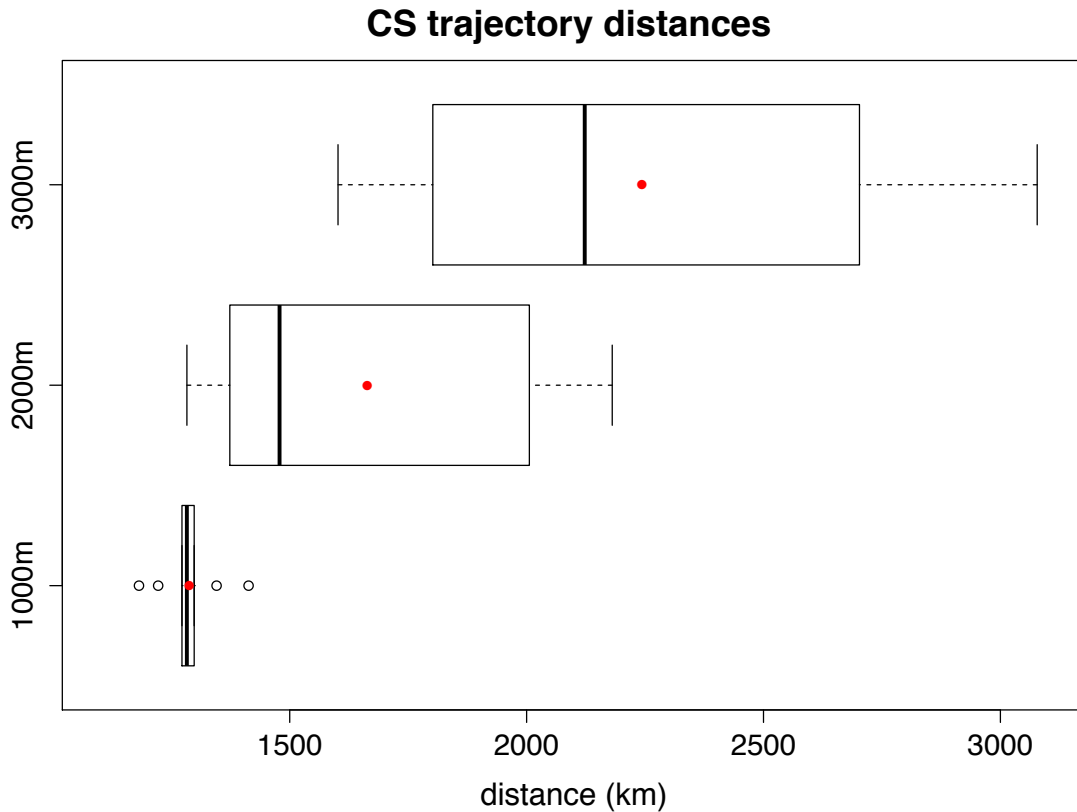


**Fig. 3.20** Boxplots depicting AR trajectory distances for the 021717 case study event according to landfall level. Box and whiskers depict interquartile range with median (black lines) and mean (red dots) distances. Outliers are depicted as open circles

### 3.5 Conclusions

We use a Lagrangian backward trajectories model (HYSPLIT) to compute backward trajectories of 159 ARs landfalling along the U.S.'s west coast from December 2004 to December 2015 for the hour of landfall and hourly for 72–h before landfall. We then compare SCA ARs to ARs landfalling farther north. One-degree GDAS data is used to force HYSPLIT with 3D atmospheric variables. For each AR nine trajectories are modeled at each of the three ending atmospheric levels, 1000 m, 2000 m, and 3000 m MSL, for a total of 27 backward trajectories calculated for each AR.

In the 72 hours before landfall, differences arise in trajectory distances as well as measured along trajectory characteristics.

In general, ARs landfalling in the western U.S. and ending at 1000 m MSL exhibit quasi-zonal orientations and cyclonic curvatures. They become less zonal and begin to extend in a northeastward orientation typical to ARs landfalling in North America (e.g. Neiman et al. 2008a) at higher altitudes with SCA AR trajectories displaying more zonal orientations (e.g. Harris and Carvalho 2017). SCA ARs trajectories appear farther south and trajectory locations 72-h before landfall are farther eastward in Pacific which is consistent with previous North American AR studies (Harris and Carvalho 2017). In the 72 hours before landfall very few AR trajectories travel below 30°N which indicates that water vapor origins (within 72-h of landfall) of many ARs may not be tropical in nature as ARs gather their water vapor through direct horizontal transport as well as local convergence (Bao et al. 2006). SCA AR have the shortest trajectories at all levels, thus in the 72-h before landfall, these ARs are slower. This implies that these ARs are likely to have differing relationships with extratropical cyclones than their more northern counterparts.

With along trajectory characteristics at all regions, parcels ending at 1000 m and 2000 m MSL show moistening (1-3 g kg$^{-1}$) as well as subsidence ($\leq$1.75hPa hr$^{-1}$) along the course of their trajectories. In the hours directly before landfall (0-15 hours) there is a decrease in pressure, high (~70%) relative humidity values, and drops in temperature indicating orographic uplift. SCA AR trajectories ending at 1000 m and 2000 m MSL tend to be warmer both with maximum along trajectory temperatures as well as landfall temperatures. This may be in part due to lower latitudes but indicates that these ARs have an increased potential to hold more moisture and are more likely to result in rainfall as opposed to snow. In regards to specific humidity, for trajectories ending at 1000 m MSL SCA ARs have higher maximum specific humidities values as well as higher specific humidities at landfall than both NCA and PNW ARs. At 2000 m MSL this difference is only seen

with SCA and PNW. Although the difference between maximum specific humidities and specific humidities at landfall (qdelta) show no differences between ARs in different landfall regions indicating that ARs regardless of landfall location are likely losing similar amounts of moisture due to condensation and precipitation along the course of their trajectories. As SCA ARs tend to have very high qmax and qland values, when these events make landfall they result in high-intensity storms. These differences help to account for the variances seen with SCA ARs which landfall less frequently than their more northern counterparts but are still capable of extreme storms and destruction.

An analysis of a strong February 2017 AR reveals a high-intensity storm with some characteristics that vary from typical ARs indicating that this was an extreme event. IMERG precipitation data show rainfall throughout the state of California with a narrow band of high values corresponding with the AR in the pre-cold frontal area of the storm (Eiras-Barca et al. in review). Reanalysis fields show that the day before SCA landfall, there is strong 850mb flow and a corresponding plume of high TPW extending from Hawaii to southern Oregon and northern California. A frontal wave emerges and develops into a cyclone, shifting the axes of the offshore trough as well as augmenting moisture due to increased convergence. This channels moisture and winds to SCA. With the HYSPLIT analysis, this event differs from other SCA ARs in that trajectories remain at low altitudes and do not experience subsidence in the hours before landfall. This event has increased moisture values that surpass the 75th percentile of the other SCA ARs examined as well as higher maximum temperatures although temperatures at landfall are comparable to other SCA ARs. Over the course of 72–h, these trajectories travel short distances indicating that this event moved rather slowly in the hours before landfall. This combination of warm temperatures, slow movement, and high specific humidity values resulted in one of the most extreme regional storms seen in years. It also brings into question the future of other AR storms

affecting SCA and how their intensity and duration may change under climate change scenarios (e.g. Dettinger 2011).

Understanding the differences of trajectories between ARs landfalling in various areas is imperative to understanding AR manifestation and lifecycles. This is especially true for SCA ARs which are infrequent but responsible for high-intensity storms as well as large proportions of the regional annual precipitation totals. Knowing how the environment affects these events and how these episodes progress will be vital for future forecasts and hazard mitigation.

**Acknowledgements**

## Chapter 4

## Conclusions

Atmospheric rivers are important components of west coast hydrological cycles. In North America, they often lead to extreme rainfall events resulting in hazards such as flooding. For SCA where annual precipitation totals are often met from only a handful of events per season, understanding and forecasting ARs is of critical importance as any changes to the frequency or intensity of local rainfall events may have devastating consequences. Yet, few studies focus on AR events leading to precipitation in SCA and instead concentrate on latitudes farther north. A better understanding of SCA ARs is imperative for forecasting as well as hazard mitigation. **This dissertation provides a novel perspective to AR research by improving the understanding of mechanisms and characteristics of AR events that landfall in SCA through the following research objectives:**

1. Design an algorithm that identifies historical AR events landfalling along the western coast of North America within reanalysis fields (Chapter 2);

2. Organize and categorize said AR events according to landfall regions and determine the climatological atmospheric characteristics during SCA ARs. Differentiate SCA ARs from ARs landfalling farther north on the day of as well as the days leading to AR landfall (Chapter 2);

3. Determine the relationships of defined AR groups with modes of variability known to affect western North America (Chapter 2);

4. Investigate the movement and change of AR groups and their along trajectory characteristics in the hours before landfall using a backward trajectories model (Chapter 3).

In chapter two we introduce a new method for AR detection within CFSR reanalysis fields of TPW. This algorithm builds off an already established procedure for AR detection but differs in that it uses a fit ellipse approach and a finer spatial resolution reanalysis. This provides a more selective identification method for AR detection as shown in the validation. We use the algorithm to identify ARs landfalling on the western coast of North America (landfalling between latitudes of 30.0°–55.0°N) during Oct-Mar seasons between 1979 and 2013. The algorithm identifies 719 independent AR events that we separate and categorize according to landfall region designated by landfall latitude. We create composites of various atmospheric features from additional reanalysis fields for each landfall area. Daily composites are created for the ten days before, day of, and three days after landfall to determine the common atmospheric characteristics present throughout an AR event and to identify the differences between ARs landfalling in different regions. We also statistically investigate AR occurrences with several modes variability known to affect the background atmospheric characteristics important to precipitation in North America.

Through daily composites of atmospheric variables, we see that on landfall days all ARs regardless of landfall region have anomalously high TPW anomalies flanked by regions of anomalously low TPW. This plume of moisture represents the AR event and corresponds to regions with high temperatures and an offshore 500mb trough. These features vary in location, shifting north/southward in accordance to where an AR makes landfall and are consistent with baroclinic wave train systems. Several days before AR landfall (~5 days), a 500mb trough develops over eastern Asia with a corresponding ridge over Alaska. The deepest troughs and most amplified ridges occur for SCA ARs whereas shallower troughs are consistent with ARs landfalling farther north. This trough-ridge couplet affects the merger and eastward extension of the upper-level (200mb) jet core ($\geq$60ms$^{-1}$) with deeper troughs leading to increased zonal flow of wind and moisture farther eastward in the Pacific basin. For ARs landfalling farther north, the jet core

retracts westward and has decreased zonal flow, consistent with previous AR studies. This indicates that wave phase, position, and amplitude are important components of ARs landfalling in western North America and are the primary drivers behind an AR's landfall location.

We also compare AR regional frequencies to occurrences and phases of variability modes that affect North America's west coast to establish conditions most likely to encourage AR manifestation and progression. The specific modes examined are the PNA, ENSO, and the MJO. We find that ARs are more frequent for all landfall areas during PNA+ but the difference between PNA+ and PNA- for SCA ARs is not significant. Additionally, SCA ARs have atmospheric features more consistent with PNA- conditions. This indicates that the PNA may not be a strong driver of AR conditions, especially for ARs landfalling in SCA. With ENSO, SCA AR conditions occur evenly between warm, cold, and neutral phases whereas NCA, SPNW, and NPNW ARs are more frequent during neutral conditions which is consistent with the occurrence of ENSO phases. For the MJO, all regions experience greater AR frequency during active MJOs yet, for most areas the frequency differences between active and inactive MJO are not significant. Also, while there are more ARs during certain phases of the MJO lifecycle, this relationship does not exist when ARs are separated according to landfall region. These varying relationships hint at the complexity of ARs that landfall on the western coast of North America. They suggest that while SCA ARs share some commonalities with other AR events, that there are also important differences in their occurrence and that these modes of variability may not be the sole drivers behind AR events landfalling in certain regions.

The following identifies the main conclusions from the methods and results presented in chapter two. First, although there are several modes of variability that affect the atmospheric conditions in North America, there are no defined relationships between any one variability mode and AR development, progression, or landfall in a specified region. This indicates that these modes

of variability are not the main drivers behind AR development or their landfalling locations. On the other hand, wave train characteristics such as phase, position, and amplitude in the days before AR development are the main drivers behind AR landfall location in western North America. Wave train dynamics over eastern Asia and western Pacific Ocean basin lead to the extension or retraction of upper-level jet core winds which drive wind and moisture towards North America's west coast with variations in the initial dynamics leading to ARs landfalling at different latitudes. The methods along with conclusions drawn in chapter two fulfill the first three objectives of this dissertation: **Design an algorithm that identifies historical AR events landfalling along the western coast of North America within reanalysis fields; Organize and categorize said AR events according to landfall regions and determine the climatological atmospheric characteristics during SCA ARs. Differentiate SCA ARs from ARs landfalling farther north on the day of as well as the days leading to AR landfall; Determine the relationships of defined AR groups with modes of variability known to affect western North America.**

In chapter three we investigate AR movements and lifecycles using the Lagrangian model HYSPLIT. We force HYSPLIT with GDAS 3D meteorological fields and calculate backward trajectories for 159 AR events landfalling on the western U.S. coast for the Oct-Mar seasons of Dec. 2004 to Dec. 2015. We apply the previously defined algorithm (chapter 2) using CFSR fields of TPW to identify these AR events. Each AR has a total of 27 calculated trajectories, 9 at each of the three levels investigated, 1000 m, 2000 m, and 3000 m MSL. Trajectories are calculated for the hour of landfall and hourly for 72 hours before landfall with outputs of air parcel locations as well as along trajectory characteristics including specific humidity and temperature.

According to average locational trajectories for all landfall regions, trajectories ending at 1000 m MSL, are shortest and are quasi-zonal. Trajectories lengthen and become less zonal,

adhering to the southwest-to-northeast orientation typical to ARs landfalling in North America at higher altitudes with SCA AR trajectories remaining the most zonally oriented. Within 72-h, very few trajectories travel south of 30°N and no trajectories travel below 25°N hinting at possible local moisture sources (within the 72-h) and pathways particularly as local convergence is a strong AR moisture source. All levels and landfall areas exhibit trajectories with cyclonic curvature. SCA ARs have significantly shorter 72-h trajectories than either NCA or PNW ARs for trajectories ending at 1000 m and 2000 m MSL. This indicates that SCA AR events move slower and/or may be more stationary implying differing behaviors with extratropical cyclones than their more northern counterparts.

With temporal variations before landfall (15-72 hours) for all regions, air parcel trajectories experience an overall moistening (1-3 g kg$^{-1}$) and subsidence ($\leq$1.75 hPa hr$^{-1}$) which can be from evaporation or moisture advection. Directly before landfall (0-15 hours) variables consistent with orographic uplift and subsequent precipitation for all regions occur including decreases in pressure, increases in relative humidity, decreases of temperature, and decreases of specific humidity. Along-trajectory variables for trajectories ending at 1000 m and 2000 m MSL show that SCA ARs tend to be warmer both at the maximum recorded temperature along the trajectory as well as at landfall with less cooling over the course of the trajectory as indicated by tdelta. This demonstrates that SCA AR air parcels have greater potential to hold moisture than ARs landfalling farther north which are cooler. SCA ARs are also more likely to result in rainfall as opposed to snow events. Additionally, increased temperatures suggest that SCA ARs are more likely to originate and/or move through more tropical (i.e. warmer) air masses. SCA ARs also have higher maximum and landfall specific humidity values for trajectories ending at 1000 m and 2000 m MSL demonstrating that these ARs do indeed contain more moisture than other ARs. However, the average qdelta values for SCA ARs are comparable to the other landfall groups indicating that

97

although SCA ARs have higher overall moisture values that ARs in general experience similar moisture losses along the course of their trajectories regardless of landfall location. The movement of warm temperatures and moisture results in high-intensity precipitation upon landfall through orographic forcing. With greater moisture values, SCA ARs are capable of producing very high-intensity rainfall.

A case study of a particularly intense AR event affecting SCA on February 17, 2017 is also investigated. We use IMERG precipitation data as well as CFS reanalysis fields to visualize this event and its conditions. Backward air parcel trajectories are calculated using HYSPLIT to determine air characteristics and movement. At the time of landfall, low precipitation values (≤5mm) consistent with an extratropical cyclone exists throughout much of the state of California. There is a narrow plume of high rainfall values (≥11mm) in the pre-cold frontal region of the storm bearing onto mountains along the California coastline. Reanalysis fields at the 850mb and 500mb levels reveal that before AR landfall around the coast of SCA there are strong offshore winds associated with a low-pressure system along with a narrow band of high TPW and an offshore trough resulting in strong flow of wind and moisture towards SCA. Also prior to SCA landfall a mesoscale frontal wave develops and progresses into a low-pressure system. This augments moisture within the already existing AR as it landfalls in SCA through increased convergence along the cold front. With HYSPLIT commonalities appear between this event and the average temporal trajectory qualities related to orographic uplift at landfall. Although, there are also differences in parcel behavior. In the 72-h before landfall air parcels occur at low altitudes and there is very little vertical movement of parcels until uplift occurs. This differs from average regional parcels that experience subsidence in the 72-h hours before landfall. Also these air parcels travel shorter distances in the course of 72-h demonstrating the slow-moving nature of this event. Finally, this event has maximum and landfall along trajectory specific humidity values that are

much higher than all ARs at all levels and at some levels surpass the 75th percentile of moisture of other SCA ARs. Maximum temperature values for this event are higher than all other landfall regions although, temperatures at landfall are similar to other SCA ARs. The overall low altitudes of the parcels and lack of vertical movement may help to explain why this event retained much of its heat and moisture throughout the trajectory and the very high specific humidity accounts for the event's extreme intensity upon landfall.

The analyses in chapter three demonstrate the following main conclusions. That ARs landfalling in SCA share similar characteristics with ARs landfalling farther north along the U.S. west coast. SCA ARs display temporal trajectory variations before and during landfall similar to NCA and PNW ARs indicating that ARs regardless of landfall locations undergo similar lifecycle development. Additionally, all ARs regardless of landfall region move high temperatures and moisture values to their designated landfall area with similar losses of moisture (qdelta) and cooling (tdelta) along the course of their trajectories. This movement of high heat and moisture along with orographic uplift leads to high-intensity precipitation common to most AR events regardless of landfall region. Yet, some important distinctions between SCA ARs and ARs landfalling farther north do arise. SCA ARs have higher maximum temperature values along their trajectories as well as higher temperatures at landfall which increases their potential to hold moisture as well as indicates they are more likely to result in rainfall events. Additionally, they have higher maximum specific humidity values along their trajectories and also at landfall indicating that these events have greater moisture contents. The higher heat and moisture values of SCA ARs explain why these events have some of the most extreme rainfall episodes even though they tend to occur less frequently compared to ARs landfalling farther north. These methods and their conclusions fulfill the fourth and final research objective: **Investigate the movement and change of AR groups**

**and their along trajectory characteristics in the hours before landfall using a backward trajectories model.**

These findings suggest that although SCA ARs share commonalities with other ARs affecting western North America, that there are also differences in how they manifest and progress. They differ in their pre-landfall as well as day-of landfall atmospheric characteristics and dynamics as well as their trajectory lifecycles and connections with other modes of variability. This information can be used to improve modeling and forecasts of AR events affecting the western coast of North America which in turn is important for hazard mitigation as well as long-term water management. Additionally, while this research focuses on a specific area, certain aspects of this work such as the detection algorithm may be applied to other regions of the world affected by similar events.

**Suggestions for Future Work**

These findings help to identify the characteristics of SCA ARs before and during landfall, and are important to understanding the progression and dynamics of SCA ARs. Yet, there are still areas of AR research and SCA AR research that need development. In the following section we identify possibilities for future research endeavors.

This research relies on the AR detection algorithm presented in chapter 2. While the validation studies conclude this is robust method for AR detection within reanalysis fields, it is by far not the only reliable method. Other studies such as Guan and Waliser (2015) use integrated vapor transport vapor (IVT) instead of TPW as a proxy for AR detection as IVT is believed to better capture the movement of AR moisture. Neiman et al. 2008a and Dettinger et al. 2011 are examples of studies that show SSM/I data to be very useful for AR detection, although there is not yet an automated AR detection method using SSM/I data. While these and the presented

algorithm provide valuable tools for historical AR detection and identification, they are in part flawed and subjective. They will require modifications to improve detection and future algorithms will most likely combine a series of data and procedures to create more accurate AR detectors.

Additionally, the research presented in this dissertation does not discern differences between ARs of varying strengths. Extreme AR events may have unique atmospheric characteristics and dynamics. An analysis by Payne and Magnusdottir (2014) concludes that there are differences between high-intensity and low-intensity AR events that affect North America's west coast. They investigate ARs affecting 20°-60°N during Nov.-Mar. between 1979 and 2011 and compare some the highest-intensity AR events (≥95th percentile moisture flux and rainfall) to less extreme events and the climatological averages. They conclude that high-intensity events occur in conjunction with the formation of Rossby Wave Breaking in the eastern Pacific and changes in the 200mb jet. The highest-intensity events may also have alternative relationships with modes of variability. An analysis by Guan et al. (2010) looks at 45 ARs affecting the Sierra Nevada between 2004 and 2010. Upon investigating ARs with the highest SWE conditions they find that several of the highest SWE events in this region occur during La Niña seasons which is inconsistent with findings from these studies (chapter 2). Neither of these studies focus on SCA ARs which behave differently from their more northern counterparts. Even though extreme events (such as the case study presented in 3.4) provide a small proportion of the events experienced, they are climatologically significant to the SCA landscape and are worth understanding in greater detail.

Finally, the studies presented in this dissertation do not make any predictions about future AR frequencies or storm intensities which are expected to vary and are of interest due to changing climatic conditions. Dettinger (2011) determines that ARs are projected to warm in a warming climate, although not at the same rate. This increases their potential to hold moisture by 7% for each 1K increase of temperature. The frequencies of AR days and years with increased AR activity

are also projected to increase in a changing climate (Dettinger 2011). A study by Hagos et al. (2016) uses Community Earth System Model Large Ensemble simulations to predict future AR frequencies. They find that comparing the last two decades of the 20th and 21st centuries, there is a 35% ± 8% increase in the number of AR landfall days in western North America (32°-60°N). The number of AR days with extreme precipitation also increases by 28% ± 7%. Additionally, it is expected that changing climate conditions will modify dynamical characteristics of the atmosphere known to affect ARs. Shields and Kiehl (2016) use the fully coupled half-degree version of the Community Climate System Model, version 4 to show an equatorward shift in the subtropical jet which results in the southward shift of AR events affecting North America's west coast during a warming climate scenario. Specifically, there is an increased number of AR events affecting the latitudes of 32°-35°N, consistent with a previous study by Payne and Magnusdottir (2015) who also show an equatorward shift in ARs affecting the U.S. west coast in climate change projections. These changes may affect how AR storms manifest and progress as well as how they interact with extratropical cyclones and modes of variability. Proper forecasting and preparation requires understanding the modifications of AR events in changing climate scenarios.

While this dissertation provides valuable information regarding the development and landfall of atmospheric rivers in western North America, it is only one piece to a large puzzle. A comprehensive understanding of high-intensity precipitation including causes, linkages with various phenomena, climatic changes, and mitigation against its impacts requires communication between various disciplines and across management sectors. The main goal of this research is to provide information that may be used by the scientific and water management communities to improve our current understanding of and help prepare for atmospheric events leading to high-intensity precipitation in North America.

# References

Anderson RS, Anderson SP (2010) Geomorphology: The Mechanics and Chemistry of Landscapes. Cambridge University Press: pp. 340 pp.

Anderson TW, Finn JD (1996) The New Statistical Analysis of Data. Springer–Verlag pp. 712

Bao JW, Michelson SA, Neiman PJ, Ralph FM, Wilczak JM (2006) Interpretation of enhanced integrated water vapor bands associated with extratropical cyclones: Their formation and connection to tropical moisture. Mon Wea Rev 134:1063-1080

Bell GD, Higgins W (2005) National Oceanic and Atmospheric Administration, Climate Prediction Center. 18 December 2004 – 17 January 2005: U.S. Storms and Flooding in the West and Midwest Exceptional Warmth in the Midwest and East. Climate Prediction Center Web. http://www.cpc.ncep.noaa.gov/products/expert_assessment/california_assessment_ 2005.pdf 23 February 2016

Caine N (1980) The rainfall intensity: duration control of shallow landslides and debris flows. Geogr Ann Ser A: Phys Geogr 62:23-27

Campmany E, Bech J, Rodríguez-Marcos J, Sola Y, Lorente J (2010) A comparison of total precipitable water measurements from radiosonde and sunphotometers. Atm Res 97:385-392

Dettinger MD (2004) Fifty-two years of "pineapple-express" storms across the West Coast of North America. U.S. Geological Survey, Scripps Institution of Oceanography for the California Energy Commission, PIER Project Rep CEC-500-2005-004:20

Dettinger MD (2011) Climate change, atmospheric rivers, and floods in California – A multimodel analysis of storm frequency and magnitude changes[1]. J Amer Water Resour Assoc 47:514-523

Dettinger MD, Ralph FM, Das T, Neiman PJ, Cayan DR (2011) Atmospheric rivers, floods, and the water resources of California. Water 3:455–478

Dettinger M, Ralph FM, Lavers D (2015) Setting the stage for a global science of atmospheric rivers. Eos, 96 doi:10.1029/2015EO038675

Draxler RR, Hess GD (1997) Description of the HYSPLIT_4 modeling system. NOAA Tech Memo ERL ARL-224: 25

Draxler RR, Hess GD (1998) An overview of the HYSPLIT_4 modelling system for trajectories. Australian meteorological magazine 47:295-308

Eiras-Barca J, Ramos AM, Pinto JG, Trigo RM, Liberato MLR, Miguez-Macho G (in review) The concurrence of atmospheric rivers and explosive cyclogenesis in the North Atlantic and North Pacific basins. Submitted for review in Earth Sys Dyn

Guan B, Molotch NP, Waliser DE, Fetzer EJ, Neiman PJ (2013) The 2010/11 snow season in California's Sierra Nevada: Role of atmospheric rivers and modes of large-scale variability. Water Resour Res 49:6731–43

Guan B, Waliser DE, Molotch NP, Fetzer EJ, Neiman PJ (2012) Does the Madden-Julian Oscillation influence wintertime atmospheric rivers and snowpack in the Sierra Nevada? Mon Wea Rev 140:325-342

Guan B, Waliser DE (2015) Detection of atmospheric rivers: Evaluation and application of an algorithm for global studies. J Geophys Res Atmos 120:12514–12535 doi:10.1002/2015JD024257.

Harris SM, Carvalho LMV (2017) Characteristics of southern California atmospheric rivers. Theor Appl Climatol 1-17 doi:10.1007/s00704-017-2138-1

Huffman GJ, Bolvin DT, Braithwaite D, Hsu K, Joyce R, Kidd C, Nelkin EJ, Sorooshian S, Xie P (2017) NASA Global Precipitation Measurement (GPM) Integrated Multi-satellitE Retrievals for GPM (IMERG), Algorithm Theoretical Basis Document (ATBD) Version 4.6. NASA/GSFC, Greenbelt, MD, USA: 32

Iverson RM (2000) Landslide triggering by rain infiltration. Water Resour Res 36:1897-1910

Jiang T, Deng Y (2011) Downstream modulation of North Pacific atmospheric river activity by East Asian cold surges. Geophys Res Lett 38: doi:10.1029/2011GL049462

Jiang T, Evans KJ, Deng Y, Dong X (2014) Intermediate frequency atmospheric disturbances: A dynamical bridge connecting western U.S. extreme precipitation with East Asian cold surges. J Geophys Res: Atmospheres 119: doi:10.1002/2013JD021209

Jibson RW (1989) Debris flows in southern Puerto Rico. In: Schultz AP, Jibson RW (eds) Landslide processes of the eastern United States and Puerto Rico. Geological Society of America Special Paper 236. Geological Society of America, Boulder, pp 29–55.

Jones C (2000) Occurrence of extreme precipitation events in California and relationships with the Madden–Julian Oscillation. J Clim 13:3576–87

Jones C, Carvalho LMV (2012) Spatial-intensity variations in extreme precipitation in the contiguous United States and the Madden-Julian Oscillation. J Clim 24:4898–4913

Jones C, Gottschalck J, Carvalho LMV, Higgins W (2011) Influence of the Madden-Julian Oscillation on forecasts of extreme precipitation in the contiguous United States. Mon Wea Rev 139:332-350

Kanamitsu M (1989) Description of the NMC global data assimilation and forecast system. Wea Forecasting 4:335-342

Kim J, Waliser DE, Neiman PJ, Guan B, Ryoo JM, Wick GA (2013) Effects of atmospheric river landfalls on the cold season precipitation in California. Clim Dyn 40: doi:10.1007/s00382-012-1322-3

Leathers DJ, Yarnal B, Palecki MA (1991) The Pacific/North American teleconnection pattern and United States climate. Part I: Regional temperature and precipitation associations. J Clim 4:517-528

Madden RA, Julian PR (1994) Observations of the 40-50-day tropical oscillation-A review. Mon Wea Rev 122:814-837

Martinković M, Mahović NS, Jurković PM, Renko T, Pelajić I, Smiljanić I (2017) Relationship between atmospheric rivers and extreme precipitation events. Perspectives on Atmospheric Sciences 385-390 doi:10.1007/978-3-319-35095-0_54

Mechoso CR, Robertson AW, Ropelewski CF, Grimm AM (2005) The American monsoon systems: An introduction. WMO Tech Doc 1266(TMRP Rep. 70):197–206

Mo KC, Higgins RW (1998) Tropical influences on California precipitation. J Clim 11:412–31

Moore BJ, Neiman PJ, Ralph FM, Barthold FE (2012) Physical processes associated with heavy flooding rainfall in Nashville, Tennessee, and Vicinity during 1-2 May 2010: The role of an atmospheric river and mesoscale convective systems*. Mon Wea Rev 140:358-378

Naftaly M, McFarland J, Paley J, Parker M (1998) 1998 Flood Report. Santa Barbara: Santa Barbara County Flood Control and Water Conservation District: print

Neiman PJ, Persson POG, Ralph FM, Jorgensen DP, White AB, Kingsmill DE (2004) Modification of fronts and precipitation by coastal blocking during an intense landfalling winter storm in Southern California: Observations during CALJET. Mon Wea Rev 132:242–273

Neiman PJ, Ralph FM, White AB, Kingsmill DE, Persson POG (2002) The statistical relationship between upslope flow and rainfall in California's coastal mountains: Observations during CALJET. Mon Wea Rev 130:1468–1492

Neiman PJ, Ralph FM, Wick GA, Lundquist JD, Dettinger MD (2008a) Meteorological characteristics and overland precipitation impacts of atmospheric rivers affecting the West Coast of North America based on eight years of SSM/I satellite observations. J Hydrometeorol 9:22–47

Neiman PJ, Ralph FM, Wick GA, Kuo YH, Wee TK, Ma Z, Taylor GH, Dettinger MD (2008b) Diagnosis of an intense atmospheric river impacting the Pacific Northwest: Storm summary and offshore vertical structure observed with COSMIC satellite retrievals. Mon Wea Rev 136: doi:10.1175/2008MWR2550.1

Neiman PJ, Schick LJ, Ralph FM, Hughes M, Wick GA (2011) Flooding in western Washington: The connection to atmospheric rivers*. J Hydrometeorol 12: doi:10.1175/2011JHM1358.1

Neiman PJ, Ralph FM, Moore BJ, Hughes M, Mahoney KM, Cordeira JM, Dettinger MD (2013) The landfall and inland penetration of a flood-producing atmospheric river in Arizona. Part I: Observed synoptic-scale, orographic, and hydrometeorological characteristics. J Hydrometeorol 14:460-484

Newell RE, Newell NE, Zhu Y, Scott C (1992) Tropospheric rivers?–A pilot study. Geophys Res Lett 19:2401-2404

Newman M, Kiladis GN, Weickmann KM, Ralph FM, Sardeshmukh PD (2012) Relative contributions of synoptic and low-frequency eddies to time-mean atmospheric moisture transport, including the role of atmospheric rivers. J Clim 25: doi:10.1175/JCLI-D-11-00665.1

Payne AE, Magnusdottir G (2014) Dynamics of landfalling atmospheric rivers over the North Pacific in 30 years of MERRA reanalysis. J Clim 27: doi:10.1175/JCLI-D-14-00034.1

Ralph FM, Dettinger MD (2011) Storms, floods, and the science of atmospheric rivers. Eos, Trans Amer Geophys Union 92:265–272

Ralph FM, Dettinger MD (2012) Historical and national perspectives on extreme west coast precipitation associated with atmospheric rivers during December 2010. Bull Amer Meteor Soc 93:783-790

Ralph FM, Neiman PJ, Kingsmill DE, Persson POG, White AB, Strem ET, Andrews ED, Antweiler RC (2003) The impact of a prominent rain shadow on flooding in California's Santa Cruz Mountains: A CALJET case study and sensitivity to the ENSO cycle. J Hydrometeorol 4:1243-1264

Ralph FM, Neiman PJ, Wick GA (2004) Satellite and CALJET aircraft observations of atmospheric rivers over the eastern North Pacific Ocean during the winter of 1997/98. Mon Wea Rev 132:1721–45

Ralph FM, Neiman PJ, Rotunno R (2005) Dropsonde observations in low-level jets over the northeastern Pacific Ocean from CALJET-1998 and PACJET-2001: Mean vertical-profile and atmospheric-river characteristics. Mon Wea Rev 133:889-910

Ralph FM, Neiman PJ, Wick GA, Gutman SI, Dettinger MD, Cayan DR, White AB (2006) Flooding on California's Russian River: Role of atmospheric rivers. Geophys Res Lett 33: doi:10.1029/2006GL026689

Ralph FM, Neiman PJ, Kiladis GN, Weickmann K, Reynolds DW (2011) A multi-scale observational case study of a Pacific atmospheric river exhibiting tropical–extratropical connections and a mesoscale frontal wave. Mon Wea Rev 139: doi:10.1175/2010MWR3596.1

Ramos AM, Nieto R, Tomé R, Gimeno L, Trigo RM, Liberato MLR, Lavers DA (2016) Atmospheric rivers moisture sources from a Lagrangian perspective. Earth Sys Dyn 7:371-384

Rutz JJ, Steenburgh WJ (2012) Quantifying the role of atmospheric rivers in the interior western United States. Atm Sci Lett 13: doi:10.1002/asl.392

Rutz JJ, Steenburgh WJ, Ralph FM (2014) Climatological characteristics of atmospheric rivers and their inland penetration over the western United States. Mon Wea Rev 142:905–921

Rutz JJ, Steenburgh WJ, Ralph FM (2015) The inland penetration of atmospheric rivers over western North America: A Lagrangian analysis. Mon Wea Rev 143: doi:10.1175/MWR-D-14-00288.1

Ryan G (1994) The climate of Santa Barbara, California. Santa Maria: National Weather Service, print.

Saha S, Moorthi S, Pan HL, Wu X, Wang J, Nadiga S, Tripp P, Kistler R, Woollen J, Behringer D, Liu H, Stokes D, Grumbine R, Gayno G, Wang J, Hou YT, Chuang Hy, Juang HMH, Sela J, Iredell M, Treadon R, Kleist D, Van Delst P, Keyser D, Derber J, Ek M, Meng J, Wei H, Yang R, Lord S, van den Dool H, Kumar A, Wang W, Long C, Chelliah M, Xue Y, Huang B, Schemm JK, Ebisuzaki W, Lin R, Xie P, Chen M, Zhou S, Higgins W, Zou CZ, Liu Q, Chen Y, Han Y, Cucurull L, Reynolds RW, Rutledge G, Goldberg M (2010) The NCEP climate forecast system reanalysis. Bull Am Meteorol Soc 91:1015-1057

Schoenherr AA (1992) A natural history of California, vol 56. Univ of California Press, pp. 8

Shakesby RA (2011) Post-wildfire soil erosion in the Mediterranean: Review and future research directions. Earth-Science Rev 105:71-100

Sodemann H, Stohl A (2013) Moisture origin and meridional transport in atmospheric rivers and their association with multiple cyclones*. Mon Wea Rev 141:2850-2868

Stohl A, Forster C, Sodemann H (2008) Remote sources of water vapor forming precipitation on the Norwegian west coast at 608N—A tale of hurricanes and an atmospheric river. J Geophys Res 113:D05102 doi:10.1029/2007JD009006

Trenberth KE (1999) Atmospheric moisture recycling: Role of advection and local evaporation. J Clim 12:1368-1381

Waliser D, Guan B (2017) Extreme winds and precipitation during landfall of atmospheric rivers. Nat Geosci 10:179-183 doi:10.1038/NGEO2894

Wallace JM, Gutzler DS (1981) Teleconnections in the geopotential height field during the Northern Hemisphere winter. Mon Wea Rev 109:784-812

Zhang C (2005) Madden-Julian Oscillation. Rev Geophys 43:1-26

Zhu Y, Newell RE (1994) Atmospheric rivers and bombs. Geophys Res Lett 21:1999–2002

Zhu Y, Newell RE (1998) A proposed algorithm for moisture fluxes from atmospheric rivers. Mon Wea Rev 126:725–35